1-1-2021

RESPONSES OF PREDATORY MYXOBACTERIA TO PREY SIGNALING MOLECULES & FEATURES OF A PSEUDOMONAS PREY AVOIDING PREDATION

Shukria Akbar
University of Mississippi

RESPONSES OF PREDATORY MYXOBACTERIA TO PREY SIGNALING MOLECULES & FEATURES OF A PSEUDOMONAS PREY AVOIDING PREDATION

A Dissertation
presented in partial fulfillment of requirements
for the degree of Doctor of Philosophy
in the Department of Biomolecular Sciences
The University of Mississippi

By

SHUKRIA AKBAR

May 2021

ABSTRACT

Gram-negative unicellular myxobacteria, along with their multicellular lifestyle and biologically active specialized metabolites, are known for the predatory interactions with Gram-negative/Gram-positive bacteria and fungi. Although myxobacterial predation range have been exploited extensively, little is known about the prey associated molecules contributing to myxobacterial predator-prey dynamics. By employing transcriptomics and untargeted metabolomics approaches, we demonstrate two structurally distinct classes of signaling molecules from Gram-negative bacterial prey elicit significant *omics* responses from myxobacteria, *Myxococcus xanthus* and *Cystobacter ferrugineus*. An overlapping and general response to acyl-homoserine lactones, whereas a distinctive response to a quinolone signaling molecule is observed from both myxobacteria. Similarly, by employing transcriptomics and classical microbiological assays, we demonstrate higher production of molecules like pyoverdine, phenazine-1-carboxylic acid, and alginate and resistance to aminoglycosides and tetracycline antibiotics are unique to a predation survivor *Pseudomonas putida* phenotype. In a predator-prey co-culturing, the predatory stress from myxobacterium *C. ferrugineus* selects for this *P. putida* phenotype that eludes subsequent myxobacterial predation. Overall, our study confirms that prey associated chemical components significantly direct responses from predatory myxobacteria.

DEDICATION

To my mom for always being there for me and making me feel loved, cared for, and special.

LIST OF ABBREVIATION AND SYMBOLS

AHL	*N*-acyl-homoserine lactone
antiSMASH	antibiotics and Secondary Metabolite Analysis Shell
ACN	Actinorhodin
BGC	Biosynthetic gene cluster
C6-AHL	*N*-Hexanoyl-L-homoserine lactone
CTTYE	Casitone Yeast Extract medium
DNA	Deoxyribonucleic acid
D-HSL	D-homoserine lactone
EIC	Extracted ion chromatograph
EtOAC	Ethyl acetate
GNPS	Global natural products social
HHQ	4-hydroxy-2-heptylquinoline
HQNO	2-heptyl-4-hydroxyquinoline *N*-oxide
LC-MS	Liquid Chromotography-Mass Spectrometry

LC-MS/MS	Liquid Chromotography-Tandem Mass Spectrometry
L-HSL	L-homoserine lactone
MS/MS	Tandem Mass Spectrometry
NPs	Natural products
3-oxo-C6-AHL	3-oxo-Hexanoyl-L-homoserine lactone
PQS	Pseudomonas quinolone signal
PQS-NO	2-heptyl-3,4-dihydroxyquinoline-*N*-oxide
PCA	Principal component analysis
P1CA	Phenazine-1-carboxylic acid
RNA	Ribonucleic acid
RNAseq	Ribonucleic acid sequencing
VY/2	Half-strength Yeast cell Vitamin B12 medium
XCMS-MRM	Various forms (X) of chromatography mass spectrometry

ACKNOWLEDGEMENTS

Accomplishing a Ph.D. away from my family was not possible without some extra support from God. I thank Him for giving me enough strength to stay collected and for making me feel lucky throughout this journey.

I believe the addition of prayers boosts one's success, and I thank my mom for her endless prayers and unconditional love. I appreciate her support and staying connected.

I thank my advisor, Prof. Cole Stevens, for introducing me to the world of scientific research and predatory bacteria. I enjoyed both a lot! I thank him for providing a stress-free research environment, and I appreciate his tolerance and kindness.

My family's support remained an asset during this journey. I thank my brother, Khalil Ahmed, for encouraging my decision and supporting me to come to the USA for higher education. Many thanks to my sister Rabia for providing me strength at every moment. A big thanks to my now ten years old nephew, Muhammed Shafey, for keep suggesting that I should read stuff online instead of asking him questions. He is second to my advisor in emphasizing the importance of reading. I thank my sisters Nadia, Nasia, Sobia, and Sundus for their care and insights and for pushing me to enjoy life during my Ph.D.

I started my Ph.D. journey with some fears and ending it with confidence, much credit to this transformation goes to the interactions I had in the Department of BioMolecular Sciences. I thank all the professors, staff members, and students from BMS for their kindness and love. I thank my dissertation committee members, Prof. Marc Slattery, Prof. Patrick Curtis, and Prof. Sudeshna Roy, for their guidance. I also say thanks to Prof. Paul Boudreau, Prof. Kristine Willett, Ms. Sherrie Gussow, Prof. Robert Doerksen, Prof. Nicole Ashpole, and Prof. Jason Paris for being very supportive and affectionate. I thank Barbara Adaikpoh for her sincere suggestions; having her as my colleague was one of the great things that happened to me. I also thank my colleague Mohammed Salahuddin for his insightful discussions. Lastly, I say thank to myself for my persistence and patience in the last one year of earning of this degree.

TABLE OF CONTENTS

Abstract ……..……..ii

Dedication……...iii

List of Abbreviations and Symbols…….…….…...iv

Acknowledgments……...…...vi

Table of contents.……..…….……...viii

List of Figures……..…….xiii

List of Tables…….xvi

Chapter 1 Myxobacterial predatory dynamics with their preys……..1

1.1. Abstract…….1

1.2. Myxobacteria…….……...2

1.3. Predation strategies…….……...……..….5

1.4. Predation range of myxobacteria…….……...……..….7

1.4.1. Predation on Gram-negative bacteria……...……...….7

1.4.2. Predation on Gram-positive bacteria……...…….....11

1.4.3. Predation on cyanobacteria……..…….....13

1.4.4. Predation on fungi…….……...…….....….15

1.5. Prey avoiding myxobacterial predator.…….……..……17

1.5.1. Prey specialized metabolites involved in predation avoidance……..…...18

1.5.2. Non-antibacterial substances involved in predation avoidance.……..….19

1.5.3. Other predation avoidance mechanisms ……...……...……..20

1.6. Concluding remarks……...…….……...……..…20

Chapter 2 Draft genome sequence and metabolic potential of myxobacterium *Cystobacter ferrugineus*……...……...…..22

2.1. Abstract……...22

2.2. Introduction...…….…….23

2.3. Results and discussion…….……...…….24

2.3.1. Whole genome sequencing of *C. ferrugineus*...……...…….....24

2.3.2. Biosynthetic potential of *C. ferrugineus*……...…...……..24

2.3.3. Tubulysins production by *C. ferrugineus*.……...…….....26

2.4. Conclusion.…….…….……..…….28

2.5. Material and method…...…….…….……..…….28

2.5.1. Bacterial culturing and DNA isolation……...28

2.5.2. Genome sequencing and annotation…….....28

2.5.3. Analysis for biosynthetic potential……...……...…..…29

2.5.4. Metabolic extraction and untargeted mass spectrometry…….....29

2.5.5. Data analysis on GNPS platform…….……...…...30

2.6. Acknowledgements…….……...…….30

Chapter 3 Myxobacterial *omics* responses to prey signaling molecules……..…..……31

3.1. Abstract……..…….31

3.2. Introduction...…….…….…32

3.3. Results…….……...…….34

3.3.1. C6-AHL induces a general transcriptional downregulation in both *C. ferrugineus* and *M. xanthus*……...……..34

3.3.2. HHQ elicits contrasting transcriptomics responses from *M. xanthus* and *C. ferrugineus*……...…...……..38

3.3.3. Prey signals differentially impact genes included in specialized metabolites biosynthetic gene clusters……..…….....42

3.3.4. Differential metabolomic impact of AHL and HHQ signals…….....….44

3.3.5. The core structural moiety of AHLs is an elicitor of myxobacterial conserved metabolomic response to AHLs…….....48

3.3.6. Oxidative detoxification of HHQ observed from *C. ferrugineus*…....….50

3.4. Discussion……...52

3.5. Material and method...…….……...…….57

3.5.1. Cultivation of *M. xanthus* and *C. ferrugineus*..……..57

3.5.2. Signal exposure experiments…….……...…….58

3.5.3. RNAseq analysis……...58

3.5.5. Metabolite extraction……..……...59

3.5.6. XCMS-MRM analysis..……..……...60

3.6. Acknowledgements……...……...…60

Chapter 4 Features associated with predation avoiding *Pseudomonas putida* phenotype selected by *Cystobacter ferrugineus*……...…….61

4.1. Abstract……...…61

4.2. Introduction...…….62

4.3. Results…….……...…….63

4.3.1. Selection of *P. putida* phenotype avoiding predation…….63

4.3.2. *P. putida* survivor eludes subsequent predation of *C. ferrugineus*…….65

4.3.3. *P. putida* survivor competes to survive *C. ferrugineus* predation in the presence of nutrients…..……...…...…….66

4.3.4. Differential gene expression of survivor phenotype...…….....67

4.3.5. Increased pyoverdine production by survivor phenotype…….....71

4.3.6. Increased production of phenazine-1-carboxylic acid by survivor phenotype…..……...……...…...…….71

4.3.7. Increased production of alginate by survivor phenotype……75

4.3.8. Antibiotic resistance of survivor phenotype…..…….76

4.4. Discussion …….....77

4.5. Materials and Methods ……...81

4.5.1. Bacterial strains and cultivations……...81

4.5.2. Predation assays...…….……...…….82

4.5.3. CFU assays...……83

4.5.4. RNA sequencing...…….……...……83

4.5.5. Assessment of extracellular Pyoverdine……..……..…85

4.5.6. Metabolite extraction and analysis……..……..…….85

4.5.7. Swarming assay with culture supernatant of parent and survivor *P. putida*...……..…….86

4.5.8. Carbazole assay...…….…….86

4.5.9. Anti-alginate dot plots...…….……...……..…87

4.5.10. Antibiotic susceptibility assays...…….……..…….87

4.6. Acknowledgements...…….…….88

Chapter 5 Conclusion and contribution……...89

5.1. Introduction…….89

5.2. Results…….…….....90

5.3. Contribution…….……...……..……..91

Bibliography…….…….92

Appendix…….…….114

Vita...…….……...120

LIST OF FIGURES

Figure 1.1. Predatory myxobacteria…… 3

Figure 1.2. Myxobacterial predation strategies……..……..….. 6

Figure 2.1. Biosynthetic capacity of *C. ferrugineus* predicted by antiSMASH……..... 25

Figure 2.2. Tubulysin biosynthetic gene cluster organization in *C. ferrugineus*…...……..... 25

Figure 2.3. Tubulysins molecular network……...……..... 27

Figure 2.4. *De novo* MS/MS assignment to m/z 844.45 detected for tubulysin A structure in the crude metabolic extract of *C. ferrugineus*…….……..... 27

Figure 3.1. Differential gene expression from myxobacteria when exposed to C6-AHL signal……. 36

Figure 3.2. Putative roles of annotated genes impacted by C6-AHL……...…. 37

Figure 3.3. Differential gene expression from myxobacteria when exposed to HHQ signal. 39

Figure 3.4. Putative roles of annotated genes impacted by HHQ exposure…….. 40

Figure 3.5. Differentially impacted genes included in antiSMASH predicted specialized metabolite biosynthetic gene clusters ……...…….…… 42

Figure 3.6. Comparison of metabolomics responses of myxobacteria to prey signals…..… 44

Figure 3.7. Prey signals impact on the peak intensities of the metabolic features…… 46

Figure 3.8. Comparison of combined impact of prey acylhomoserine lactone and quinolone signals on metabolic features of myxobacteria……...…… 47

Figure 3.9. *C. ferrugineus* overlapping response to L-homoserine lactone and prey associated acyl-homoserine lactones……...……...…… 48

Figure 3.10. Box-plot showing *C. ferrugineus* overlapping response to L-homoserine lactone and acylhomoserine lactone……...……...…… 49

Figure 3.11. Extracted ion chromatograph of the oxidized products of HHQ from *C. ferrugineus* crude extracts……..…… 50

Figure 3.12. Comparison of MS/MS spectra of HHQ oxidized products from *C. ferrugineus* extract with the commercial standards. ……..……..... 118

Figure 3.13. MS/MS spectrum of PQS-NO from HHQ exposed *C. ferrugineus* extract…. 119

Figure 4.1. *C. ferrugineus* predation on *P. putida*…..……...….. 64

Figure 4.2. Subsequent predation assay on nutrient-free WAT agar medium.…….…... 65

Figure 4.3. Subsequent predation assay on nutrient-rich VY/2 agar medium…….. 67

Figure 4.4. Differentially expressed genes in survivor phenotype compared to parent *P. putida*…… 68

Figure 4.5. Pyoverdine production from survivor *P. putida*. ……...…… 72

Figure 4.6. Metabolic crude extract analysis of both phenotypes of *P. putida*. ……...…… 73

Figure 4.7. *P. putida* survivor phenotype produces higher quantities of alginate. …….. 75

Figure 4.8. *P. putida* survivor phenotype demonstrates resistance to aminoglycosides and tetracycline antibiotics……... 76

LIST OF TABLES

Table 1.1. Tested Gram-negative bacterial preys..……...……. 8

Table 1.2. Tested myxobacterial predators……... 10

Table 1.3. Tested Gram-positive bacterial preys……..…….……...…… 11

Table 1.4. Tested cyanobacterial preys…….....…...……..... 13

Table 1.5. Tested fungal preys...…….…...…...…… 16

Table 1.6. Prey bacteria exhibited avoidance to *M. xanthus* predation……...……. 18

Table 2.1. Similarity of tubulysin BGC proteins from *C. ferrugineus* with known BGC… 25

Table X Abbreviations of microorganisms…… 115

Table 3.1. Prey signaling molecules impact on myxobacterial genes included in biosynthetic gene clusters…….…...……..… 117

Chapter 1

Myxobacterial predatory dynamics with their preys

1.1. Abstract

Myxobacteria are Gram-negative Deltaproteobacteria that live in multicellular communities, exhibit gliding motility, and predate on other microorganisms. The bacteriolytic myxobacteria exhibit efficient and diverse predation strategies to lyse and digest the biomass of their prey. The prey range for myxobacteria is enormous and expands from Gram-negative and Gram-positive bacterial strains to photosynthetic cyanobacteria as well as fungi. The generalist predatory lifestyle lets myxobacteria prey on a wide variety of preys; however, lytic efficiencies vary significantly across predatory myxobacteria, and an individual myxobacterial strain exhibits variable predation rates and unique specificities to its preys. In addition to myxobacterial predatory capacities, specific characteristics associated with prey organisms contribute to myxobacterial predation efficiencies. Here, we have summarized myxobacterial specialized hunting strategies, their predation range, and prey features contributing to resistance to *Myxococcus xanthus* predation.

1.2. Myxobacteria

Myxobacteria are Gram-negative rod shaped bacteria that are ubiquitous and can be found in the soil, associated with tree bark, tree compost, animal dung, bogs, caves, as well as in the marine environments (1,2). *Myxococcales* is a monophyletic order in Deltaproteobacteria that contains myxobacteria and is further divided into three suborders; *Cystobacterineae*, *Sorangiineae*, and *Nannocystineae,* comprising ten families, 29 genera, and 58 species (3). All myxobacteria are specialized to degrade biomacromolecules and are categorized into two groups according to their nutritional needs. One group is cellulolytic myxobacteria, which includes *Sorangium* and *Byssovorax* genera from *Sorangiineae* and decomposes cellulose to obtain nutrients. The other group is predatory myxobacteria that can lyse and digest other microorganisms and acquire their macromolecules as nutrients (4,5).

The complex developmental cycle, biologically active natural products, and predatory lifestyle are characteristic features of these microbes (6–8). Myxobacterium *Myxococcus xanthus* **(Figure 1.1A-C)** is a model organism that has been extensively utilized to investigate myxobacterial physiology, motility, and predatory interactions (9,10). In a nutrient-rich environment, myxobacterial cells form multicellular communities, known as swarms, covered with a slimy extracellular matrix, and aggregate into mounds termed as fruiting bodies when starved **(Figure 1.1G-I)** (9,11). Within fruiting bodies, cells differentiate to form myxospores **(Figure 1.1I)** that are metabolically dormant and can withstand a prolonged period of starvation, desiccation, and harsh environmental conditions (8). Due to their multicellular life cycle and cooperativity, myxobacteria are known as social bacteria (10).

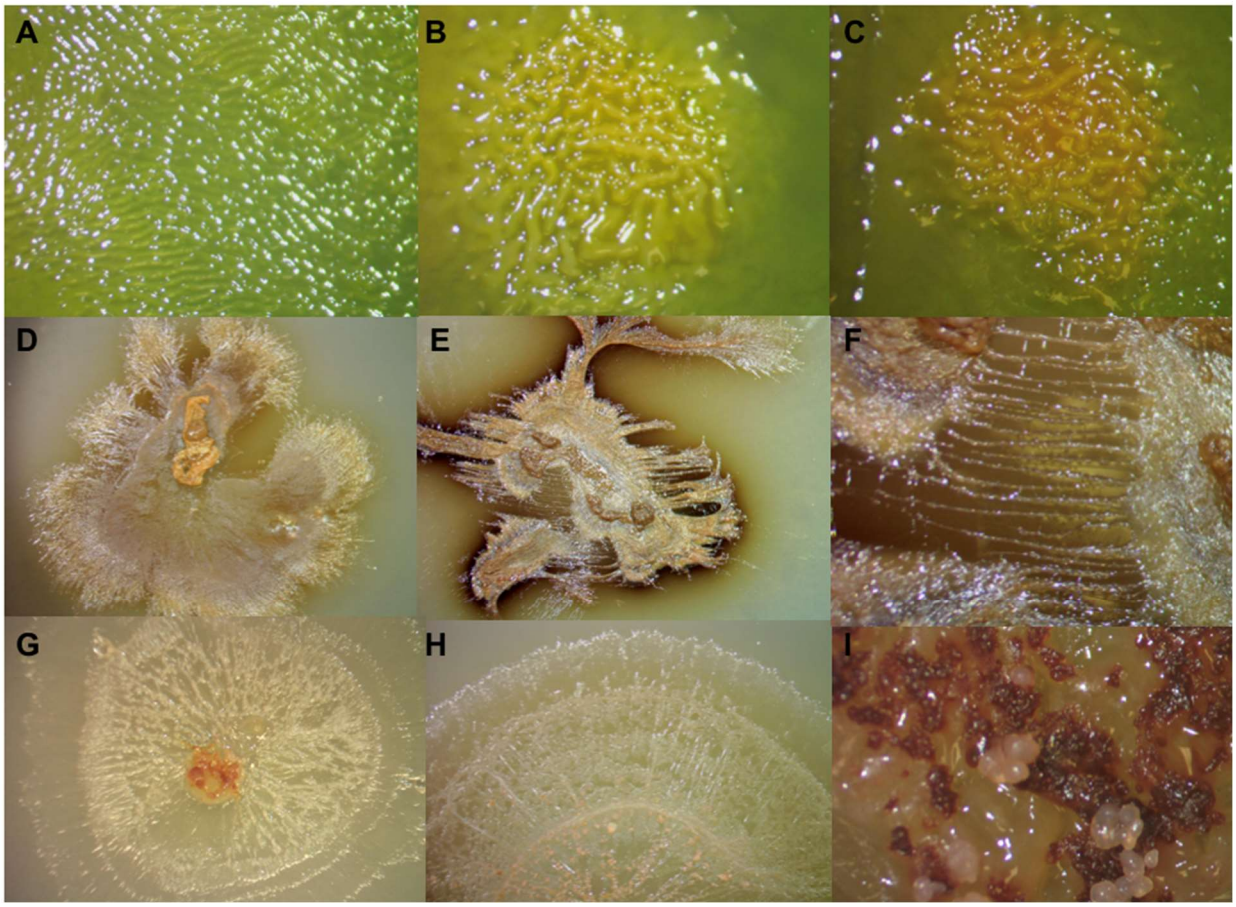

Figure 1.1. Predatory myxobacteria. *Myxococcus xanthus* (A) swarm, (B) early stage cells aggregate, (C) late stage cells aggregate, (D, E, F) *Archangium violaceum* swarm, *Cystobacter ferrugineus* (G) swarm, (H) swarm with fruiting bodies, (I) fruiting bodies with colored spores.

The motility of myxobacteria is another aspect of their complexity. Their coordinated movement also called swarming, allows them to spread over the solid surfaces. Myxobacteria are non-flagellated bacteria that utilize two different motility systems to glide over the surfaces (12,13). The social (S) motility is responsible for the movement of the cells in groups. This motility system is powered by the retraction of type IV pili present at the pole of *M. xanthus* cells. Retraction of pili is mediated by binding with the extracellular matrix, also known as fibrils (14,15). In addition to S-motility, *M. xanthus* individual cells from the swarm edges move independently by employing adventurous (A) motility. A-motility is powered by slime secretion

and periodic movement of fixed protein complexes, also known as focal adhesion complexes (16). The motility of *M. xanthus* is crucial to its developmental cycle; it plays roles in swarm spreading, aggregation and fruiting body formation, as well as predation. Both S- and A- motility systems are synergistic. The absence of one or both of these systems results in defects in cells aggregation and fruiting body formation (17).

The complexity of myxobacterial multicellular life cycle and motility is matched by their extraordinary genome size, reflecting their complex life cycle and its regulation at a genetic level (18). Compared to other bacteria, they have larger genomes with an average of 9-14 million base pairs and %GC content of 66-72% (18,19). A large portion of the myxobacterial genome is dedicated to the biosynthesis of natural products, also known as specialized metabolites (20). They produce compounds that belong to all major natural product classes such as polyketide, non-ribosomal peptides, terpenoids, phenylpropanoids, and alkaloids (21). Up till 2016, almost 110 distinct chemical scaffolds with diverse biological activities, including antimicrobial and anticancer activities, have been isolated from myxobacteria (7,21,22). The production of specialized metabolites has made myxobacteria a central focus of natural products research.

Although the specialized metabolism of myxobacteria is correlated with their predation (23–25), only two metabolites are identified so far that are utilized in the predation. Myxovirescin and myxoprincomide are the antibiotics that *M. xanthus* utilize during the predation of *Escherichia coli* and *Bacillus subtilis*, respectively (26,27). Except for these two metabolites from *M. xanthus*, there is no evidence of specialized metabolites involved in predation from the other myxobacteria. In fact, many genera of the isolated myxobacterial strain have been investigated for natural product discovery efforts (7,21,22); however, majorly the genera of *Myxococcus* and *Corallococcus* have been scrutinized for their predatory activities (28,29).

Different myxobacterial strains exhibit differential predatory activity against a single prey organism (29,30), even though being generalist predators, myxobacteria predate a diverse variety of microbes, including Gram-negative and Gram-positive strains of bacteria, human pathogens and plant pathogenic bacteria, cyanobacteria, and a variety of phytopathogenic fungi (2,29,31). Notably, a handful of prey bacteria evade *M. xanthus* predation by employing diverse resistance mechanisms (32–36). The observations of differential predation among the myxobacteria and the employment of particular specialized metabolites against a distinct prey emphasize the importance of investigating the predatory interactions of each isolated myxobacterial strain thoroughly. Similarly, to unravel potential other prey species and their employed mechanisms to avoid myxobacterial predation, scrutinizing additional myxobacteria in pairing with different prey would be important. In an effort to present currently utilized myxobacteria and their prey in a predator-prey dynamic, here we have summarized myxobacterial hunting strategies, the prey range, and prey defenses against myxobacterial predation.

1.3. Predation strategies

Bacteriolytic myxobacteria hunt in swarms and demonstrate wolf pack predation. Employing gliding motility, a group of myxobacterial cells invades and surrounds prey and lyse prey biomass by secreting a cocktail of lytic enzymes and antimicrobial substances (6,24). They exhibit contact-dependent predation, which means direct contact with prey is essential for successful predation (37–39). Although a certain quorum and cooperativity among myxobacterial cells are required for efficient predation (40–42), a single *M. xanthus* cell can successfully lyse cells of Gram-negative and Gram-positive prey bacteria (37,38).

Although wolf packing is the primary predation strategy of myxobacteria, their swarm, as suggested by Pérez et al., displays different predatory patterns during predation (43). These patterns include a frontal attack and an attack involving myxobacterial swarm moving along the periphery of the prey. Throughout the frontal attack, myxobacterial swarms exhibit a direct invasion in the prey colony along with moving forward around the prey colony edges **(Figure 1.2 A&B).** This frontal attack is employed for denser prey colonies (35). In circumstances when myxobacteria cannot lyse prey due to underlying predation avoidance mechanisms, cells in the swarm move alongside the prey colony and fully surround it **(Figure 1.2 C)** (35). Other than different attacking techniques, myxobacteria utilize efficient tactics to digest the biomass of their prey effectively. One such strategy is myxobacterial rippling behavior. During their development, myxobacterial cells exhibit collective, coordinated motility in self-organized bands of traveling alternating-density waves known as rippling **(Figure 1.2 D)** (44,45). Rippling has been suggested as a predatory behavior in *M. xanthus*, as its induction requires extracellular peptidoglycan or the presence of prey cells (46). Rippling results in an increased rate of *M. xanthus* spreading over prey. It allows *M. xanthus* to stay longer on prey and efficiently consume non-diffusible molecules from the lysed prey (45).

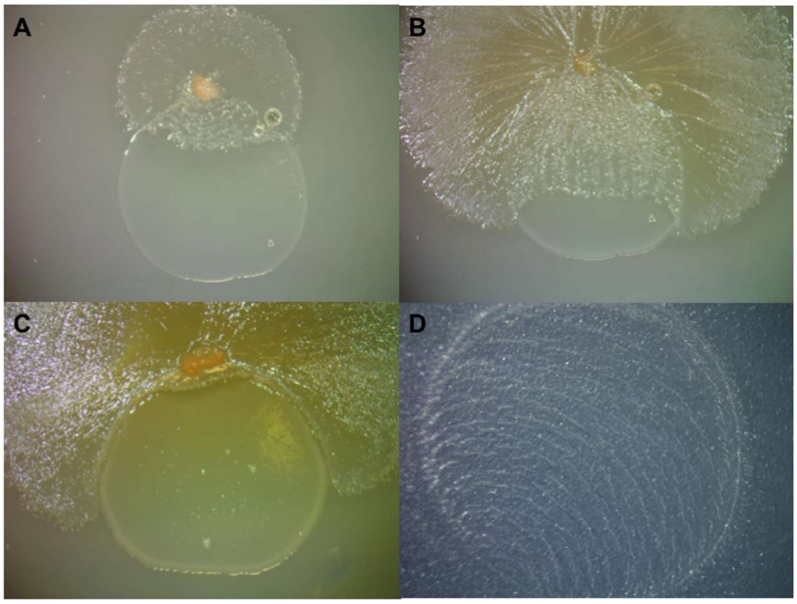

Figure 1.2. Myxobacterial predation strategies. (A) the frontal attack, (B) swarming around the prey along with frontal attack, (C) swarming along the prey colony border, (D) rippling.

Different strategies that myxobacteria utilize to predate on their prey on solid surfaces are well-understood; however, little is known about myxobacterial predation in aquatic environments. Even though there is an increase in marine myxobacterial isolates (1), only two studies demonstrating myxobacterial predation in the liquid media are currently available. Just like the solid media, in the aqueous media, predation of *M. xanthus* PCO2 on a cyanobacterium *Phormidium luridum* (47) and *M. xanthus* DK1632 on *E. coli* (39) is contact-dependent. Planktonic *M. xanthus* cells co-aggregate and flocculate with its cyanobacterial as well as *E. coli* prey cells and ultimately lyse the entrapped prey (39,40). Overall, myxobacteria display very effective predation strategies due to their multicellular lifestyle and motility, which allow them to move over prey cells, and by employing lytic enzymes and antibiotic factories, they lyse and digest biomass of their prey efficiently.

1.4. Predation range of myxobacteria

1.4.1. Predation on Gram-negative bacteria

Broadly considered generalist predators, myxobacteria display a more predatory inclination towards Gram-negative prey over Gram-positive bacterial strains (29,48–51) and demonstrate predation on a variety of Gram-negative bacteria **(Table 1.1)**. Rhizosphere bacterial networks in the greenhouse mesocosm reveal most of the myxobacteria link with Gram-negative bacteria (51). The members of *Cystobacteraceae*, in particular, exhibit rapid assimilation of Gram-negative *Pseudomonas putida* biomass compared to Gram-positive *Agrobacter globiformis* in a soil microcosm experiment (50). The myxobacterium *M. xanthus*, the most thoroughly studied member of the *Myxococcales*, displays rapid predation on Gram-negative *E. coli* compared to Gram-positive *Micrococcus luteus* (48).

E. coli, due to the rapid assimilation of its biomass by myxobacteria is a commonly employed prey to study myxobacterial predatory characteristics (6,48,52). In addition to ecological and evolutionary aspects of myxobacteria, several of their developmental phenomena involving predation have been examined in a predator-prey interaction of *M. xanthus* and *E.coli* (6,9,48,52–54). The constitutive toxicity of *M. xanthus* in the presence of *E. coli* prey contributes to its characteristics as a generalist predator (53). Additionally, the evolutionary adaptation of *M. xanthus* in the form of "an enhanced searching rate" for low density prey (55) and co-evolution of the genome of *M. xanthus* and its prey are evaluated with *E. coli* (54). Although cell aggregation and fruiting body formation are an essential part of *M. xanthus* developmental cycle under starving conditions (9,11), *M. xanthus* forms well-organized fruiting bodies upon the loss of prey availability when co-cultured with *E. coli* prey (56). Finally, the *E. coli* baiting method is one of the employed methods for isolating myxobacteria from soils as well as marine environmental samples (57–60). In fact, some marine myxobacteria lyse *E. coli* efficiently, and it is interesting to note that these marine myxobacterial isolates of *Nannocystis exedens* DSM 71Ta, *Enhygromyxa salina* DSM 15217Tc, and *Enhygromyxa* sp. show significantly less lysis of yeast cells (58,60). In addition to predation on *E. coli* prey, the myxobacterium *M. xanthus* effectively predates several

Table 1.1. Tested Gram-negative bacterial prey

Prey	Refences
Escherichia coli	(38,39,45,48,52-56)
Escherichia freundii	(62)
Enterococcus faecalis	(30)
Klebsiella pneumoniae	(30,64)
Mycobacterium phlei	(63)
Pectobacterium carotovorum subsp. *carotovorum*	(61)
*Proteus X*19	(63)
Proteus mirabilis	(30,64)
Pseudomonas aeruginosa	(30,64,98)
Pseudomonas mildenbergii	(62)
Pseudomonas putida	(50,62)
Pseudomonas syringae pv. *alisalensis*	(61)
Rhizobium vitis	(29)
Salmonella paratyphosa	(63)
Salmonella typhosa	(63)
Salmonella typhosa Vi-I	(63)
Salmonella typhosa H-901	(63)
Salmonella typhosa O-901	(63)
Serratia marcescens	(61)
Shigella dysenteriae Shiga	(63)
Shigella paradysenteriae Flexner	(63)
Shigella sonnei	(63)
Sinorhizobium meliloti	(32,35)
Sphingomonas suberifaciens	(61)
Vibrio cholerae Ogawa 49514	(63)
Vibrio cholerae Rough 49515	(63)
Xanthomonas campestris pv. *vitians*	(61)
Xanthomonas fragariae	(29)

other Gram-negative prey bacteria. The human pathogenic *Serratia marcescen* is susceptible to *M. xanthus* lysis (61). Although with the variability in rates, *M. xanthus* also prey efficiently on plant pathogens, including *Xanthomonas campestris* pv. *vitians, Pectobacterium carotovorum* subsp. *carotovorum, Pseudomonas syringae* pv. *alisalensis, Sphingomonas suberifaciens* (61).

While *M. xanthus* is the most commonly used myxobacterium to investigate the predatory lifestyle of myxobacteria, representatives from *Myxococcaceae* (62) and other myxobacterial genera have also been utilized as predators to study myxobacterial predation **(Table 1.2)**. Among these, many show similarities in the lytic spectrum against a prey species. Pure cultures of myxobacteria *Myxococcus virescens* and *Myxococcus fulvus* show preferential predation on living cells of *P. putida* compared to *Escherichia freundii* and *Pseudomonas mildenbergii* (62). Both myxobacteria also exhibit overlapping lytic activity for human pathogens *Salmonella typhosa H*-901, *Proteus X*19, and *Salmonella paratyphosa*, and lyse them completely. Whereas both *M. virescens and M. fulvus* only partially lyse *Shigella dysenteriae* Shiga, and *S. typhosa O*-901, and none can lyse *Mycobaderium phlei* (63). Natural isolates of *Corallococcus* spp., *Pyxidicoccus* spp., *Myxococcus macrosporus, M. xanthus, and M. virescens* have also demonstrated activity against the clinically relevant human pathogens. The mean predatory activity of these myxobacteria is highest on *Klebsiella pneumoniae* and moderate on *Proteus mirabilis,* and *Enterococcus faecalis*. Simultaneously, these myxobacterial isolates show limited lytic activity on *Pseudomonas aeruginosa* (30). Singh also noticed complete lysis of several living phytopathogenic bacteria by *M. virescens, M. fulvus,* and *Corallococcus exiguus* (49).

Along with similarity in predatory activity, lytic efficiencies vary significantly across predatory myxobacteria. The lytic activity of *C. exiguus* against Gram-negative bacteria is comparatively lower than *M. virescens* and *M. fulvus* (49). However, the predatory activity of *C.*

exiguus DSM 14696^T outweighs the predation of several *Corallococcus* species (64). In fact, it is able to efficiently prey on *P. aeruginosa, K. pneumoniae,* and *P. mirabilis*, and its predatory activity on these prey bacteria is higher compared to other *Corallococcus* species (64). Similarly, *Myxococcus flavescens, M. macrosporus*, *M. virescens,* and seventeen strains of *M. xanthus* exhibit differential predation of Gram-negative prey from different classes of proteobacteria (29). While *M. virescens* completely lysed human pathogens *Shigella sonnei, Shigella paradysenteriae* Flexner, *Vibrio cholerae* Ogawa 49514, *S. typhosa,* and *S. typhosa* Vi-*I* with variability in rate, *M. fulvus* can lyse these pathogens only partially. *M. fulvus,* on the other hand, completely lysed *V. cholerae* Rough 49515, and *M. virescens* lysed it partially (63). Likewise, the susceptibility of plant pathogenic *Rhizobium vitis* and *Xanthomonas fragariae* to the predation of *M. flavescens, M. virescens,* and *M. macrosporus,* and several strains of *M. xanthus* is variable. Even though these myxobacteria capably swarm both phytopathogens, their swarming is comparatively better on *R. vitis* (29). Overall, myxobacteria competently predate Gram-negative bacteria, except for a few human pathogens; most tested pathogenic bacteria are susceptible to myxobacterial predation, albeit with variable rates and unique specificities to the predators.

Table 1.2. Tested myxobacterial predators

Myxobacterial predators	References
Myxococcus flavescens	(29,92)
*Myxococcus fulvus**	(40,49,62,63,65,79,80,92,93)
Myxococcus macrosporus	(29,30,73)
Myxococcus stipitatus	(73,92)
Myxococcus spp., KYC 1126, KYC 1136, and KYC 2001	(87)
*Myxococcus virescens**	(29,30,49,62,63,65,66,73,92, 93)
*Myxococcus xanthus**	(26,27,29,30-39,46-48,52-56,63,70,73,79,92)
Myxobacter strain 8	(41)
Corallococcus coralloides	(93)
*Corallococcus exiguus**	(49,64,93)
Corallococcus sp. EGB	(95,96)
Corallococcus spp.*	(28,30,64)
Chondrococcus coralloides	(65)
Pyxidicoccus caerfyrddinensis	(73)
Pyxidicoccus fallax type strain DSM 14698^T	(73)
Pyxidicoccus spp.	(30)
Pyxidicoccus trucidator	(73)
Polyangium fumosum	(93)
Polyangium parasiticum	(81)
Archangium gephyra	(93)
Jahnia thaxteri	(93)
Enhygromyxa salina DSM 15217Tc	(58)
Enhygromyxa sp.	(60)
Nannocystis exedens DSM71Ta	(58)

* Multiple strains of these myxobacteria have been tested for the predatory activity.

1.4.2. Predation on Gram-positive bacteria

Even though Gram-negative bacterial prey support myxobacterial growth more effectively (29,48–51), efficient myxobacterial predation against Gram-positive prey bacteria has also been observed (29,37) **(Table 1.3)**. *M. virescens* and *Chondrococcus coralloides* exhibit lytic activity on Gram-positive *Aerobacter aerogenes, Aerobacter* sp., and *B. subtilis* (65). The well-known antibiotic producers Gram-positive *Streptomyces* (66–69) are also susceptible to myxobacterial predation (70). *M. xanthus* cells cause intense lysis of hyphae of *Streptomyces coelicolor* upon entering its colony in co-culture experiments. The number of *S. coelicolor* colonies after co-culturing w ith *M. xanthus* in a liquid culture are fewer than *S. coelicolor* colonies observed when not co-cultured with *M. xanthus* (70). Although *S. coelicolor* produces pigmented antibiotic actinorhodin, *M. xanthus*, due to its production of myxochelin - an iron siderophore, dominates this interaction. Interestingly, myxochelin alone, even without physical contact between these two bacterial species, results in actinorhodin production in *S. coelicolor* (71).

Table 1.3. Tested Gram-positive bacterial prey

Prey	References
Aerobacter aerogenes	(65)
Aerobacter sp.	(65)
Agrobacter globiformis	(50)
Bacillus subtilis	(26,34,64,65,105)
Clavibacter nebraskensis DSM 7483	(73)
Micrococcus luteus	(29,41,48,72)
Staphylococcus aureus	(30,63,64)
Staphylococcus epidermidis	(64)
Staphylococcu saprophyticus	(30,64)
Streptomyces coelicolor	(70)

Notably, some myxobacteria display a predatory preference for Gram-positive bacteria over Gram-negative bacterial prey. The genus *Haliangium*, in particular, assimilates comparatively more biomass of Gram-positive *A. globiformis* than Gram-negative *P. putida* in a soil microcosm experiment (50). Likewise, in a greenhouse mesocosm experiment, some of *Haliangiacea* and *Polyangiaceae* interact with actinomycetes and actinomycetes-like Gram-positive bacteria in rhizosphere bacterial networks (51). In addition to *Haliangiaceae*, a few

members of *Myxococcaceae* show their predatory attraction for Gram-positive bacterial prey. For example, germination of myxospores of *Myxobacter* strain 8 is only observable in the presence of *M. luteus,* whereas its germination is not observed with *E. coli* (41,72). Although it is more due to characteristic of media condition, *M. xanthus* displays efficient predation on high density prey patches of *M. luteus* compared to *E. coli* on soft agar (48). For the genus *Pyxidicoccus*, a relatively more predatory inclination for Gram-positive bacteria is observed. Two out of three species of *Pyxidicoccus* show higher average predatory activity on Gram-positive *C. nebraskensis* DSM 7483 compared to Gram-negative *E. coli* or the fungus *Ustilago maydis* DSM 14603 (73). In addition to *Pyxidicoccus*, some species of *Coralococcus* grow particularly well in the presence of *B. subtilis* instead of their Gram-negative prey (64).

Like variability in the predation of Gram-negative prey, varying predation capacities of myxobacteria are also observed for their Gram-positive bacterial prey. For instance, *C. exiguus* DSM 14696^{T} is able to efficiently prey on Gram-positive *Staphylococcus aureus*, *Staphylococcus* epidermidis, and *Staphylococcus saprophyticus* (64). On the other hand, natural isolates of *Corallococcus* spp., *Pyxidicoccus* spp., *M. macrosporus, M. xanthus, and M. virescens* show limited lytic activity on *S. aureus, S. saprophyticus* (30). *M. virescens and M. fulvus* also only partially lyse *S. aureus* (63). Moreover, from among a panel of myxobacteria that also included *M. flavescens,* and *M. virescens,* and several different strains of *M. xanthus*, only *M. macrosporus* exhibit the largest swarm expansion on *M. luteus* prey lawn (29). Similarly, *M. fulvus*, *Myxococcus stipitatus*, and *M. macrosporus* exhibit higher average predation on Gram-positive *Clavibacter nebraskensis* DSM 7483 when compared to *M. xanthus* and *M. virescens* (73). Compared to *Pyxidicoccus trucidator, Pyxidicoccus fallax* type strain DSM 14698^{T} and *Pyxidicoccus caerfyrddinensis* show higher average predatory activity on *C. nebraskensis* DSM 7483 (73).

Collectively, like their Gram-negative bacterial prey, myxobacteria can efficiently predate Gram-positive bacterial strains, and different myxobacterial predators demonstrate differential predation rate and variability in the specificity of their Gram-positive bacterial prey.

1.4.3. Predation on cyanobacteria

Photoautotrophic cyanobacteria, also known as blue-green algae, are eubacteria found in aquatic and terrestrial environments (74,75). *Lysobacter* was mistaken for myxobacteriales for cyanobacterial and algal predation in some early studies due to gliding motility-like features shared with myxobacteria (76–78); however, there are numerous observations of true myxobacterial predation of cyanobacteria **(Table 1.4)**. *M. xanthus* PCO2, for instance, can survive in the presence of prey cyanobacterium *P. luridum* as a sole food source. in a liquid media, its colonial aggregates and floccules with the prey cyanobacterium are observable with scanning electron micrographs (47). *M. fulvus* can also lyse *Nostoc muscorum* in a cell density dependent manner. It can only lyse *Nostoc muscorum* when the initial inoculum of *M. fulvus* is more than 5 x 10^6 cells per ml in inorganic media (40). Notably, this might be a fair illustration of a possible mechanism that marine myxobacteria utilize during predation in aquatic environments.

Table 1.4. Tested cyanobacterial prey

Prey	References
Nostoc muscorum	(40)
Phormidium luridum	(47,79)

Consistent with Gram-negative and Gram-positive bacterial prey, the lytic capabilities for cyanobacterial predation vary among different myxobacterial strains. Compared to *M. xanthus* BG03 and *M. xanthus* PCO2, myxobacterium *M. fulvus* BG02 depicts the maximum lysis of *P. luridum* (79). The variation in the predatory performance of a single predator can also vary for different cyanobacteria (80). *M. fulvus* (S-l-8) shows differential lytic activity for several cyanobacteria. It can lyse *Anabaena solitaria* within 15 min and lyse *Anacystis affinis, Anacystis*

circinalis, P. luridum, Microcystis viridis, and *Anacystis cylindrica* overnight. At the same time, *Anacystis nidulans, Microcystis aeruginosa* (N-11) & (NIES-99), *Microcystis flos-aquae, Microcystis elabens* undergo lysis within two days (80). However, quite surprisingly, *M. fulvus* (S-l-8) cannot lyse *E. coli, B. subtilis,* or *S. cerevisiae*. In contrast, generally myxobacteria lyse these prey quite efficiently (80), which poses a concern that the observed lytic predator from this study (80) may have been incorrectly identified as a myxobacterium at the time of the study. In addition to cyanobacteria, myxobacterial predation to cyanobacterial close eukaryotic algal neighbor is also observed, however only in one study. The study demonstrates a myxobacterium *Polyangium parasiticum* to be parasitic towards a green alga, *Cladophora*. It is able to lyse and puncture holes in the cell wall of *Cladophora* and forms fruiting bodies inside and on the surface of algal filament (81).

Like myxobacteria, cyanobacteria are abundantly present in the soil (74,82,83), and like cyanobacteria myxobacteria have also been found in the aquatic environment (1,74,84,85). It is interesting to note that quite a few studies describing interactions between cyanobacteria and myxobacteria are available. Nevertheless, the available studies depict common features associated with myxobacterial predation, such as requiring a certain initial inoculum for the successful predation (40) and differential predatory efficiencies for different cyanobacteria (80). Notably, contrary to other bacterial prey, there is only one study that presents the production of lysin, a lytic enzyme, by a myxobacterium in the presence of a blue-green alga – *Lyngbya* sp., (86). Further studies describing the interaction between these two phyla can unravel many exciting research findings regarding bacterial chemical ecology.

1.4.4. Predation on fungi

The broad predatory range of myxobacteria also includes fungal prey. Extracts of *Sorangium cellulosum* KYC 3270, a cellulolytic myxobacterium, has antifungal activity against gray mold, anthracnose fungus, *Batrytis cinerea,* and *Colletotrichum acutatum* (87,88). Similar to extracts from cellulolytic myxobacteria (89), predatory myxobacterial extracts are active against fungal phytopathogens (87). Besides cellular extracts, predatory myxobacteria depict antagonistic interactions with fungi. Perforations in the cell wall of plant pathogenic *Rhizoctonia solani* hyphae and *Cochliobolus miyabeanus* conidia have been observed when co-cultured with myxobacterial isolates that belong to the genus *Polyangium* (90), and *Myxococcus* spp., KYC 1126, KYC 1136, and KYC 2001 repress the mycelial growth of *Phytophthora capsica* (87). Although not a pathogen, the cell components of *Saccharomyces cerevisiae* support myxobacterial growth (91), and to date, Baker's yeast is a component of VY/2 growth medium (www.dsmz.de/microorganisms/medium/pdf/DSMZ_Medium9) for many myxobacteria. Even though genus *Sorangium* is not known for fungal lytic activity, two of its members exhibit lysis of the plant fungal pathogens, *Pythium intermedium, R. solani, Fusarium oxysporum, and Fusarium solani* (89). However, the lytic activity suggests that these myxobacteria possibly were miss-identified as genus *Sorangium*.

Like bacterial prey, myxobacterial differential predatory efficiency is observable for fungal prey **(Table 1.5)**. Myxobacterial isolates from the strawberry rhizosphere exhibit different inhibitory activity against plant fungal pathogens. In particular, the lytic activity of isolated *Myxococcus coralloides* outweighs the lytic activity of other co-isolated myxobacteria. When co-cultured, it completely inhibits the growth of phytopathogenic fungi that comprise *Phytophthora capsica*, *Pythium ultimum*, *Rhizoctonia* spp., *Verticillium dahlia, Verticillium albo-*

atrum, *Cylindrocarpon* spp., *Fusarium oxysporum* f. sp. *apii,* and two fungal biological control agents, including *Gliocladium virens* and *Trichoderma viride*. Whereas, *Sclerotinia minor* is a fungus that *M. coralloides* does not entirely inhibit. On the other hand, inhibition of *S. minor* is observed when co-cultured with *M. flavescens*, *M. fulvus*, *Myxococcus stipitatus*, *M. virescens*, *M. xanthus* strain K, and strain L myxobacterial isolates. Notably, none of these isolates could inhibit *V. dahlia, V. albo-atrum*, *C.* spp., and *F. oxysporum* f. sp. (92). Additionally, some myxobacterial inhabitants of the acidic soil comprising *M. virescens, M. fulvus, C. exiguus, Corallococcus coralloides, Archangium gephyra, Polyangium fumosum,* and *Jahnia thaxteri* also display fungal inhibitory activity. Strains of the species *M. virescens* from pine tree soil and *C. exiguus* from birch and oak tree soil, in particular, show the most substantial antagonism to fungal pathogens of pine seedlings, including *R. solani, F. oxysporum*, *Fusarium culmorum,* and *Cylindrocarpon destructans* (93). *C. destructans* appeared to be most sensitive among these fungal pathogens, and *F. culmorum* is the most resistant pathogen. In addition to standard *in-vitro* inhibition of fungal pathogens, strains of *M. virescens* and *C. exiguus* also protect the roots of pine seedlings, *Pinus sylvestris*, against the *R. solani* (93). Besides co-culture antagonism from *C. exiguus,* the crude extracts of two *C. exiguus* isolates from karst limestone and soil in Indonesia also suppress the growth of *Fusarium odoratissimum,* a fungal pathogen of banana plants (94). Myxobacteria isolated from saline soil are also inhibitory towards

Table 1.5. Tested fungal prey

Prey	References
Cochliobolus miyabeanus	(90)
Cylindrocarpon destructans	(93)
Cylindrocarpon spp.	(92)
Fusarium culmorum	(93)
Fusarium odoratissimum	(94)
Fusarium oxysporum	(89,93,95)
Fusarium oxysporum f. sp. *apii*	(92)
Fusarium solani	(89)
Gliocladium virens	(92)
Phytophthora capsica	(87,92)
Pythium intermedium	(89)
Pythium ultimum	(92)
Rhizoctonia solani	(89,90,93)
Rhizoctonia spp.	(92)
Saccharomyces cerevisiae	(91)
Sclerotinia minor	(92)
Trichoderma viride	(92)
Ustilaginoidea virens	(95)
Verticillium albo-atrum	(92)
Verticillium dahlia	(92,95)

phytopathogenic fungi. Among them, *Corallococcus* sp. EGB is a promising antifungal biocontrol agent as it exhibits excellent inhibitory activity against fungal pathogens *F. oxysporum*, *V. dahlia,* and *Ustilaginoidea virens.* It exhibits excellent biocontrol efficiency against *Fusarium* wilt of cucumber (95,96). Additionally, a glycoside hydrolase, β-1,6-glucanase, from *Corallococcus* sp. strain EGB efficiently decomposes *Magnaporthe oryzae* fungus and prevents rice plant from the fungal infection (97). Taken together, myxobacteria isolated from diverse soil habitats display fungal lytic activities, and similar to the bacterial lysis, some myxobacterial strains demonstrate more efficient lysis of a specific fungal species.

1.5. Prey avoiding myxobacterial predator

These predator-prey dynamics are crucial to the regulation of soil microbial biodiversity, myxobacterial predators predate a range of prey microorganisms with varying predation efficiencies (29,31). Where the predatory efficiency is characteristic of a predator itself (98), certain characteristics associated with prey organisms also contribute to their differential susceptibility to myxobacterial predation (32–35,70). The prey organisms respond to myxobacterial presence. For instance, pathogenic *S. minor* fungus produce sclerotium, a persistent fungal resting structure (99), only in the absence of myxobacteria, and its sclerotium is not observable in the presence of predatory myxobacteria (92). Some bacterial species also respond to myxobacterial predation by employing diverse mechanisms and elude *M. xanthus* predation **(Table 1.6)** (32-35,70,105). Even though examples of predatory avoidance are a few, it is interesting to note that each observed interaction employs a distinct mechanism to avoid *M. xanthus*.

1.5.1. Prey specialized metabolites involved in predation avoidance

Although many soil-borne bacteria produce specialized metabolites (67,68,100), the role of specialized metabolites in protection from microbial predation has only recently been reported (34,70,92). It is observed that soil-dwelling pigmented bacterial strains are generally resistant to myxobacterial predation compared to non-pigmented strains (49). Antibiotic actinorhodin (ACT) production protects Gram-positive *S. coelicolor* from *M. xanthus* predation (70). The enhanced production of myxochelin, a siderophore for iron quenching from *M. xanthus,* triggers ACT production in *S. coelicolor* that protects *S. coelicolor* from *M. xanthus* (71). Bacillaene, another specialized antibacterial metabolite produced by Gram-positive prey *B. subtilis* (101) has been associated with avoidance of *M. xanthus* predation. Besides its inhibitory effect, bacillaene provides sufficient time for the *B. subtilis* cells to develop into mature spores, enabling *B. subtilis* to escape predation (34). Notably, purified bacillaene also results in limited predation of the otherwise sensitive *E. coli* cells (34). Like Gram-positive bacteria, antibiotics from Gram-negative bacterial prey also contribute to their protection from predation. For example, phenazines antibiotic produced by a rhizobial bacterium *Pseudomonas aureofaciens* 30-84 has been reported to protect it from myxobacteria. Phenazine protects *P. aureofaciens* 30-84 from *M. stipitatus*, *M. xanthus* L, and *M. fulvus*. On the contrary, an isogenic mutant of strain 30-84, *P. aureofaciens* 30-84Z, does not produce phenazine and undergoes comparatively better lysis by *M. stipitatus and M. fulvus* (92). Similarly, the specialized metabolites 2,4-diacetyl-phloroglucinol, pyoluteorin, and pyrrolnitrin are produced by

Table 1.6: Prey bacteria exhibited avoidance to *M. xanthus* predation

Prey	Involved mechanism	References
*Escherichia coli**	Surface curli matrix	(33)
*Sinorhizobium meliloti**	Galactoglucan & Melanin	(32,35)
Bacillus subtilis[#]	Bacillaene & spore filled megastructures	(34,105)
Bacillus licheniformis[#]	Oxidation of myxovirescin of *M. xanthus*	(36)
Streptomyces coelicolor[#]	Actinorhodin production	(70,71)

* Gram-negative bacteria, #Gram-positive bacteria.

Pseudomonas fluorescens strains CHA0 and Pf-5. The regulatory element of these metabolites, *gacS*, is involved in inhibiting myxobacterial growth and protecting the strain CHA0 from *M. stipitatus*, *M. xanthus* L, and *M. fulvus* predation. Interestingly, a *gacS* mutant strain of *P. fluorescens* does not produce above mentioned specialized metabolites and undergoes lysis by the same myxobacteria. However, it is not evident yet which molecule, in particular, is involved in predation avoidance (92). Besides myxobacteria, eukaryotic predators in the soil also preferably predate *gacS* mutant of *P. fluorescens* (102), further emphasizing the significance of specialized metabolites under GacS control in combating predators.

1.5.2. Non-antibacterial substances involved in predation avoidance

To resist predation, in addition to antibacterial small molecules, some prey bacteria utilize molecules with no apparent antibacterial activity (32,98). For instance, *Sinorhizobium meliloti* produces antioxidant pigment melanin in the presence of copper. Melanin polymer accumulates at the predator-prey interface and contributing a defensive role during the predatory interaction of *S. meliloti* with *M. xanthus* (32). Similarly, *P. aeruginosa* is known to secrete toxic formaldehyde that might protect *P. aeruginosa* from the predatory myxobacteria lacking formaldehyde detoxifying enzyme (98). In addition to secreted molecules, different matrix components of the prey bacteria offer various levels of resistance against myxobacterial predators (33,35). The dense curli protein matrix present at the surface of *E. coli* (103) protects *E. coli* from *M. xanthus* predation (33). Wild type *E. coli* survives *M. xanthus* predation, whereas a mutant deficient in curli fiber formation could not avoid predation (33). Similarly, galactoglucan, a linear heteropolysaccharide consisting of glucose and galactose disaccharide subunits, contributes to the mucoidy appearance of *S. meliloti* (104) and protect it from *M. xanthus* predation (35).

1.5.3. Other predation avoidance mechanisms

Other than chemical defense, prey structural components protect them from the *M. xanthus* predation. Stress-resistant spore filled megastructures of *B. subtilis* are inherently resistant to predation by *M. xanthus* (105). *B. subtilis* produces these megastructures as a response to predatory stress, and their formation is independent of the production of bacillaene, which also protects *B. subtilis* from *M. xanthus*. In fact, the mutant *B. subtilis* cells that cannot produce bacillaene produce megastructures more rapidly than normal cells, ensuring the long-term survival of these cells via sporulation within the megastructure (105). It is evident that myxobacteria utilize specialized metabolites in the killing of prey during predation. Myxovirescin and myxoprincomide are two antibiotics that *M. xanthus* utilizes during predation of *E. coli* and *B. subtilis*, respectively (26,27,106). Myxovirescin is a macrocyclic polyketide with antibacterial activity against Gram-negative and some Gram-positive bacteria (22,107). Some strains of prey *Bacillus licheniformis* deactivates myxovirescin (36). *B. licheniformis* deactivates myxovirescin by glucosylation, and this glycosylation prevents the prey *B. licheniformis* from *M. xanthus* DK1622 predation (36). It is worth noticing that each prey has mechanisms unique to it to resist the predation, and emphasizes the importance of understanding mechanisms involving predation avoidance at the individual prey level.

1.6. Concluding remarks

Since the first observation of myxobacterial lytic activity (108), several features associated with myxobacterial predation have been investigated (6,9,48,52–54). Extensive work has identified the lytic enzymes involved in the lysis of the prey (6,24,37,49), possibly involved small molecules (26,27,106), the predatory strategies (24,37–39), and their prey range (29,31,37). Most of the predatory interactions of myxobacteria are observed for *Myxococcus* and *Coralococcus*

species. This might be because these two genera are among the most abundant culturable isolates of myxobacteria (28,57). However, metagenomic and 16 S rRNA analysis depict that genera of *Sorangiineae*, *Nannocystineae, Haliangiaceae, and Polyangiaceae* are abundant in soil (51,109,110). The variability in the prey sensitivity even to the different strains of a single myxobacterial species is well observed (29). This predation selectivity among myxobacterial predators is also recognizable at the genomic level (98). The overlapping genes associated with the predatory activity as well as genes possibly exclusive to the predation for an individual prey are present in myxobacterial genomes (98). The uniqueness of the accessory pan-genomes of myxobacterial strains from a single genus (28) results in this variability in the predatory activity against specific prey by phylogenetically similar myxobacteria (30). This varying predation capacities of myxobacteria (30,31) and the presence of genes unique to a predator for a specific prey (28,37) emphasize the importance of the utility of additional myxobacterial strains from unique or less utilized genera to investigate predatory range.

For this, new strategies to isolate and culture myxobacteria would be needed. The utility of diverse prey organisms (111) and clinically relevant pathogens instead of widely employed *E. coli* baiting method (57–60) might lead to the isolation of unique myxobacterial strains able to lyse the pathogens competently. Additionally, since the prey characteristics play an essential role in predatory interactions with myxobacteria as observed from the prey organisms' employed mechanisms to avoid predation (32–36,70,105), additional prey species should be tested to decipher the other unknown predation avoidance mechanisms. More precisely, the predator-prey dynamic of myxobacterial strains from less utilized myxobacterial genera and additional prey species would provide the possibility to recognize a greater number of specialists myxobacterial predators, competent to prey on both the human and the plant infectious microorganisms.

Chapter 2

Draft genome sequence and metabolic potential of myxobacterium *Cystobacter ferrugineus*

2.1. Abstract

Myxobacteria are a relatively underexplored source of natural products when compared to actinobacteria. In an effort to explore myxobacterial natural product biosynthetic potential, the draft genome sequence of *Cystobacter ferrugineus* strain Cbfe23 has been obtained. Analysis of the genome using antiSMASH suggests the presence of a multitude of unique natural product biosynthetic pathways including a biosynthetic pathway responsible for the production of cytotoxic natural product, tubulysin. Metabolomic investigation of *C. ferrugineus* using untargeted mass spectrometry confirms the presence of tubulysin A and other tubulysin analogs in the crude organic extracts of *C. ferrugineus*. This study highlights the tremendous metabolic potential of myxobacteria and the significance of advancing the use of genomics and metabolomics bioinformatics tools to discover natural products.

2.2. Introduction

Myxobacteria are a prolific source of natural products with prominent biological activities (1,7,112). The genus *Cystobacter,* in particular, has been shown to produce a variety of structurally diverse bioactive molecules (7), including cystobactamid (113), althiomycin(114), macyranones (115), and cystochromones (116). Since the sequencing of the first bacterial genome in 1995 (117), a vast number of bacterial genomes have been sequenced and contributed to the discovery of biologically active small molecules (118–125). Like other bacteria, access to myxobacterial sequenced genomes has increased due to the low cost of genome sequencing (126). With accessibility to the sequenced genomes, the development of bioinformatics tools has revolutionized the identification of biosynthetic potential of the sequenced genomes (118,127,128). Among the bioinformatic tools capable of predicting biosynthetic potential in the bacterial genomes, antibiotics and secondary metabolite analysis shell – antiSMASH is an open-source genome mining platform (128,129). It predicts biosynthetic gene clusters (BGCs) based on homology with experimentally proven BGCs (128,129). Due to high accuracy in the predicted biosynthetic by antiSMASH, it is one of the well utilized genome mining platforms (130).

Besides genomic level biosynthetic potential predicting tools (125,130,131), the development of platforms to process metabolomics data has significantly contributed to the natural products discovery efforts (132–135). Available to the general public, Global natural products social – GNPS platform generates molecular networks from untargeted mass spectrometry data (135). Utilizing publicly available natural products libraries and publicly submitted mass spectrometry data of characterized small molecules, it detects molecules present in its database and creates molecular networks among the detected metabolites inferred from their shared fragmentation patterns (136,137).

Isolated from a soil sample in China collected in 1982, *Cystobacter ferrugineus* strain Cb fe23, DSM 52764, was recently reported to produce the novel diterpene cystodienoic acid (138). In an effort to explore the biosynthetic potential of *C. ferrugineus* strain Cbfe23, we sequenced its genome and determined its biosynthetic potential by using the antiSMASH platform. We further explored the metabolic potential of the strain by employing untargeted mass spectrometry based metabolomics and GNPS molecular networking.

2.3. Results and discussion

2.3.1. Whole genome sequencing of *C. ferrugineus*

Compared to other bacteria, myxobacteria have a relatively larger genome with an average of 9-14 million base pairs (bp) and a %GC content of 66-72% (18,19). The draft genome of *C. ferrugineus* contains 12,051,756 bp with 74 identified RNAs, 9,992 coding sequences, and a 68.5% GC content across 42 contigs containing protein-encoding genes. This whole-genome shotgun project has been deposited in DDBJ/ENA/GenBank under the accession number MPIN00000000. The version described in this paper is the first version, MPIN00000000.1. (139).

2.3.2 Biosynthetic potential of *C. ferrugineus*

Using antiSMASH version 5.0 (129), we identified 44 secondary metabolite biosynthetic pathways in *C. ferrugineus* genome. These pathways include twelve ribosomally synthesized and post-translationally modified peptides including four lantipeptides, ten terpenes, ten nonribosomal peptides, four polyketides; three type I polyketides, one type III polyketide, four hybrid nonribosomal peptide-polyketides, and grouped together as “others” one aminoglycoside, and a nucleoside **(Figure 2.1)**.

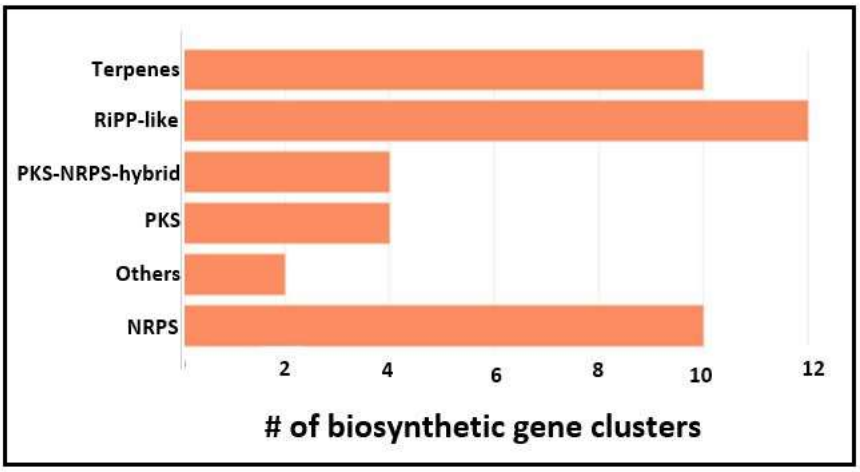

Figure 2.1. Biosynthetic capacity of *C. ferrugineus* predicted by antiSMASH. RiPP-like=Ribosomally synthesized post translationally modified peptides, PKS=Polyketide synthase, NRPS=Nonribosomal peptide synthetase, other=Aminoglycoside & Nucleoside.

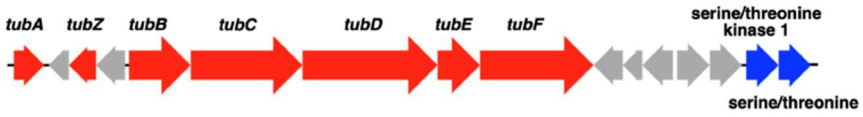

Figure 2.2. Tubulysin biosynthetic gene cluster organization in *C. ferrugineus*.

Table 2.1. %identity of tubulysin BGC proteins from *C. ferrugineus* with known BGC

Protein ID *Cystobacter ferrugineus*	**Protein homolog of *Cystobacter* sp. SBCb004**	**Identity**	**Reference**	**Proposed function**
WP_071905043.1	TubA	90.28%	ADH04674.1	NRPS
WP_084737959.1	TubZ	90.96%	ADH04676.1	NRPS
WP_071905046.1	TubB	92.99%	ADH04678.1	NRPS
WP_071905047.1	TubC	92.91%	ADH04679.1	NRPS
WP_071905048.1	TubD	92.28%	ADH04680.1	Hybrid PKS/NRPS
WP_071905049.1	TubE	93.80%	ADH04681.1	NRPS
WP_071905050.1	TubF	92.14%	ADH04682.1	PKS

BGC= biosynthetic gene cluster; NRPS= nonribosomal peptide synthetase; PKS= polyketide synthase

Notably, a biosynthetic gene cluster with significant homology (~70%) to the characterized tubulysin cluster from *Cystobacter* sp. SBCb004 (121) is present in the *C. ferrugineus* genome **(Figure 2.2)** with ≥ 92% identity for all core nonribosomal peptide synthetases **(Table 2.1)**. Sequence homology between the identified pathways and reported myxobacterial biosynthetic pathways suggests that along with tubulysins, *C. ferrugineus* may produce metabolites structurally similar to myxobacterial natural products myxochelin, and cystobactamid (113,122,140). Except for 4-5 BGCs that exhibit similarity to already known BGCs, other antiSMASH predicted BGCs have no similarity to known clusters. This suggests *C. ferrugineus* has the potential to produce natural products with unique scaffolds.

2.3.3. Tubulysins production by *C. ferrugineus*

To further explore the metabolic potential of *C. ferrugineus,* we analyzed metabolic crude extracts of *C. ferrugineus* obtained after growing bacterium on VY/2 agar medium. The crude extracts were subjected to untargeted mass spectrometry, and analyzed by Global Natural Product Social Molecular Networking (GNPS) (135). Molecular networking using GNPS provides networks depicting similarities in detected metabolite scaffolds inferred from shared fragmentation patterns. Myxobacterial metabolite tubulysin A as $[M+H]^+$ ion at m/z 844.45 was identified by GNPS in *C. ferrugineus* extracts from ionized fragment commonalities with a deposited library spectrum with a cosine score of 0.71 **(Figure 2.3)**. Tubulysins are a family of cytotoxic nonribosomal peptides with antitumor activity (7,122). Previously, their production has been reported from several myxobacteria including *Angiococcus disciformis* An d48 (141,142) reclassified as *Archangium disciforme* (143), *Archangium gephyra* Ar 315 (141,142), and *Cystobacter* sp. SBCb004 (122). The tubulysin A MS/MS spectrum from *C. ferrugineus* extracts shared 38 fragment peaks with the deposited library spectrum for tubulysin A in GNPS. We also

determined the structure with *De novo* analysis of MS/MS spectra of m/z 844.45, $[M+H]^+$ ion **(Figure 2.4)**. Tubulysin production by *C. ferrugineus* corroborates the presence of predicted tubulysin BGC in its genome **(Figure 2.2)**. Within the molecular network generated by GNPS from *C. ferrugineus* extracts, 3 additional metabolites detected as $[M+H]^+$ ions at 802.407 m/z, 816.422 m/z, and 830.438 m/z, were determined to be structurally similar to tubulysin A and assumed to be tubulysin I, tubulysin C, and tubulysin B, respectively **(Figure 2.3)**.

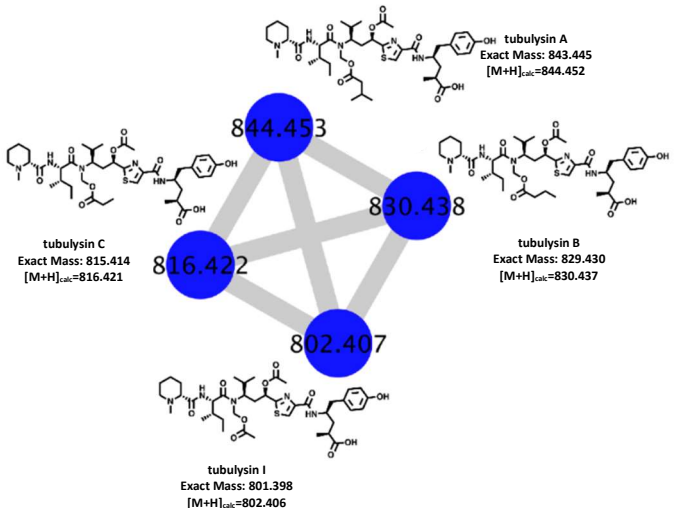

Figure 2.3. Tubulysins molecular network. Molecular family from crude extract of *C. ferugineus* samples that includes tubulysins A, B, C, and I provided by GNPS analysis.

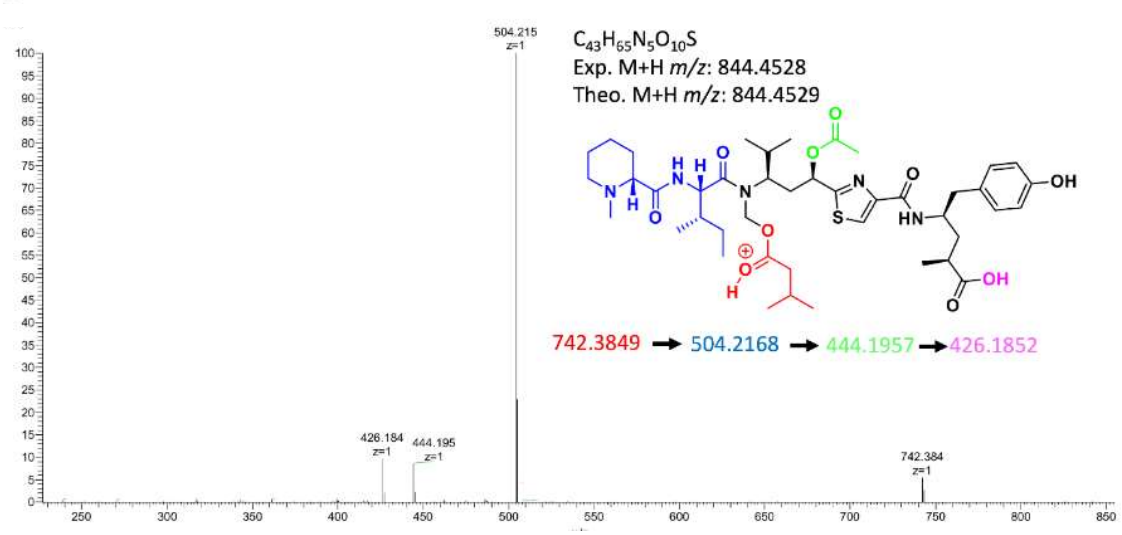

Figure 2.4. *De novo* MS/MS assignment to m/z 844.45 detected for tubulysin A structure in the crude metabolic extract of *C. ferrugineus*.

We confirmed in addition to previously known tubulysins producers myxobacteria, myxobacterium *C. ferrugineus* produces tubulysin A and other tubulysins analogs. LC-MS/MS data for this analysis were deposited in the MassIVE Public GNPS data set (ftp://massive.ucsd.edu/MSV000086742).

2.4. Conclusion

We confirmed the production of tubulysins in the crude extracts of *C. ferrugineus*, gene cluster of which was also predicted during *C. ferrugineus* genome analysis. The draft genome sequence exhibits the tremendous potential of *C. ferrugineus* to biosynthesize novel natural products. Further crude extract analysis of *C. ferrugineus* would allow us to explore structurally unique natural products.

2.5. Material and method

2.5.1. Bacterial culturing and DNA isolation

C. ferrugineus was acquired from the German Collection of Microorganisms (DSM) in Braunschweig (DSM 52764) and cultivated using VY/2 agar (1.4% w/v agar, 0.1% w/v $CaCl_2$ * 2 H_2O, 0.5% w/v Baker's yeast, 500 µM vitamin B12) media at 30 °C for 5-7 days. After 5-7 days, myxobacterial cells were removed from the agar plates, and genomic DNA was isolated using a GeneJET genomic DNA purification kit (ThermoFisher).

2.5.2. Genome sequencing and annotation

Genome sequencing was performed at MR DNA (Shallowater, TX) using an Illumina HiSeq system. The libraries were prepared using a Nextera DNA sample preparation kit (Illumina) following the manufacturer's user guide. Following the library preparation, the final concentration of the library (13.0 ng/L) was measured using the Qubit dsDNA HS assay kit (Life Technologies),

and the average library size (845 bp) was determined using the Agilent 2100 Bioanalyzer (Agilent Technologies). The libraries were pooled and diluted (to 10.0 pM) and sequenced paired end for 500 cycles with an average coverage of 50. An initial annotation was completed using the Rapid Annotations using Subsystems Technology (RAST) server (144), with further annotation requested by the NCBI Prokaryotic Genome Annotation Pipeline (145). This whole-genome shotgun project has been deposited in DDBJ/ENA/GenBank under the accession number MPIN00000000. The version described in this paper is the first version, MPIN00000000.1.

2.5.3. Analysis for biosynthetic potential

AntiSMASH version 5.0 (129) was utilized with the default settings to identify secondary metabolite biosynthetic gene clusters in the sequenced genome of *C. ferrugineus*. Protein BLAST search from NCBI database (https://www.ncbi.nlm.nih.gov/) was employed to confirm the protein similarity of tubulysins BGC from *C. ferrugineus* to the known tubulysins pathway from the myxobacterium *Cystobacter* sp. SBCb004.

2.5.4. Metabolic extraction and untargeted mass spectrometry

Metabolic extraction was performed after culturing *C. ferrugineus* on VY/2 agar media at 30 °C for 5-7 days. Agar with bacterial culture was chopped and extracted with ethyl acetate (EtOAC). The EtOAc extracts were dried in vacuo to produce crude extracts for LC-MS/MS analysis. LC–MS/MS analysis was performed on an Orbitrap Fusion instrument (Thermo Scientific, San Jose, CA) controlled with Xcalibur version 2.0.7 and coupled to a Dionex Ultimate 3000 nanoUHPLC system. Samples were loaded onto a PepMap 100 C18 column (0.3 mm × 150 mm, 2 μm, Thermo Fisher Scientific). Separation of the samples was performed using mobile phase A (0.1% formic acid in water) and mobile phase B (0.1% formic acid in

acetonitrile) at a rate of 6 µL/min. The samples were eluted with a gradient consisting of 5 to 60% solvent B over 15 min, ramped to 95% B over 2 min, held for 3 min, and then returned to 5% B over 3 min and held for 8 min. All data were acquired in positive ion mode. Collision-induced dissociation (CID) was used to fragment molecules, with an isolation width of 3 m/z units. The spray voltage was set to 3600 V, and the temperature of the heated capillary was set to 300 °C. In CID mode, full MS scans were acquired from m/z 150 to 1200, followed by eight subsequent MS2 scans on the top eight most abundant peaks. The orbitrap resolution for both the MS1 and MS2 scans was 120,000. The expected mass accuracy was < 3 ppm.

2.5.5. Data analysis on GNPS platform

LC-MS/MS generated data was converted to .mzML files using MS-Convert, and the GNPS platform was utilized as a dereplication tool to look for the small molecules' library hits within publicly available natural products libraries. A GNPS library match for tubulysin A was observed with a cosine score of 0.71. LC-MS/MS data for this analysis were deposited in the MassIVE Public GNPS data set (ftp://massive.ucsd.edu/MSV000086742).

2.6. Acknowledgements

I appreciate funding and support from the University of Mississippi and from American association of Colleges of Pharmacy (AACP) new investigator award. I thank Dr. Scot E. Dowd at MR DNA, Molecular Research LP for assistance throughout sequencing services provided, Dr. Sandeep Misra Manager of the Analytical and Biophysical Chemistry Core associated with the Glycoscience Center of Research Excellence (GlyCORE; P20GM130460) for LC-MS/MS analysis. I also thank Prof. Joshua Sharp for assisting in *De novo* analysis of tubulysins A MS/MS fragmentation pattern.

Chapter 3

Myxobacterial *omics* responses to prey signaling molecules

3.1. Abstract

Abundantly present in the soil, the predatory myxobacteria preferably interact with their Gram-negative bacterial prey. Even though predatory eavesdropping of *M. xanthus* on Gram-negative bacterial prey signaling molecules has been observed, the impact of these signaling molecules on the shared chemical space of predator and prey is not explored yet. Here, we employ a combined transcriptomics and metabolomics approach to demonstrate two structurally distinct classes of signaling molecules from Gram-negative bacteria elicit significant responses from predatory myxobacteria, *M. xanthus* and *C. ferrugineus*. Both myxobacteria exhibit general transcriptomics and metabolomics response to acyl-homoserine lactone (AHLs) type signals and present an overlapping metabolomics response to the core homoserine lactone structural moiety present in all AHL-type signals. On the other hand, both bacteria show distinctive omics response to a quinolone virulent factor (HHQ). Upon exposure to HHQ, *C. ferrugineus*, contrary to

M. xanthus, exhibits profound omics responses and oxidizes HHQ to HQNO, PQS, and PQS-NO metabolites. Altogether, our results provide additional evidence of myxobacterial eavesdropping on prey signals and present myxobacterial ability to respond to these prey signals distinctively.

3.2. Introduction

The uniquely multicellular lifestyles of myxobacteria have motivated continued efforts to explore the myxobacterium *Myxococcus xanthus* as a model organism for cooperative behaviors including development, motility, and predation (9,10). Often attributed to their need to acquire nutrients as generalist predators (24,29,31), myxobacteria have also been a valuable resource for the discovery of novel specialized metabolites (7,21,120). The diversities in structural scaffolds and observed activities as well as the unique chemical space associated with myxobacterial metabolites when compared with more thoroughly explored Actinobacteria make myxobacteria excellent sources for efforts focused on the discovery of therapeutics (21,66,146). However, the connection between myxobacterial predation and production of these biologically active metabolites remains relatively theoretical (23,24,147). Currently, only the metabolites myxovirescin and myxoprincomide have been directly implicated to be involved during *Myxococcus xanthus* predation of *Escherichia coli* and *Bacillus subtilis,* respectively (26,27,106). Even though it is demonstrated *M. xanthus* produce different metabolites depending on its different prey presence (26,27,106), the components of prey responsible for eliciting this response are unknown. In fact, a comprehensive understanding of the chemical ecology of predator-prey interactions between myxobacteria and their prey remains underexplored.

Ubiquitous to Proteobacteria (excluding myxobacteria) (148–150) and numerous other non-Proteobacteria genera (151), acylhomoserine lactones (AHLs) are the most common class of quorum signal autoinducers and are often implicated in interspecies communication within

polymicrobial communities (148–150). Recently, AHLs based modulating microbial secondary metabolic machineries has received a significant focus in expression of BGCs that fail to be expressed under axenic laboratory cultivation conditions (152–154). Also associated with the modulation of interspecies and interkingdom behaviors (155), slightly antibacterial, the quinolone signal HHQ (155–157) contributes to the pathogenicity of *Pseudomonas aeruginosa* by participating in the regulation of various virulence factors (156,158,159). In addition to *P. aeruginosa*, some pathogenic *Burkholderia* species also produce quinolone signals (160,161). Notably, the evidence of several bacteria modifying HHQ implicates the complexity of metabolic interactions in microbial communities (162,163). As a generalist predator, myxobacteria prey on a broad range of Gram-negative bacteria (29,31). However, only recently the impact of AHL quorum signals from prey microbes on the predatory capacity of *M. xanthus* has been reported (164) suggesting quorum signals might influence predator-prey interactions and induce biosynthesis of predation-associated specialized metabolites. Myxobacteria are not known participants in AHL quorum signaling and although 2 orphaned, functional AHL synthases have been reported, no myxobacteria have been observed to produce AHLs (165). However, a recent survey of signaling systems within the family *Myxococcaceae* reported the presence of conserved AHL receptor (LuxR) homologues and inferred that many myxobacteria within the two genera *Myxococcus* and *Corallococcus* are capable of sensing quorum signaling molecules that might contribute to the predatory eavesdropping of myxobacteria on prey quorum signaling (166).

Even though Gram-negative bacterial prey quorum signals influence predatory capacity of *M. xanthus*, myxobacterial metabolic interactions with the prey signals, either of AHL or HHQ, have not been explored yet. Herein we utilize a combination of transcriptomics and metabolomics to assess the myxobacterial response to prey quorum signals. Utilizing this omics approach, we

sought to determine response from myxobacteria *M. xanthus* GJV1 and *C. ferrugineus* Cbfe23 to structurally and functionally dissimilar signals from their Gram-negative bacterial prey. For these experiments we exposed each myxobacterium to *N*-Hexanoyl-L-homoserine lactone (C6-AHL), and the quinolone signal 4-hydroxy-2-heptylquinoline (HHQ). We anticipate transcriptomic and metabolomic data would play an indispensable role in understanding the shared chemical space of predator-prey interaction and the impact of prey signals on the metabolic capacity of myxobacteria. We expect an exploration of the myxobacterial response to prey quorum signals would not only provide insights into the impact that shared chemical signals might have on predator-prey interactions and specialized metabolism of myxobacteria but may also inform a general approach to modulate the specialized metabolism of myxobacteria that leverages their unique predatory roles and any sensory responses to detected prey.

3.3. Results

3.3.1. C6-AHL induces a general transcriptional downregulation in both *C. ferrugineus* and *M. xanthus*

As a model organism for developmental studies, *M. xanthus* is the best characterized myxobacterium (9,10) and has already demonstrated a behavioral response to exogenous AHLs (164). We employed developmentally proficient laboratory reference strain *M. xanthus* GJV1, a derivative clone of *M. xanthus* DK1622 and is distinguished from it by five accumulated mutations of unknown effect (167–169). However, we suspected that routine use as a laboratory strain (29,48,168,170–174), constitutive toxicity (53), and well-explored specialized metabolism of *M. xanthus* (175) might diminish its viability as the sole myxobacterium for these experiments. Therefore, *C. ferrugineus* was also included as a more recent myxobacterial isolate with a lesser explored biosynthetic capacity (139). Neither *M. xanthus* or *C. ferrugineus* possess a homologous

PqsR-type HHQ receptor (176,177). Whereas, both *M. xanthus* and *C. ferrugineus* have an annotated LuxR-type AHL receptor present in their genomes (WP_011555271.1 and WP_071900454.1). However, the homology-based annotation of these features only indicates the helix-turn-helix DNA-binding domain of LuxR receptors, and neither include an AHL-binding site motif (PF03472). Despite the absence of a canonical receptor, exogenous AHLs have been observed to stimulate the motility and predatory activity of *M. xanthus* (164). Exposure experiments utilizing a 9 μM concentration of C6-AHL, previously shown to elicit a predatory response from *M. xanthus* (164), were conducted in triplicate for both *M. xanthus* and *C. ferrugineus.* DMSO exposures served as a vehicle, negative control for comparative transcriptomic analysis.

Preliminary comparative transcriptomic analysis from RNAseq data revealed C6-AHL exposure impacted transcription of a total of 76 genes from *C. ferrugineus* experiments **(Figure 3.1A)** and only 3 total genes from *M. xanthus* experiments with ≥4-fold change in transcription at $p \leq 0.01$. In order to see whether C6-AHL impacted *M. xanthus* transcriptome at all, we expanded our analysis to include differentially impacted genes with $p \leq 0.05$ and ≥4-fold change for *M. xanthus*. RNAseq data from *M. xanthus* at $p \leq 0.05$ with ≥4-fold change provided an updated total of 59 differentially expressed genes when exposed to C6-AHL **(Figure 3.1B)**. Over all, these data revealed that C6-AHL exposure elicited a general downregulation of genes with a total of 51 downregulated genes from *C. ferrugineus* and 55 downregulated genes observed from *M. xanthus*. Total 25 upregulated genes were observed from *C. ferrugineus* during C6-AHL exposure, and only 4 features were observed to be upregulated by *M. xanthus* when exposed to C6-AHL **(Figure 3.1)**.

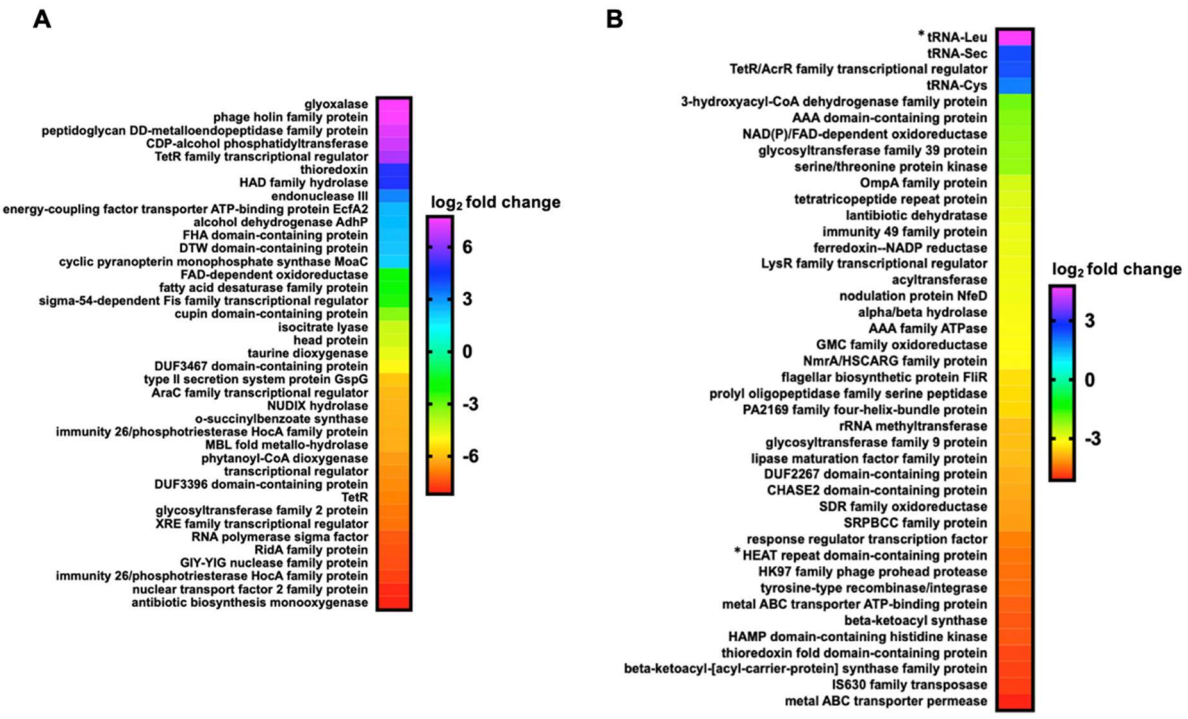

Figure 3.1. Differential gene expression from myxobacteria when exposed to C6-AHL signal. (A) Differentially expressed genes from *C. ferrugineus* exposed to C6-AHL when compared to signal unexposed *C. ferrugineus* control, p-value ≤0.01 **(**B) Differentially expressed genes from *M. xanthus* exposed to C6-AHL when compared to signal unexposed *M. xanthus* control, p-value ≤0.05. Data depicted as an average from 3 biological replicates, with genes annotated as hypothetical not included.

Comparing annotated genes impacted by C6-AHL exposure across both datasets and their putative roles by general system, numerous genes involved in signal transduction pathways and transcriptional regulation were included in both datasets with 7 regulatory genes downregulated by *M. xanthus* and 6 downregulated by *C. ferrugineus* **(Figure 3.2)**. Both myxobacteria also had a TetR family transcriptional regulator upregulated by C6-AHL exposure. Multiple genes associated with primary and specialized metabolisms and cell wall biogenesis and maintenance were downregulated by C6-AHL exposure across both datasets. Considering previous reports that C6-AHL exposure suppresses *M. xanthus* sporulation (164), we sought to determine if C6-AHL

exposure effected either of the transcriptional regulators associated with *M. xanthus* sporulation FruA (178,179) or MrpC (180,181). While no significant change in FruA (WP_011553167.1) was observed, transcription of the gene product MrpC (WP_002634092.1) was downregulated 1.7-fold by *M. xanthus* exposure to C6-AHL. However, transcription of the FruA (WP_071904077.1) or MrpC (WP_071900118) homologs from *C. ferrugineus* was not significantly changed by C6-AHL

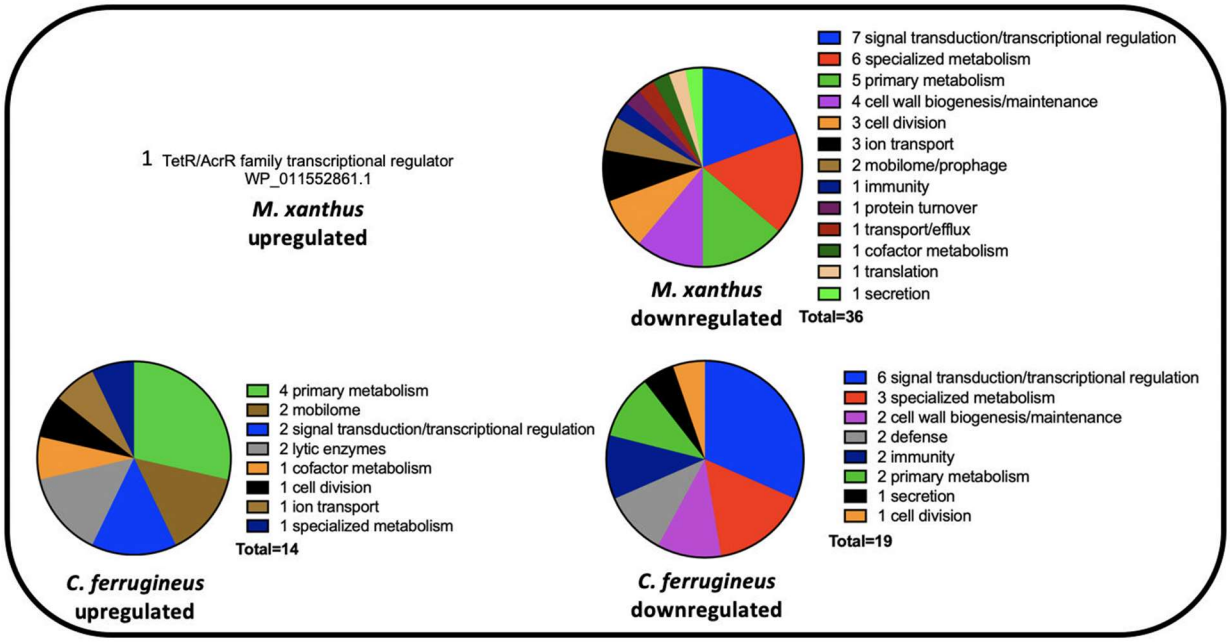

Figure 3.2. Putative roles of annotated genes impacted by C6-AHL exposure to *M. xanthus,* p-value ≤0.05 and *C. ferrugineus* p-value ≤0.01. Data depicted as an average from 3 biological replicates with genes annotated as hypothetical not included.

exposure. MrpC is a key transcription regulator and controls the expression of many developmentally regulated genes and multicellularity in *M. xanthus* (181,182). Furthermore, no obvious predatory features associated with motility or lytic enzymes were directly impacted in our C6-AHL exposed *M. xanthus* results, we suspect that this could be due to the previously reported constitutive toxicity of *M. xanthus* observed in both the presence and absence of prey (53). Notably, the increased transcription of lytic enzymes and mobile genetic elements observed from

C. ferrugineus exposed to C6-AHL suggest a predatory response; however, these features could also be associated with a defense response akin to phage defense. Transcription of neither of the annotated LuxR-type receptors (*M. xanthus*, WP_011555271.1; *C. ferrugineus*, WP_071900454.1) was affected by C6-AHL exposure. Overall considering the most significantly impacted genes across both datasets, C6-AHL exposure elicited somewhat similar responses from both myxobacteria including impacting numerous genes associated with transcriptional regulation and signal transduction, primary and specialized metabolisms, and cell wall maintenance.

3.3.2. HHQ elicits contrasting transcriptomics responses from *M. xanthus* and *C. ferrugineus*

Changes in the gene expression were also analyzed after exposing *M. xanthus* and *C. ferrugineus* to 9 μM HHQ and DMSO serving as HHQ unexposed, negative control. Comparative transcriptomic analysis from RNAseq data revealed HHQ exposure led to a ≥4-fold change in transcription of a total of 185 genes from *C. ferrugineus* **(Figure 3.3A)**, whereas we see 31 total impacted genes from *M. xanthus* with a p-value ≤0.05 **(Figure 3.3B)**. Unlike the similar responses elicited by C6-AHL exposure in both myxobacteria, contrasting responses were apparent when comparing data between these myxobacteria upon exposure with HHQ. Expression of a total of 156 genes was upregulated and 29 genes was downregulated in HHQ exposed *C. ferrugineus* when compared to unexposed sample. Whereas, *M. xanthus* RNAseq data depicted 9 upregulated genes and a total of 22 downregulated genes.

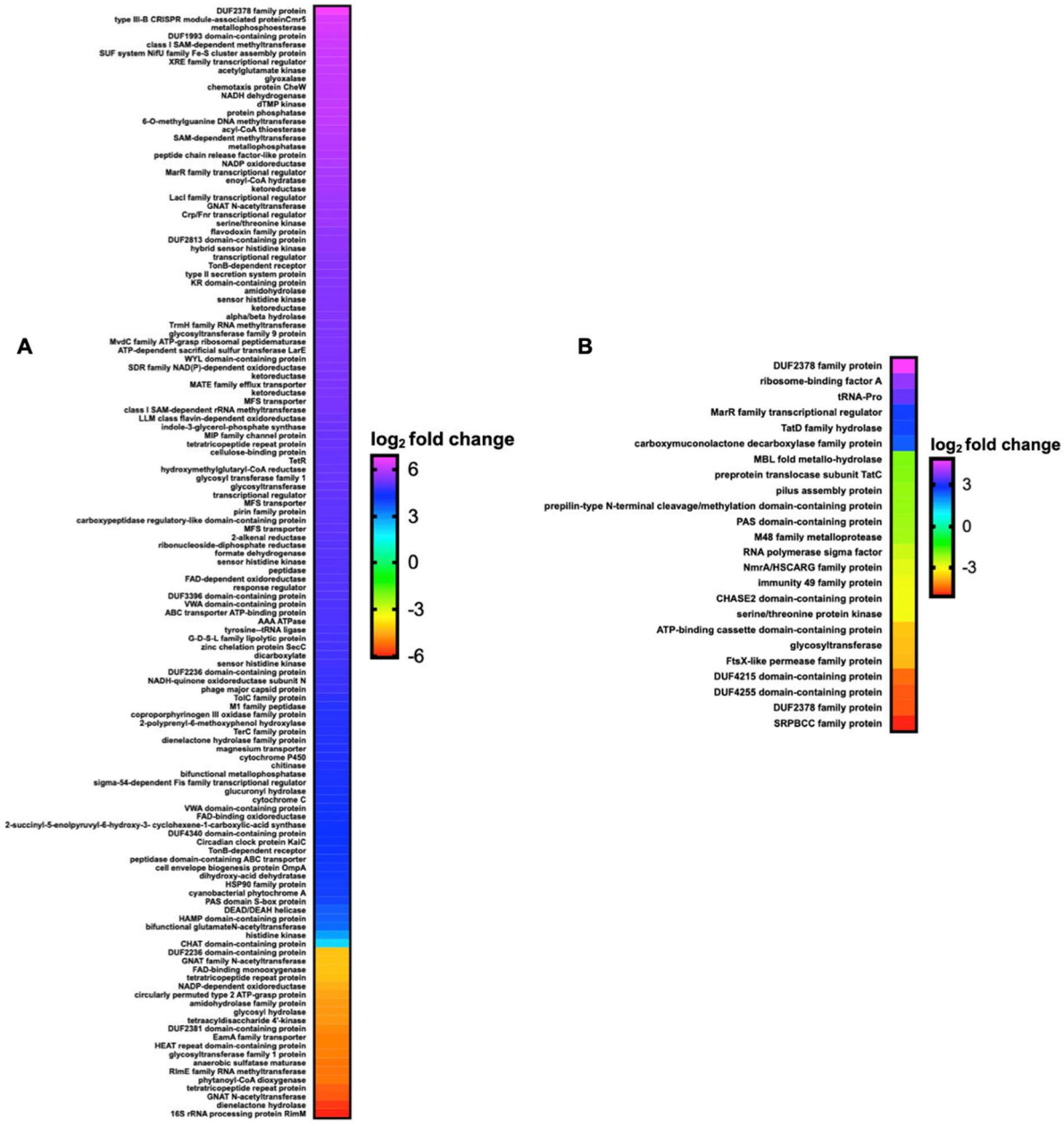

Figure 3.3. Differential gene expression from myxobacteria when exposed to HHQ signal. (A) Differentially expressed genes from *C. ferrugineus* exposed to HHQ when compared to signal unexposed *C. ferrugineus* control. (B) Differentially expressed genes from *M. xanthus* exposed to HHQ when compared to signal unexposed *M. xanthus* control. Data depicted as an average from 3 biological replicates p-value ≤0.05 with genes annotated as hypothetical not included.

Collectively, the observed contrasting impact on the impacted genes suggests both employed myxobacteria respond distinctly to HHQ signal. Furthermore, data from *M. xanthus* experiments revealed overlap between responses to prey signaling molecules. Like C6-AHL exposed transcriptome, higher number of statistically significant impacted genes were downregulated in HHQ exposed transcriptome of *M. xanthus* **(Figure 3.1B & Figure 3.3B)**. Additionally, among the downregulated genes in HHQ exposed *M. xanthus* RNAseq data, 5 genes

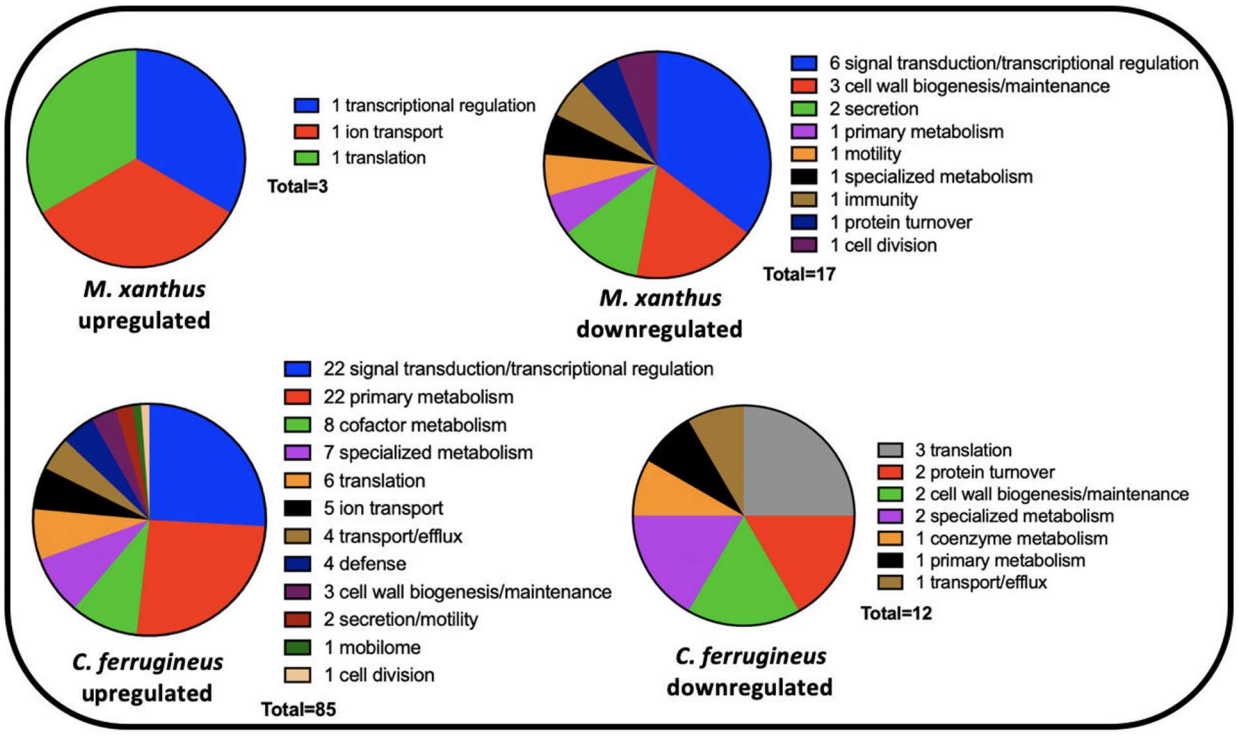

Figure 3.4. Putative roles of annotated genes impacted by HHQ exposure to *M. xanthus,* and *C. ferrugineus*. Data depicted as an average from 3 biological replicates, p-value ≤0.05, with genes annotated as hypothetical not included.

were also downregulated by C6-AHL exposure. Overlapping annotated features impacted by both C6-AHL and HHQ included an NmrA/HSCARG family protein (WP_ 011556972.1), an immunity 49 family protein (WP_011550233.1), a CHASE2 domain-containing protein (WP_011554259.1),

and 2 hypothetical proteins (WP_011555268.1 and WP_011552217.1). Overlap between putative roles of annotated genes was also observed from *M. xanthus* with multiple impacted genes predicted to be involved in transcriptional regulation and signal transduction and cell wall biogenesis and maintenance **(Figure 3.4)**. Of note, the pleiotropic regulator MrpC (WP_002634092.1) (180–182) was also downregulated 2.2-fold in *M. xanthus* exposed to HHQ which is comparable to 1.7-fold downregulation of MrpC observed with C6-AHL exposure.

Unlike the overlap in responses to both signals observed from *M. xanthus*, none of the 186 differentially impacted genes from HHQ exposure overlapped with the 76 genes impacted by C6-AHL exposure. Considering annotated genes by functional category, *C. ferrugineus* genes impacted by HHQ exposure were largely associated with signal transduction and transcriptional regulation, various metabolic pathways, and multiple genes associated with protein translation and turnover, cell wall biogenesis and maintenance, and specialized metabolism **(Figure 3.4)**. Interestingly, an annotated FAD-dependent oxidoreductase (WP_071901324.1) homologous to the monooxygenase PqsH from *P. aeruginosa* (91% coverage; 38% identity) which hydroxylates HHQ to yield 2-heptyl-3,4-dihydroxyquinoline or pseudomonas quinolone signal (PQS) (159,183–185) was upregulated 31-fold in HHQ exposed RNAseq data of *C. ferrugineus*. An outlier to the contrasting responses to HHQ, an annotated DUF2378 family protein (*M. xanthus,* WP_011553830.1; *C. ferrugineus,* WP_084736518.1) was significantly upregulated in both myxobacteria; DUF2378 family proteins are ~200 amino acid proteins with no known function that are exclusive to myxobacteria. Overall, these results indicated that *M. xanthus* exhibits a similar transcriptional response to both C6-AHL and HHQ signals whereas HHQ elicits a distinct response from *C. ferrugineus*.

3.3.3. Prey signals differentially impact genes included in specialized metabolite biosynthetic gene clusters

Genomic clustering of specialized metabolite biosynthetic gene clusters (BGCs) from bacteria (186) and the ability to broadly predict metabolite class by type from the genome sequence data (128,187,188) provided the opportunity to further scrutinize transcriptional responses potentially associated with specialized metabolite biosynthesis elicited by C6-AHL and HHQ. Using the BGC prediction platform antiSMASH (128,129), we determined biosynthetic potential of *C. ferrugineus* and *M. xanthus*. We, then, sought to evaluate if these prey signals effect the

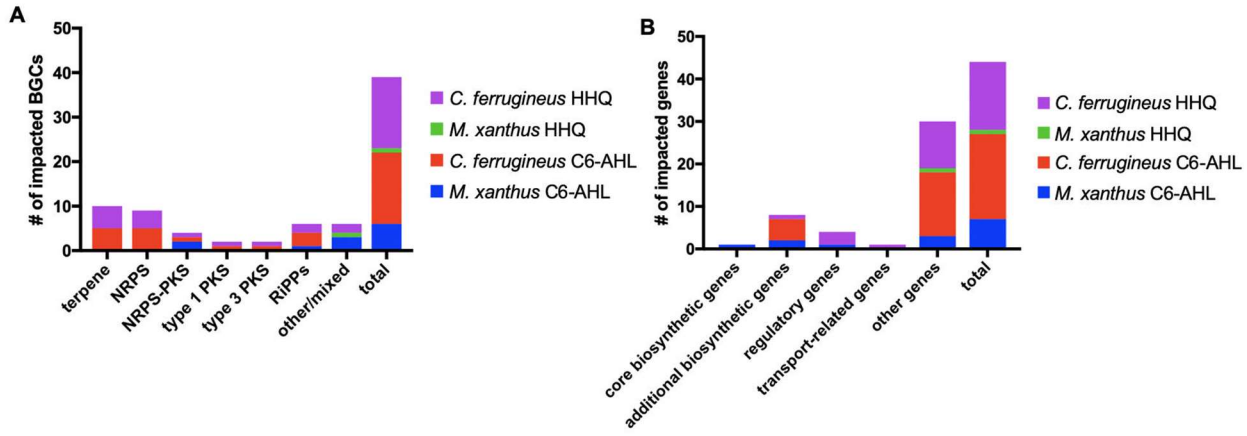

Figure 3.5. Differentially impacted genes included in antiSMASH predicted specialized metabolite biosynthetic gene clusters of *M. xanthus,* and *C. ferrugineus* when exposed to C6-AHL and HHQ signals. (A) Total number of BGCs impacted with specialized metabolite class type. (B) Predicted function of the impacted genes. Data depicted as an average from 3 biological replicates, p-value ≤0.05, fold change ≥4.

transcription of genes included in BGCs predicted by antiSMASH from each myxobacteria. In total, with a p-value ≤0.05 and ≥4-fold change, 7 out of the 59 total genes (12%) affected by C6-AHL exposure and only 1 gene of the 31 total impacted genes (3%) impacted by HHQ exposure were included in BGCs predicted from *M. xanthus*, and 20 out of 76 total (26%) genes effected by

C6-AHL exposure and 16 out of 185 total impacted genes (9%) by HHQ exposure were included in BGCs predicted from *C. ferrugineus* **(Table 3.1 in Appendix)**. antiSMASH analysis also provided a prediction for BGC type **(Figure 3.5A)** as well as categorized roles predicted for each gene within a BGC **(Figure 3.5B)**. Nine BGCs from *C. ferrugineus* were impacted by both signals while just one BGC from *M. xanthus* was impacted by both. However, no individual gene included in these BGCs was affected by both signals in either myxobacteria. In *M. xanthus* RNAseq data, the impacted genes included in BGCs were annotated as "others" when exposed to HHQ, whereas C6-AHL exposure impacted genes annotated as core biosynthetic, additional biosynthetic, and regulatory. In *C. ferrugineus* RNAseq data from HHQ exposure, the proteins encoded by the impacted genes in BGCs were mostly regulatory. While 26% of the total genes with a ≥4-fold change in transcription from *C. ferrugineus* when exposed to C6-AHL were included in BGCs, the categorized roles for these genes were predicted to be either "other" or hypothetical genes with an unknown contribution to metabolite biosynthesis or additional biosynthetic genes that likely modify the core chemical scaffold of the metabolite associated with the BGC. These results suggest that our prior assessment of responses to signal exposure by annotated enzyme category in certain cases provided an underestimate of the extent to which prey signals effect specialized metabolism. For example, 4 total genes categorized to be associated with specialized metabolism had a ≥4-fold change in transcription in our *C. ferrugineus* C6-AHL exposure experiments whereas 20 of the genes demonstrating a ≥4-fold change from these experiments were included in predicted BGCs. Overall, these results demonstrate that C6-AHL and HHQ both effect transcription of genes included in BGCs from each myxobacteria albeit to varying degrees in both utilized myxobacteria.

3.3.4. Differential metabolomic impact of AHL and HHQ signals

Subsequent exposure experiments utilizing *N*-Hexanoyl-L-homoserine lactone (C6-AHL), an additional AHL signal, 3-oxo-Hexanoyl-L-homoserine lactone (3-oxo-C6-AHL) and the quinolone signal 4-hydroxy-2-heptylquinoline (HHQ) were conducted with *C. ferrugineus* and *M. xanthus* exactly as done for our RNAseq experiments. Crude, organic phase extracts generated from these experiments were subjected to untargeted mass spectrometry and the XCMS-MRM (v3.7.1) platform was utilized for comparative statistical analysis of all detected metabolic features. Comparing features with significantly impacted intensities ($p \leq 0.02$) during these signal exposure experiments; all 3 signals elicited a prominent response from *C. ferrugineus* **(Figure 3.6A & 3.6B)**. The number of impacted metabolic features was comparable in *C. ferrugineus* when exposed to the employed AHL signals, with almost 34-36% features showed an increase in the detected ion intensity **(Figure 3.6C)**, and

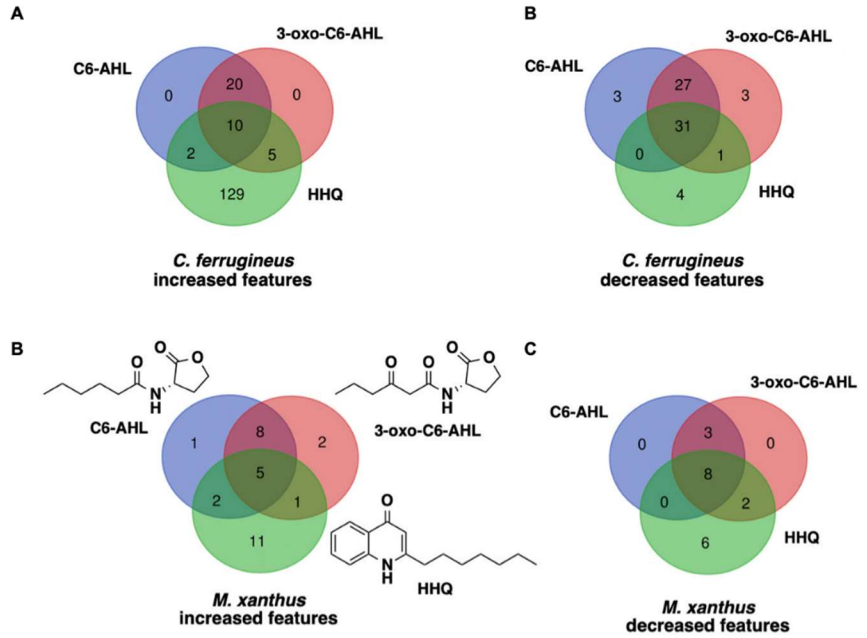

Figure 3.6. Comparison of metabolomics responses of myxobacteria to prey signals. (A, B) Number of metabolic features from *C. ferrugineus* with impacted detected ion intensity when signals were exposed (C, D) Number of metabolic features from *M. xanthus* with impacted detected ion intensity upon exposure to signals. The comparison was done with DMSO exposed myxobacteria considered as control. The included prey signals were C6-AHL and 3-oxo-C6-AHL as acylhomoserine lactones, and HHQ as employed quinolone signal. Data is provided by XCMS-multigroup analysis with n=3, p-value ≤0.02.

almost 64-66% features exhibited a decrease in the detected ion intensity in both data sets compared to DMSO exposed negative control dataset **(Figure 3.6D)**. We also noticed the impact of both AHL signals was apparently similar on a single mass feature. For example, in *C. ferrugineus* if a feature (m/z 690.3992) demonstrated decrease in intensity upon exposure of C6-AHL when compared to DMSO exposed sample, similar decline in the detected ion intensity for the same feature (m/z 690.3992) was noticed when *C. ferrugineus* was exposed to 3-oxo-C6-AHL **(Figure 3.7A)**. Despite the comparatively diminished response from *M. xanthus* with 41%-45% differentially detected features showing a decrease in ion intensity and 55%-59% exhibiting an increased detected ion intensity when exposed to either of AHLs **(Figure 3.6C & 3.6D)**, a trend similar to *C. ferrugineus* when exposed to AHLs was observed **(Figure 3.7A)**. HHQ exposure to *C. ferrugineus* resulted in a greater number of impacted features with increase in detected ion intensity, with almost 80% of the statistically significant impacted features in *C. ferrugineus* showed an increase in ion intensity **(Figure 3.6A)**, and only 20% of the detected ions were decreased in intensity compared to DMSO exposed negative control sample **(Figure 3.6B)**. Contrary to similar impact of both AHL signals on a single metabolic feature, HHQ appeared to induce a contrasting effect on the same metabolic feature in both employed myxobacteria **(Figure 3.7A)**. Which means if AHLs increased ion intensity of a particular feature, HHQ decreased the detected ion intensity of the same feature compared to DMSO exposed control sample. Interestingly, some features seemed to be activated in HHQ exposed dataset from *C. ferrugineus* with no traces detected for them in the HHQ unexposed control dataset or AHL exposed datasets **(Figure 3.7B)**. *M. xanthus*, on the other hand, showed 54% increase and 46% decrease in the intensity compared to HHQ unexposed samples when it was exposed to HHQ.

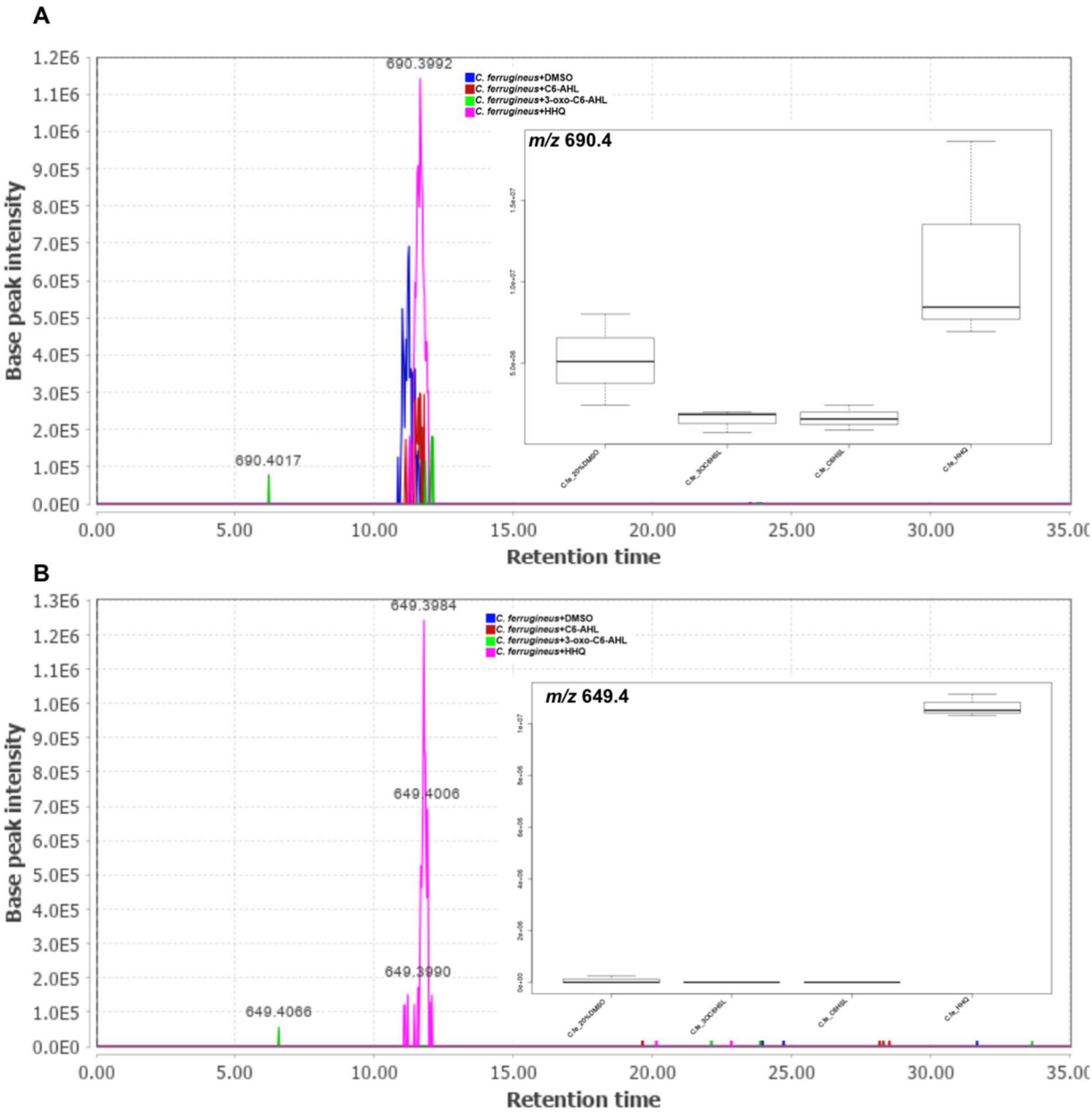

Figure 3.7. Prey signals impact on the peak intensities of the metabolic features. (A) An extracted ion chromatograph (EIC) of one of impacted metabolic feature (m/z 690.4) with its corresponding box-plot from XCMS statistical analysis. *C. ferrugineus* crude extracts depicting increased detected ion intensity when exposed to HHQ and decreased detected ion intensity when exposed to AHL signals compared to signal unexposed DMSO control sample. (B) An EIC of one of the impacted metabolic feature (m/z 649.4), with its corresponding box-plot from XSMS statistical analysis, that appeared exclusively in HHQ exposed *C. ferrugineus* sample. Chromatograph rendered with MZmine v2.37. Box-plot data is provided by XCMS-multigroup analysis with n=3, $p \leq 0.02$. On the bar-graph, the x-axis shows different exposure conditions, and y-axis showing base peak intensity of a detected ion.

Overall, two general trends were apparent when comparing the signals responses between both myxobacteria. First, both AHL signals resulted in highly similar responses from both myxobacteria with few to no uniquely impacted features specific to either C6-AHL or 3-oxo-C6-AHL signal exposure **(Figure 3.6 & Figure 3.7A)**. Second, HHQ exposure induced a dramatic change in the metabolic profile of *C. ferrugineus* that was not observed from HHQ-exposed *M. xanthus* **(Figure 3.6)**.

Intrigued by the difference in responses to AHLs and HHQ, additional experiments where both myxobacteria were exposed to combined C6-AHL and HHQ (C6-AHL + HHQ) were performed. Comparative analysis of results revealed that the addition of C6-AHL did not dramatically impact the change in metabolomic profile observed from either myxobacteria when exposed to HHQ **(Figure 3.8)**. Conversely, impacted features observed in our previous AHL exposure experiments were not observed in our C6-AHL + HHQ experiments **(Figure 3.8)**.

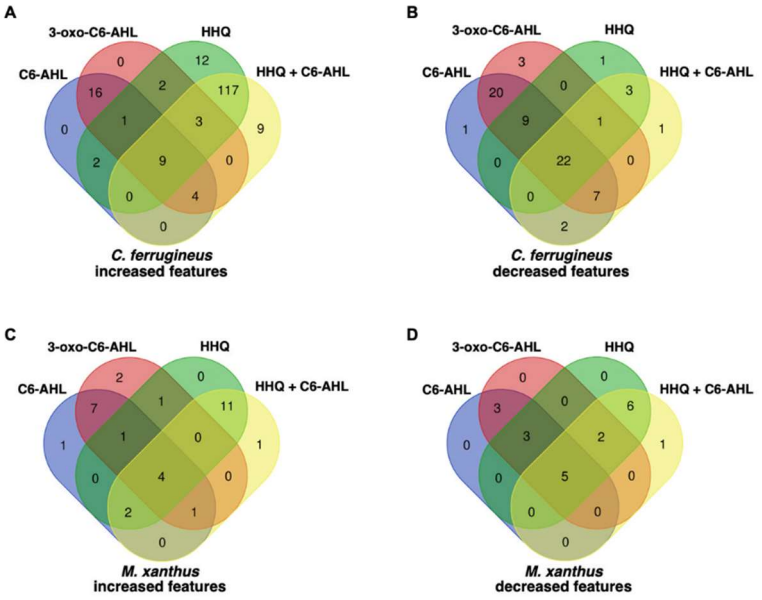

Figure 3.8. Comparison of combined impact of prey acylhomoserine lactone and quinolone signals on metabolic features of myxobacteria. (A, B) Number of metabolic features with impacted detected ion intensities compared to unexposed sample when signals were exposed to *C. ferrugineus.* (C, D) Number of metabolic features with impacted detected ion intensities compared to unexposed sample from *M. xanthus.* Two treatments were C6-AHL and 3-oxo-C6-AHL as acylhomoserine lactones, third treatment was HHQ as employed quinolone signal, and a fourth treatment was a combined C6-AHL & HHQ signals. Data is provided by XCMS-multigroup statistical analysis with n=3, p-value ≤0.02.

From these results, we determined that both myxobacteria demonstrate a metabolic response unique to either HHQ or AHL-type chemical signals with a conserved response to both C6-AHL and 3-oxo-C6-AHL. These data also revealed a unique metabolic response from *C. ferrugineus* when exposed to HHQ similar to our previous transcriptomics observations.

3.3.5. The core structural moiety of AHLs is an elicitor of myxobacterial conserved metabolomic response to AHLs

Intrigued by the overlap in metabolic responses observed from AHL signal exposure **(Figure 3.6 & Figure 3.7A)**, we were curious if the core homoserine lactone moiety present in all AHL-type quorum signals was a sufficient elicitor for a similar response. Noticing a profound metabolic response from *C. ferrugineus*, we included it for the additional metabolomic exposure assays. By including either L-homoserine lactone (L-HSL), the stereoisomer present in natural AHL-type quorum signals (151); D-homoserine lactone (D-HSL), the enantiomer of L-HSL; or boiled C6-AHL; we performed untargeted mass spectrometry and XCMS-MRM analysis to determine any overlap with previously observed responses to C6-

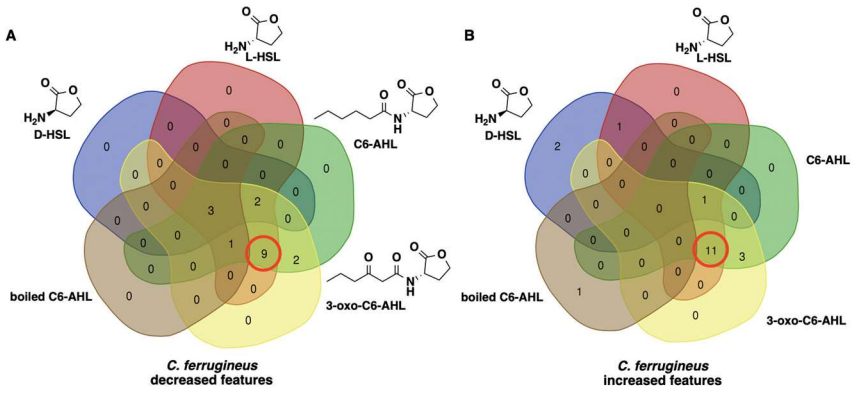

Figure 3.9. *C. ferrugineus* overlapping response to L-homoserine lactone and prey associated acyl-homoserine lactones. (A) Number of metabolic features with a decrease in the detected ion intensity compared to unexposed sample (B) Number of metabolic features with increased detected ion intensity compared to unexposed sample. The included signals were C6-AHL and 3-oxo-C6-AHL: prey associated acylhomoserine lactone (AHLs) quorum signals, and L-HSL: the stereoisomer present in natural AHL-type quorum signals, D-HSL: the enantiomer of L-HSL, and boiled C6-AHL. Red circle indicates overlapping metabolic features of L-HSL with employed AHLs. Data is provided by XCMS-multigroup analysis; n=3; p ≤0.02.

AHL and 3-oxo-C6-AHL exposure. Comparative analysis of statistically impacted features by signal intensity ($p \leq 0.02$) revealed 20 overlapping features from the L-HSL, C6-AHL, and 3-oxo-C6-AHL exposure experiments and just 3 overlapping features from the L-HSL, D-HSL, C6-AHL, and 3-oxo-C6-AHL exposure **(Figure 3.9)**. Not only same features were impacted with L-HSL, C6-AHL, and 3-oxo-C6-AHL exposure, but the effect on their detected ion intensities was also overlapping. For instance, upon exposure to either of AHLs when a mass feature showed an increase in intensity compared to DMSO control, it also depicted an increase in the detected ion intensity when exposed to L-HSL **(Figure 3.10)**. These results provide some explanation for the observed transcriptomic and metabolomic response to exogenous AHLs despite

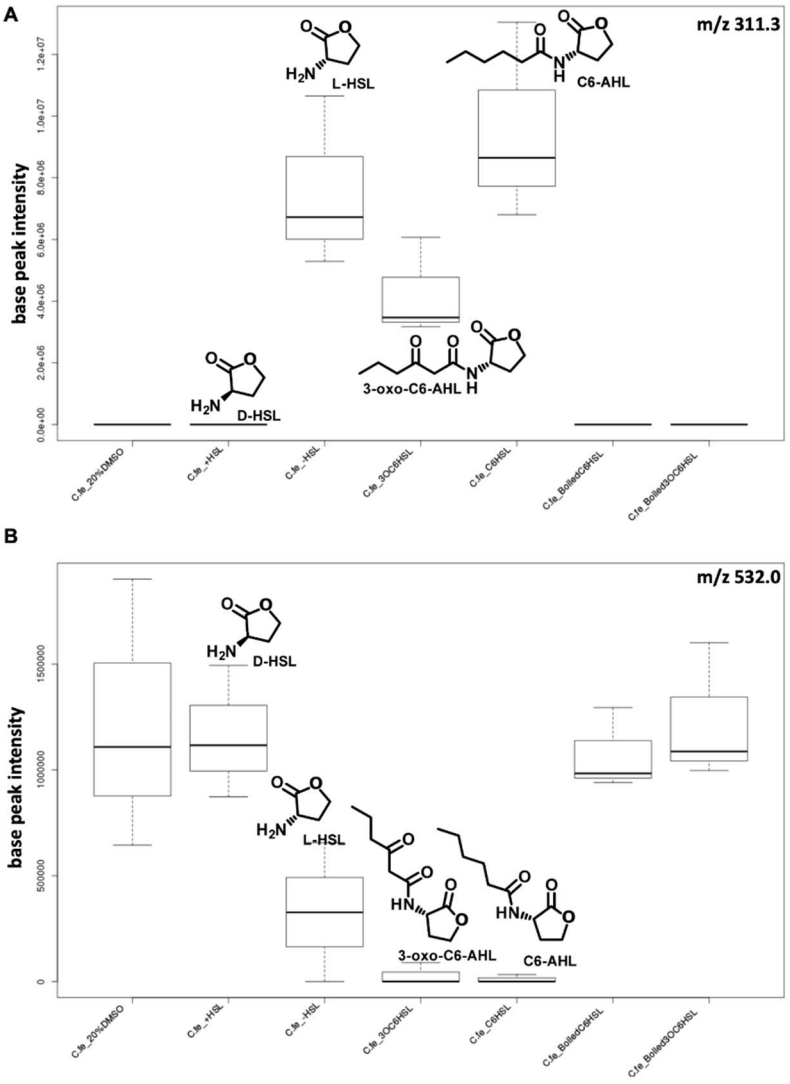

Figure 3.10. Box-plot showing *C. ferrugineus* overlapping response to L-homoserine lactone and acylhomoserine lactone. (A, B) Examples of two of the impacted metabolic features (m/z 311.3 & m/z=532.0) impacted similarly by L-HSL and AHLs, whereas ion intensities for the same features in case of D-HSL, and boiled AHLs (2 right box-plots) exposure correspond to DMSO negative control. Box-plot data is provided by XCMS-multigroup analysis with n=3, $p \leq 0.02$.

the absence of a LuxR-type AHL receptor including a canonical AHL-binding site and suggest that the core homoserine lactone present in all AHLs is sufficient for eliciting a response from myxobacteria.

3.3.6. Oxidative detoxification of HHQ observed from *C. ferrugineus*

Considering the evidences that some bacteria has shown metabolic detoxification of quinolone signaling molecules (162), we evaluated metabolomic datasets from HHQ exposure experiments for the modified products of HHQ. Comparing metabolomic datasets from HHQ exposure experiments, we detected oxidized analogs of HHQ at m/z 260.164, $[M+H]^+$ ion, and exact mass of 259.157 Da that were exclusive to the *C. ferrugineus* dataset **(Figure 3.11A)**.

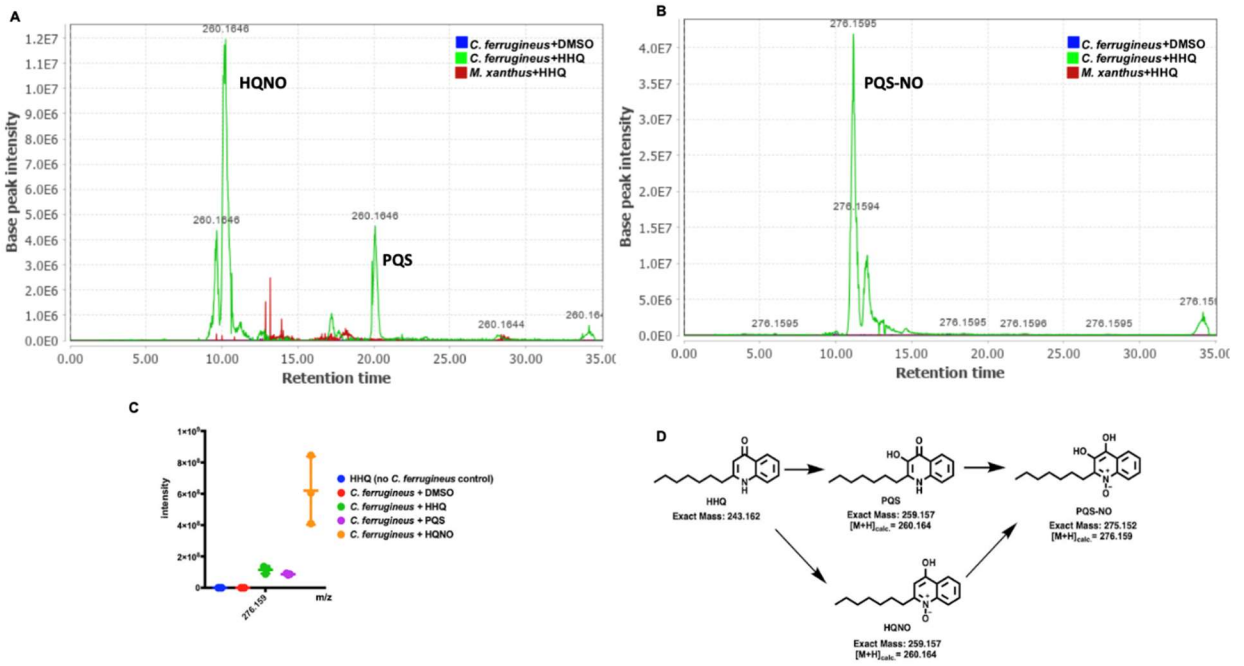

Figure 3.11. Extracted ion chromatograph (EIC) of the oxidized products of HHQ from *C. ferrugineus* crude extracts when exposed to HHQ. **(A)** EIC depicting presence of PQS and HQNO **(B)** EIC depicting presence of PQS-NO from the extracts of *C. ferrugineus.* Chromatograph rendered with MZmine v2.37. **(C)** Detected ion intensity for PQS-NO from crude extracts of *C. ferrugineus* exposed to HHQ as well as commercially available PQS and HQNO signals. **(D)** Proposed route of PQS-NO synthesis from *C. ferrugineus*.

Authentic standards for the oxidized HHQ quinolone signals *Pseudomonas* quorum signal (PQS) exact mass of 259.157 Da and 2-heptyl-4-hydroxyquinoline *N*-oxide (HQNO) also exact mass of 259.157 Da confirmed the presence of both oxidized products in HHQ exposed *C. ferrugineus* extracts **(Figure 3.12 in Appendix)**. Additionally, the presence of a metabolite with a m/z 276.159, $[M+H]^+$ ion and a similar MS/MS fragmentation pattern matching 2-heptyl-3,4-dihydroxyquinoline-*N*-oxide (PQS-NO) an oxidation product reported by Thierbach *et al*. (162) was also observed in *C. ferrugineus* extracts from HHQ **(Figure 3.11B & Figure 3.13 in Appendix)**. Oxidative detoxification of quinolone signals including quinolone signals has been reported from numerous bacteria (162,163). In an effort to get insight about the oxidative detoxification route for quinolone signals, we performed additional experiments by exposing *C. ferrugineus* to PQS and HQNO. The presence of a metabolite with an exact mass and similar MS/MS fragmentation pattern matching PQS-NO in *C. ferrugineus* extracts from both PQS, and HQNO exposure experiments suggesting subsequent oxidation of both PQS and HQNO to detoxified oxidized product **(Figure 3.11C)**. Surprisingly, none of the oxidized products were observed from the crude extracts from *M. xanthus* when exposed to HHQ or PQS. These results suggest that *C. ferrugineus* possesses a detoxification route for quinolone signals not observed from *M. xanthus* and capably oxidizes the quinolone signals HHQ, PQS, and HQNO to PQS-NO **(Figure 3.11D)**.

3.4. Discussion

Although the predatory lifestyles of myxobacteria have long been associated with their capacity as a resource for natural products (NPs) discovery (23,24,147), the chemical ecology of predator-prey interactions and its impact on myxobacterial NPs remains underexplored. The recent discovery that exogenous AHL quorum signals associated with Gram-negative prey bacteria increase the predatory capacity of *M. xanthus* (164) provides an excellent example of shared chemical space within microbial communities influencing predation. In this study, utilizing comparative transcriptomics and metabolomics, we determined the generality of predatory eavesdropping and its impact on myxobacterial metabolism by comparing omics responses from *M. xanthus* and *C. ferrugineus* when exposed to structurally distinct quorum signals C6-AHL and HHQ.

Initial transcriptomic data comparing *M. xanthus* and *C. ferrugineus* exposed to C6-AHL revealed similar transcriptional responses with downregulation of several genes from both myxobacteria. Originally referenced as predatory eavesdropping, we further sought to determine the impact of C6-AHL on genes with annotations affiliated with predation and predatory responses such as motility features, lytic enzymes, and specialized metabolism. Transcription of multiple genes associated with transcriptional regulation, metabolism, and cell wall maintenance was influenced by exogenous C6-AHL across both myxobacteria. Other than the numerous genes associated with specialized metabolism impacted across both myxobacteria, the only other potential predatory features with a transcriptional response to C6-AHL exposure were lytic enzymes from *C. ferrugineus*, and no annotated genes predicted to be involved in motility were affected by C6-AHL in either myxobacterium. Considering the original observation that AHLs stimulate predation by increasing the vegetative population of *M. xanthus* (164), we suggest that

the observed change in transcription of genes associated with metabolism and signal transduction from both myxobacteria may correspond with a similar population-based response. The decreased transcription of the gene encoding for MrpC, a developmental regulator involved in sporulation (180–182), observed in our *M. xanthus* dataset, also supports a population-based response to C6-AHL. Exogenous AHLs were also previously not observed to influence outer membrane vesical (OMV) production or OMV lytic activity (164). Secreted OMVs from myxobacteria include lytic enzymes such as proteases and amidases and contribute to prey lysis (189,190). The observed change in transcription of genes within specialized metabolite BGCs elicited by C6-AHL exposure may provide some explanation for increased predation of AHL-exposed *M. xanthus*. However, neither of the *M. xanthus* metabolites known to contribute to predation, myxovirescin (27,106) and myxoprincomide (26), were significantly impacted in our metabolomics dataset, and no genetic features within the corresponding BGCs for either metabolite were impacted by C6-AHL exposure.

The comparison of metabolomic responses elicited by C6-AHL and 3-oxo-C6-AHL signals in both myxobacteria also demonstrated a similar response from *C. ferrugineus* and *M. xanthus*. Intrigued by the observed similarity of metabolic responses to AHLs from both myxobacteria and to identify the structural moiety of AHLs responsible for the observed effect, we investigated myxobacterial metabolomic response to L-homoserine lactone (L-HSL), its enantiomer D-homoserine lactone (D-HSL), and a boiled C6-AHL. Our evaluation indicates L-HSL evoked a response similar to C6-AHL and 3-oxo-C6-AHL, whereas D-HSL and boiled C6-AHL mostly showed ion intensities similar to the unexposed samples. The overlapping response of L-HSL with the employed AHL suggests myxobacteria likely respond to the homoserine lactone moiety of acyl-homoserine lactone quorum signals. This also suggests, regardless of the difference in the

side chain of AHLs, the core homoserine lactone structure possibly allows non-discriminating perception of the prey by myxobacteria. Considering L-HSL and AHLs eliciting a similar metabolomics response from both utilized myxobacteria and no differential expression of the annotated LuxR-type receptors has been identified from either of myxobacterial RNAseq data when exposed to C6-AHL, we suggest probably myxobacteria utilize a cognate receptor required to perceive L-homoserine lactone structural moiety of AHL signals instead of full acyl-homoserine lactone signals. Notably, no cognate receptor to L-homoserine lactone has been identified yet. A future investigation of such a receptor would contribute to our understanding of chemically modulated ecological interactions within microbial communities.

Sub-inhibitory concentrations of antibiotics are suggested to influence transcriptional responses in bacteria (191). Comparing the transcriptomics responses of *M. xanthus* and *C. ferrugineus*, when exposed to HHQ virulent factor suggests distinct responses from both myxobacteria. *C. ferrugineus* demonstrate a profound differential transcriptomics response to HHQ and upregulates many of its genes. Compared to *C. ferrugineus,* a distinct response was observed from *M. xanthus* with more downregulated genes when exposed to HHQ. Contrary to *M. xanthus*, *C. ferrugineus* upregulated genes associated with signal transduction and transcriptional regulation, various metabolic pathways, and multiple genes associated with protein translation and turnover, cell wall biogenesis and maintenance, and specialized metabolism. Interestingly, an annotated FAD-dependent oxidoreductase homologous to the monooxygenase pqsH from *P. aeruginosa*, which hydroxylates HHQ to yield pseudomonas quinolone signal (PQS) (159,183–185) was upregulated 31-fold in *C. ferrugineus*. In contrast, no differential expression for *pqsH* homolog from *M. xanthus* (WP_011553431.1) could be identified.

In addition to differential transcriptomic responses, the metabolomics responses to HHQ were also contrasting in both myxobacteria. *C. ferrugineus* showed a robust metabolomic response with a higher number of metabolic features showing increased in detected ion intensities. Additionally, metabolomics data of *C. ferrugineus* obtained after exposing it to HHQ indicates some metabolic features were exclusively present in HHQ exposed samples. These observations suggest HHQ triggered a metabolic response in *C. ferrugineus* and activated previously undetectable metabolites. The metabolic response from *C. ferrugineus* correlates with the activated metabolic response from some other bacteria when exposed to chemical elicitors, including subinhibitory concentrations of some antibiotics (192–197). The drastic metabolic response corroborating transcriptional response from *C. ferrugineus,* when exposed to HHQ (155–157) suggests HHQ acted as a global elicitor to *C. ferrugineus* metabolism and activated the products associated with several BGCs. Previously antibiotic trimethoprim in subinhibitory concentrations has acted as a global metabolic elicitor and activated several of BGCs with the production of more than 100 molecules that were not detected under standard growth conditions from *Burkholderia thailandensis* (192,195). In contrast, the number of increased and decreased features are comparable when *M. xanthus* was exposed to HHQ and AHLs. However, *M. xanthus*, like *C. ferrugineus,* showed contrasting impact on a single detected metabolic feature emphasizing *M. xanthus* also recognizes both signal classes distinctly.

The detection of PQS, HQNO, and PQS-NO, the oxidized products of HHQ, in the crude extract of *C. ferrugineus* confirms that *C. ferrugineus* utilizes an oxidative metabolic pathway to detoxify HHQ. Detection of PQS also correlates with upregulated *pqsH* homolog in our transcriptomics data from *C. ferrugineus* when exposed to HHQ. It is the first report demonstrating the production of PQS and HQNO (184,198), the oxidized products of HHQ, from a bacterium

other than *P. aeruginosa*. Except for playing a role in *P. aeruginosa* pathogenesis, PQS and HQNO show inhibitory effects on the growth of other bacteria (184,199,200). The ability of *C. ferrugineus* to sense and oxidize HHQ suggests predatory eavesdropping on a potential prey's signaling molecule to utilize these oxidized molecules in repressing the growth of several of its bacterial prey. However, this hypothesis requires antibacterial testing, against Gram-positive and Gram-negative prey bacteria, of the crude metabolic extracts obtained from *C. ferrugineus* after exposing it to HHQ. Alternatively, detection of PQS and HQNO products could only be as the intermediate products while *C. ferrugineus* eavesdrops on HHQ of *P. aeruginosa* and detoxifies it to PQS-NO to reside in the same soil habitat as *P. aeruginosa* or to prey efficiently on *P. aeruginosa*. The detected PQS-NO, already reported from strains of *Arthrobacter*, *Rhodococcus* spp. and *Staphylococcus aureus* as an oxidized product of HQNO, is relatively less toxic molecule (162). Notably, none of these products could be identified in the crude extracts from *M. xanthus* after exposure to HHQ, and it might be due to no noticeable differential expression of *pqsH* homolog in *M. xanthus* genome. Individuality in the utilized myxobacterial response to HHQ emphasizes the specialized aspect of myxobacterial predation. Broadly considered generalist predator, myxobacteria prey on a wide variety of microorganisms, including Gram-negative bacteria, Gram-positive bacteria, cyanobacteria, and fungi (6,43,47). However, predatory specialization has been observed among different myxobacterial strains (29,49,63,64,73). *M. xanthus* inadequate response to HHQ signal might corroborate with its poor predation on *P. aeruginosa* (30), whereas *C. ferrugineus* comparatively significant response to HHQ signal suggests it could be a relatively good predator of *P. aeruginosa*. However, this hypothesis needs further predatory testing to be justified. Further studies identifying the predatory capability of *C. ferrugineus* towards HHQ producing *P. aeruginosa* would further add to our understanding.

Overall, we show that exogenous quorum signals from prey elicit significant responses from both *M. xanthus* and *C. ferrugineus* providing supporting evidence that predatory myxobacteria eavesdrop on prey signaling molecules. We determine that both myxobacteria exhibit a general transcriptomics and metabolomics responses to AHL signals and suggest that overlapping responses to the core homoserine lactone moiety present in all AHL-type signals could be related to the absence of a LuxR-type receptor possessing a conserved AHL-binding domain. We also show distinct responses from both myxobacteria upon HHQ exposure and determine that *C. ferrugineus* capably metabolizes HHQ similar to previously reported oxidative detoxification of HQNO signal. Altogether, our results provide additional evidence for Gram-negative bacterial prey signals eavesdropping by predatory myxobacteria. Our results also suggest distinctive response to prey signaling molecules may contribute to specialized predatory traits of myxobacteria.

3.5. Materials and Methods

3.5.1. Cultivation of *M. xanthus* and *C. ferrugineus*

Myxobacteria *Cystobacter ferrugineus* strain Cbfe23, DSM 52764, initially obtained from German Collection of Microorganisms (DSMZ) in Braunschweig, and *Myxococcus xanthus* GJV1 obtained from Professor Peter Zee as a gift were employed in this study. *C. ferrugineus* was grown on VY/2 agar (5 g/L baker's yeast, 1.36 g/L $CaCl_2$, 0.5 mg/L vitamin B_{12}, 15 g/L agar, pH 7.2). Whereas, CTTYE agar (1.4% w/v agar, 1% Casitone, 10 mM Tris-HCl (pH 7.6), 1 mM potassium phosphate (pH 7.6), 8 mM $MgSO_4$, 0.5% yeast extract) was utilized to culture *M. xanthus*.

3.5.2. Signal exposure experiments

For signal exposure conditions, required volumes for 9 μM of filter sterilized, HHQ (Sigma), C6-AHL (Cayman Chemical), 3-oxo-C6-AHL (Cayman Chemical), (-) HSL (Cayman Chemical), and (+) HSL (Cayman Chemical) from a 150 mM stock prepared in DMSO were added to autoclaved medium at 55ºC. For RNA-seq and LC-MS/MS analysis, *C. ferrugineus* was cultivated on VY/2 agar medium, and *M. xanthus* was cultured on CTTYE agar medium. *C. ferrugineus* for 10 days and *M. xanthus* 14 days were grown at 30°C.

3.5.3. RNAseq analysis

After incubation period, the myxobacterial cells were scrapped from the agar plates and stored in RNA-ladder. Total RNA was isolated from the samples using the RNeasy PowerSoil Total RNA Kit (Qiagen) following the manufacturer's instructions. 500mg sample was used for extractions. The concentration of total RNA was determined using the Qubit® RNA Assay Kit (Life Technologies). For rRNA depletion, first, 1000ng of total RNA was used to remove the DNA contamination using Baseline-ZERO™ DNase (Epicentre) following the manufacturer's instructions followed by purification using the RNA Clean & Concentrator-5 columns (Zymo Research). DNA free RNA samples were used for rRNA removal by using RiboMinus™ rRNA Removal Kit (Bacteria; Thermo Fisher Scientific) and final purification was performed using the RNA Clean & Concentrator-5 columns (Zymo Research). rRNA depleted samples were used for library preparation using the KAPA mRNA HyperPrep Kits (Roche) by following the manufacturer's instructions. Following the library preparation, the final concentration of each library was measured using the Qubit® dsDNA HS Assay Kit (Life Technologies), and average library size for each was determined using the Agilent 2100 Bioanalyzer (Agilent Technologies). The libraries were then pooled in equimolar ratios of 0.75nM, and sequenced paired end for 300

cycles using the NovaSeq 6000 system (Illumina). RNA sequencing was conducted by MR DNA (Molecular Research LP). RNAseq analysis was performed using ArrayStar V15 for differential expression data with p-values ≤ 0.01, whereas R-package, DESeq2 (201) was used for differential expression data with p-values ≤ 0.05.

3.5.4. Metabolite extraction

After cultivation, utilized myxobacterial plates were manually diced and extracted with excess EtOAc. Pooled EtOAc was filtered and dried *in vacuo* to provide crude extracts for LC-MS/MS analysis. LC-MS/MS analysis of the extracted samples was performed on an Orbitrap Fusion instrument (Thermo Scientific, San Jose, CA) controlled with Xcalibur version 2.0.7 and coupled to a Dionex Ultimate 3000 nanoUHPLC system. Samples were loaded onto a PepMap 100 C18 column (0.3 mm × 150 mm, 2 μm, Thermo Fisher Scientific). Separation of the samples was performed using mobile phase A (0.1% formic acid in water) and mobile phase B (0.1% formic acid in acetonitrile) at a rate of 6 μL/min. The samples were eluted with a gradient consisting of 5 to 60% solvent B over 15 min, ramped to 95 % B over 2 min, held for 3 min, and then returned to 5% B over 3 min and held for 8 min. All data were acquired in positive ion mode. Collision-induced dissociation (CID) was used to fragment molecules, with an isolation width of 3 m/z units. The spray voltage was set to 3600 volts, and the temperature of the heated capillary was set to 300 °C. In CID mode, full MS scans were acquired from m/z 150 to 1200 followed by eight subsequent MS2 scans on the top eight most abundant peaks. The orbitrap resolution for both the MS1 and MS2 scans was 120000. The expected mass accuracy was <3 ppm. MZmine 2.53 was used to generate extracted ion chromatograms (202–204).

3.5.5. XCMS-MRM analysis.

Generated data were converted to .mzXML files using MS-Convert. Multigroup analysis of converted. mzXML files was done using XCMS-MRM and the default HPLC/Orbitrap [136] parameters (205,206). Within the XCMS-MRM result tables, determination of signal-impacted detected features was afforded by filtering results for those with a $p \leq 0.02$.

3.6. Acknowledgements

I appreciate funding and support from the National Institute of Allergy and Infectious Diseases (R15AI137996) and the National Institute of General Medical Sciences of the National Institutes of Health (P20GM130460). I thank Scot E. Dowd at MR DNA, Molecular Research LP for assistance throughout sequencing services provided, Dr. Sandeep Misra Manager of the Analytical and Biophysical Chemistry Core associated with the Glycoscience Center of Research Excellence (GlyCORE; P20GM130460) for LC-MS/MS analysis. I also thank Prof. Peter Zee for his courtesy of gifting us *M. xanthus* GJV1 strain.

Chapter 4

Features associated with predation avoiding *Pseudomonas putida* phenotype selected by *Cystobacter ferrugineus*

4.1. Abstract

Predator-prey experiments utilizing myxobacteria have provided details into predatory mechanisms and features that facilitate the consumption of prey. However, prey resistance to myxobacterial predation remains underexplored. Utilizing a predator-prey pairing that included the myxobacterium, *Cystobacter ferrugineus,* with *Pseudomonas putida* as prey, we infrequently observed surviving phenotype capable of eluding predation. Comparative transcriptomics between parent *P. putida* and the survivor phenotype suggested that increased expression of genes responsible for iron acquisition, genes associated with mucoid conversion, efflux pumps, and various membrane features contribute to predator avoidance. The *P. putida* survivor phenotype was confirmed to be producing more pyoverdine, phenazine-1-carboxylic acid, alginate and demonstrated resistance to antibiotics kanamycin, gentamicin, and tetracycline than parent *P. putida*. The survivor phenotype also benefited from increased predator avoidance during subsequent predation assays. These results demonstrate the utility of myxobacterial predator-prey models and provide insight into prey defenses in response to predatory stress that might contribute to phenotypic diversity and the structure of bacterial communities.

4.2. Introduction

Abundant within soils and marine environments, predatory myxobacteria contribute to nutrient cycling within the microbial food web (3,10,207,208). Myxobacteria are prolific producers of antimicrobial specialized metabolites and display a cooperative, swarming predation strategy that can be readily reproduced and monitored within laboratory settings, making them uniquely appropriate for the assessment of predator-prey interactions (3,10,54,207). Broadly considered generalist predators, myxobacteria capably predate a range of prey, including both Gram-negative and Gram-positive bacteria as well as fungi (43,54). Constitutive production of specialized metabolites and lytic proteins are often associated with this predatory range, and a variety of metabolites and enzymatic features have been reported to benefit predation (26,27,53,106).

However, relatively few examples of prey resistance to myxobacterial predation have been reported (98). Compared to features associated with bacterial strategies to avoid protozoan predators, prey avoidance of predatory myxobacteria remains underexplored (209–213). Examples of prey responses correlated with resistance to myxobacterial predation include *Escherichia coli* biofilm formation (33), *Bacillus subtilis* sporulation and production of bacillaene (34,105), *Bacillus licheniformis* glycosylation of the predation-associated metabolite myxovirescin A (36), galactoglucan exopolysaccharide production, and increased melanin production by *Sinorhizobium meliloti* (32,35), and formaldehyde secretion by *Pseudomonas aeruginosa* (98). All of these features were discovered from predator-prey experiments utilizing the model myxobacterium *M. xanthus*. Considering these diverse mechanisms opted by different prey organisms, we suspect the development of predator-prey pairings that include other myxobacterial prey bacteria might provide additional insight into prey resistance to myxobacterial predation. For our predator-prey experiments, the soil-dwelling myxobacterium *Cystobacter*

ferrugineus strain Cbfe23 (139) was included due to a favorable growth profile and capability to quickly consume *P. putida* during standard predation assays. Also found within soils, root colonizing *P. putida* was chosen as prey due to an established ability to resist protozoan grazers (211). Initial predator-prey experiments provided a *P. putida* phenotype capable of avoiding *C. ferrugineus* predation. Herein we report the generation and myxobacterial predator avoidance of a *P. putida* phenotype using standard predator-prey experiments, differential gene expression data comparing the survivor phenotype with parent *P. putida*, and traits observed that potentially contribute to predator avoidance.

4.3. Results

4.3.1. Selection of *P. putida* phenotype avoiding predation

The predatory stress from the prokaryotic and eukaryotic predators (32–36,105,209–213) and sometimes competition for nutrients (71,214,215) result in predation avoidance mechanisms in the prey bacteria. Previously, *P. putida* has exhibited resistance to the predation of its protozoan grazers (211). To identify any such predation avoidance of *P. putida* when interacting with a bacterial predator, we chose to utilize a culture-based predation assay on solid agar media and investigated predatory interaction between a myxobacterium *C. ferrugineus* predator and *P. putida* prey. Utilizing predation assays (216) where an inoculum of *C. ferrugineus* was introduced to the edge of an established spot of *P. putida*, we considered swarming overtaking the *P. putida* spot with no visible prey biomass remaining to be an endpoint of predation. Typically, *C. ferrugineus* swarmed *P. putida* with no visible prey biomass within three days of co-cultivation on nutrient-free WAT agar **(Figure 4.1A)**. However, one spot of *P. putida* from the initial ten assays provided minimally consumed and readily observable biomass of *P. putida* remaining on the assay plate even after 14 days of co-culturing **(Figure 4.1B)**. To access the viability of this remaining *P.*

putida biomass, we cultured it on an LB agar plate. Interestingly, the resulting colonies were smaller **(Figure 4.1D)** compared to the *P. putida* type strain that we utilized in this study **(Figure 4.1C)** and appeared after 36 h compared to the 18 h incubation time of *P. putida*. To see the reoccurrence of this phenomenon, we accessed 90 more independent predation assays where all *P. putida* spots were utilized from an individual colony culture. Among these, 50 assays were performed on nutrient-free WAT agar and 40 on nutrient-rich VY/2 agar plates. In these replicates, we again found minimally consumed and readily observable biomass of *P. putida* twice each from the nutrient free and nutrient rich media. These undigested *P. putida* prey when struck on LB agar, the colonies that appeared from the individual collected phenotype were also small like observed from the first replicate **(Figure 4.1D)**. Further in this study, we named this small colony variant of *P. putida* as the "survivor *P. putida* phenotype" and the utilized *P. putida* type strain as "parent *P. putida"*.

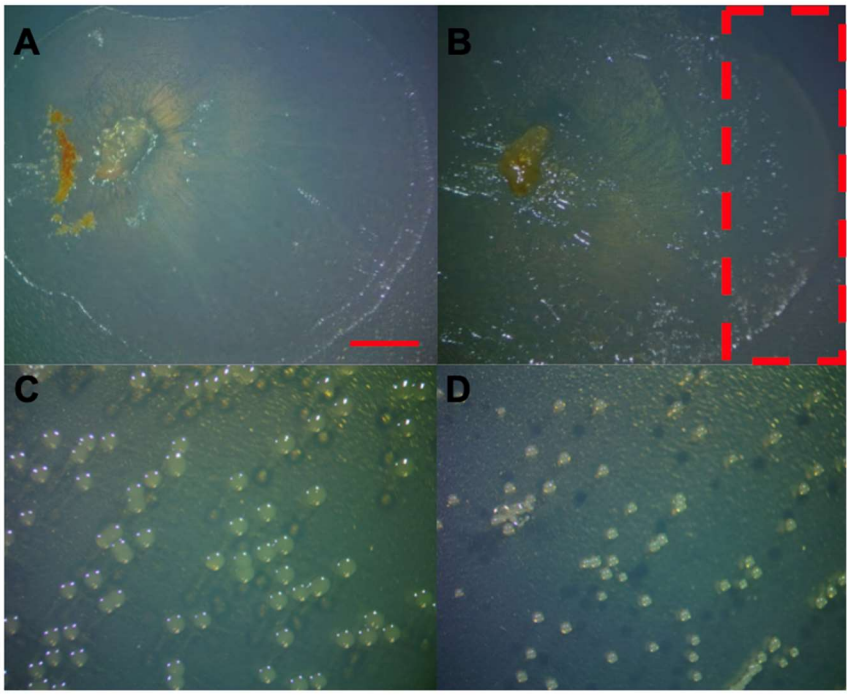

Figure 4.1. *C. ferrugineus* predation on *P. putida*. (A) Predation on type strain *P. putida* (labeled as "parent *P. putida*") with complete *C. ferrugineus* swarming on prey spot in 3 days, (B) type strain *P. putida* depicting predator avoidance (labeled as "survivor phenotype"). No full swarming observed till day 14 of co-culturing. Prey spot under red-block survived predation. Comparison of colony sizes of (C) parent *P. putida* (D) *P. putida* survivor phenotype depicting small colony variant. all scale bars depict 1mm.

4.3.2. *P. putida* survivor eludes subsequent predation of *C. ferrugineus*

Microcolonies or small colonies variants are previously observed for *Pseudomonas* sp. CM10, *P. aeruginosa*, and *Serratia marcescens* and protect them from their protozoan grazers (217–219). To confirm the predator avoidance associated with the small colony variant survivor phenotype in our study, we performed subsequent predation assays. The predation assays were performed as described previously, with predator cells directly introduced to the edge of the established prey spot on a nutrient-free WAT agar (216). Myxobacterial swarming overtaking the *P. putida* spot with no visible prey biomass remaining to be an endpoint of predation. Typically, *C. ferrugineus* swarmed over parent *P. putida* in 3 days of co-cultivation **(Figure 4.2A & 4.2C)**. However, it took almost 12-14 days to swarm over the survivor phenotype **(Figure 4.2B & 4.2C)**.

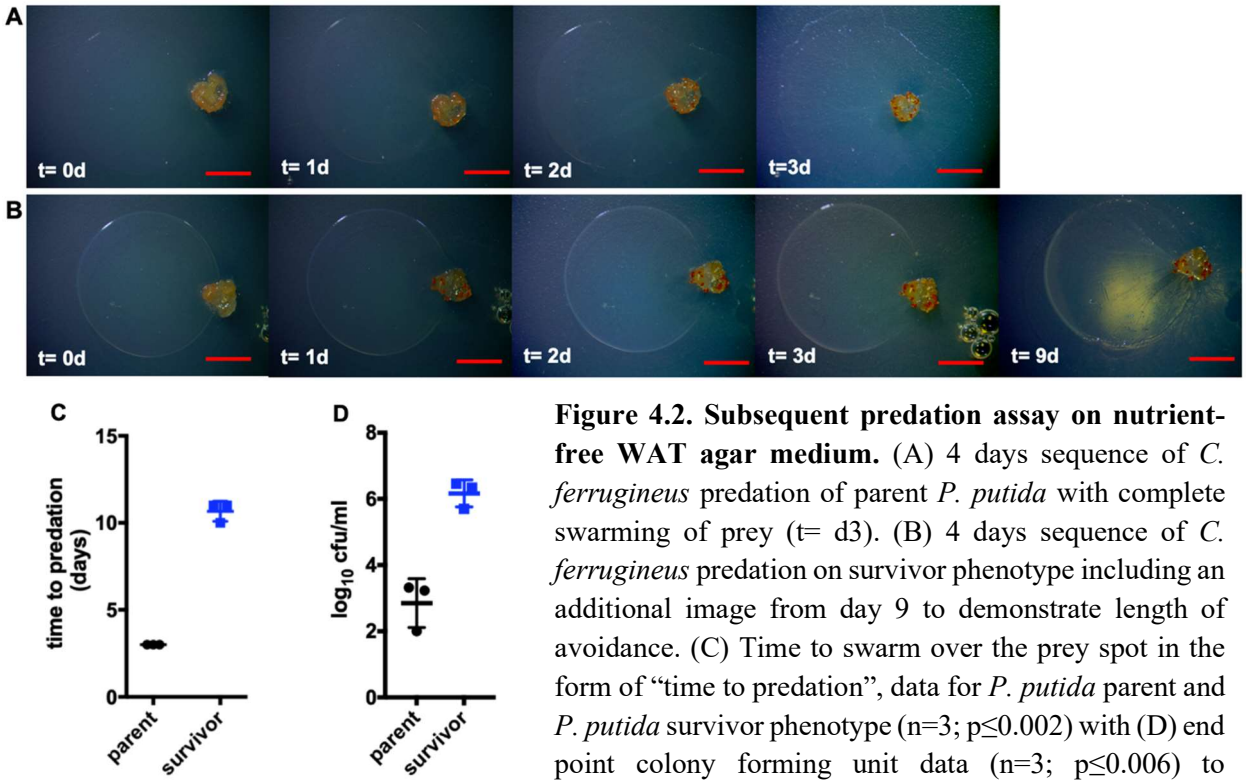

Figure 4.2. Subsequent predation assay on nutrient-free WAT agar medium. (A) 4 days sequence of *C. ferrugineus* predation of parent *P. putida* with complete swarming of prey (t= d3). (B) 4 days sequence of *C. ferrugineus* predation on survivor phenotype including an additional image from day 9 to demonstrate length of avoidance. (C) Time to swarm over the prey spot in the form of "time to predation", data for *P. putida* parent and *P. putida* survivor phenotype (n=3; $p \leq 0.002$) with (D) end point colony forming unit data (n=3; $p \leq 0.006$) to determine differences in cell viabilities post-swarming. Unpaired t-test with Welch's correction used for statistical analyses included in (D) and (E); all scale bars depict 1mm.

For the assessment of efficiency of predation after full swarming of *C. ferrugineus* over the prey spot and complete visible digestion of prey biomass, we performed colony forming unit (CFU) assays to assess remaining viable prey cells. Exponentially fewer viable colonies of parent *P. putida* were observed from endpoint CFU assays (3-4 days for parent *P. putida*; 12-14 days for *P. putida* survivor phenotype) **(Figure 4.2D)**. It depicts that even though *C. ferrugineus* fully swarmed over the survivor *P. putida* on nutrient-free WAT agar media in 14 days **(Figure 4.2C)**, the predation efficiency remained lower. Also apparent from CFU assays, colonies of the survivor phenotype were consistently smaller **(Figure 4.1C)** when compared to parent *P. putida* **(Figure 4.1D)**. These observations suggest that the survivor phenotype survive subsequent predation of *C. ferrugineus*.

4.3.3. *P. putida* survivor competes to survive *C. ferrugineus* predation in the presence of nutrients

As we collected the undigested *P. putida* biomass from the nutrient-rich media as well in our preliminary predation assays; therefore, we performed the subsequent predation assays on nutrient-rich VY/2 agar media to identify the predator avoidance phenomenon in the presence of nutrients availability. Compared to parent *P. putida* predation (3 days) **(Figure 4.3A)**, no prey biomass degradation (predation) was visible on the VY/2 assay plates for the survivor phenotype **(Figure 4.3B)**. This suggests the availability of nutrients makes the survivor phenotype relatively more competent to avoid the *C. ferrugineus*. Additionally, instead of frontal attack at the predator-prey interface when exposed to parent *P. putida* **(Figure 4.3A)**, *C. ferrugineus* swarmed along the perimeter of the survivor phenotype **(Figure 4.3B)**. *C. ferrugineus* attack on survivor phenotype is parallel to *M. xanthus* predation strategy to predation avoiding mucoid *S. meliloti* phenotypes (35).

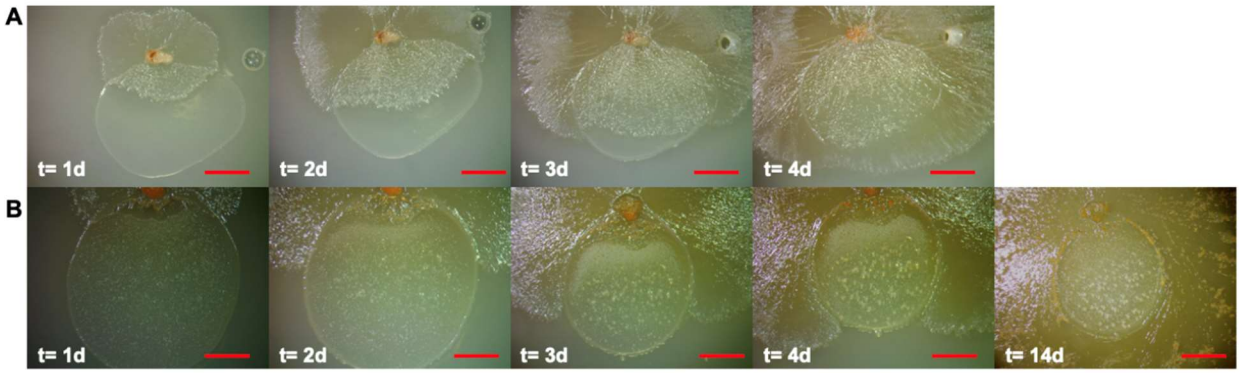

Figure 4.3. Subsequent predation assay on nutrient-rich VY/2 agar medium. (A) 4 days sequence of *C. ferrugineus* predation of *P. putida* with complete swarming of prey (t=d4). B) 4 days sequence depicting predator avoidance observed from *P. putida* survivor phenotype including an additional image from day 14 to demonstrate length of avoidance. Note the difference in swarming patterns with frontal swarming of parent (A) and perimeter swarming of survivor phenotype (B). all scale bars depict 1mm.

4.3.4. Differential gene expression of survivor phenotype

To identify the differentially regulated genes in the survivor *P. putida* phenotype compared to parent *P. putida*, we performed comparative transcriptomics. Utilizing RNA sequencing, we conducted comparative transcriptomic experiments between the parent *P. putida* (control) and the survivor phenotype. For this analysis, we employed three samples collected independently out of five initially survived *P. putida* survivor phenotypes. This comparative analysis determined that 1,178 genes were down-regulated ≥4-fold and 122 genes were up-regulated ≥4-fold across the survivor phenotype replicates when compared to parent *P. putida* replicates ($n=3$; $p \leq 0.05$).

Considering up-regulated genes from the survivor phenotype with the highest fold change values, apparent differences in overexpressed features specific to the survivor phenotype included genes involved in siderophore production, mucoid conversion, and a variety of membrane-associated proteins **(Figure 4.4A)**. Associated with iron limiting conditions, a TonB-dependent hemin, ferrichrome receptor (WP_016501290.1), a Ferric iron ABC transporter, iron-binding

protein (WP_016501876.1), a Bacterioferritin (WP_143999490.1), and a Bacterioferritin-associated ferredoxin (WP_016488781.1) was upregulated in the survivor phenotype. The TonB-dependent hemin, ferrichrome receptor, the Ferric iron ABC transporter are responsible for the transportation of siderophore, whereas the Bacterioferritin and the Bacterioferritin-associated ferredoxin are responsible for iron storage and iron release under iron depleted conditions,

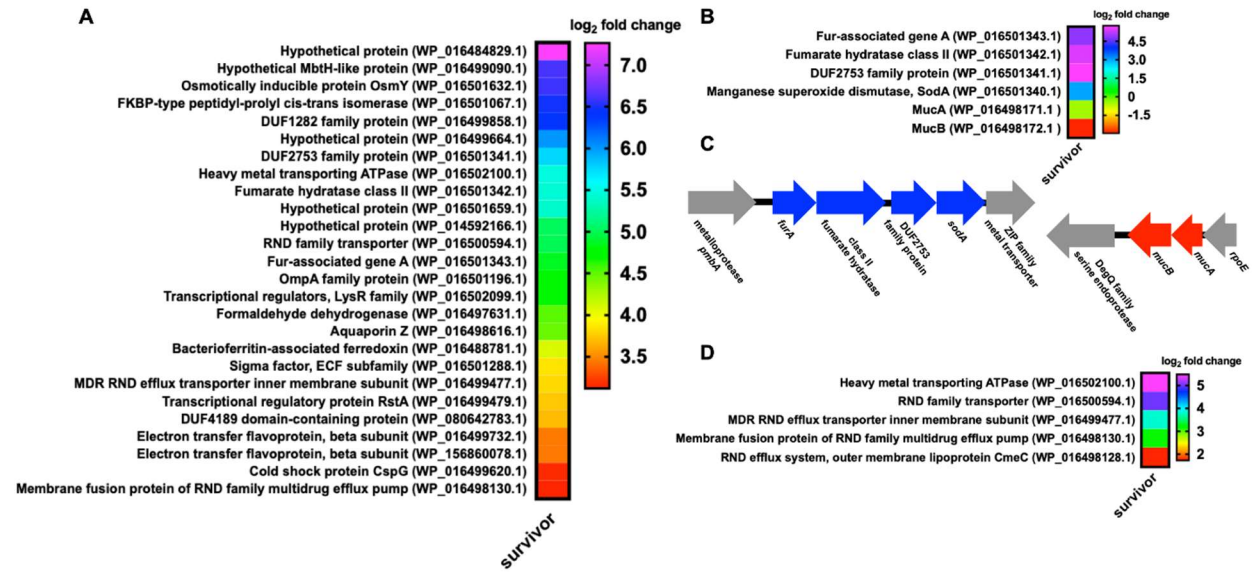

Figure 4.4. Differentially expressed genes in survivor phenotype compared to parent *P. putida*. (A) Most abundantly over-expressed genes from survivor phenotype when compared to predator unexposed *P. putida*. (B) Up-regulated features associated with alginate production and (C) the associated genomic context for each from (B). (D) Up-regulated transport proteins including those associated with antibiotic efflux. All data depicted as an averages from 3 biological replicates ($p \leq 0.05$).

respectively (220,221). Also, associated with iron limitation, regulatory and biosynthetic genes contributing to the production of the siderophore pyoverdine were significantly up-regulated in the survivor phenotype. These included PvdA an L-ornithine monooxygenase (WP_016499102.1) and PvdH a diaminobutyrate-2-oxoketoglutarate transaminase (WP_016498669.1), both involved in pyoverdine precursor biosynthesis, a regulatory transcription factor PvdS (WP_016498655.1), a proximal MbtH-like protein (WP_016499090.1), and a core nonribosomal peptide synthetase

homologous to PvdL from *P. aeruginosa* (NP_746359.1) **(Figure 4.5A)** (222–225). Upregulation of the genes responsible for the iron acquisition suggest that the survivor phenotype probably was selected under high iron competing interaction. Iron competition is common in different bacterial interactions (71,214,215,226). Previously enhanced production of the primary myxobacterial siderophore myxochelin by *M. xanthus* contributed to an iron-restrictive environment and triggered production of the pigmented antibiotic actinorhodin from *S. coelicolor* (70,71).

A 4 genes operon including a ferric uptake regulatory (*furA*) associated gene (WP_016501343.1), a fumarate hydratase (WP_016501342.1), a manganese superoxide dismutase (*sodA*) (WP_016501340.1), and a hypothetical protein with a conserved DUF2753 domain (WP_06501341.1) was significantly up-regulated in the survivor phenotype **(Figure 4.4B & 4.4C)**. Interestingly, expression of this operon from *P. aeruginosa* in response to iron limitation leads to elevated alginate production, an exopolysaccharide composed of mannuronic acid and guluronic acid monomers, and increased mucoidy (227,228). It also corroborates our observation of small colony variance from the survivor phenotype, as *P. aeruginosa* production of alginate overproduction is associated with small colony variants (227,228). Notably, the alginate regulatory elements MucA (WP_016498171.1) and MucB (WP_016498172.1) were both significantly down regulated in the survivor phenotype **(Figure 4.4B)**. The anti-sigma factor MucA and the associated binding partner MucB inhibit mucoid conversion by sequestering the alternative sigma factor AlgU required for alginate production in *P. aeruginosa* (229–232). Increased transcription from the 4 genes, *furA* operon combined with decreased transcription of MucA and MucB, indicates that mucoid conversion might contribute to predator avoidance which parallels *Pseudomonas* sp. CM10, *P. aeruginosa*, and *Serratia marcescens* predatory avoidance mechanisms when exposed to grazing amoeba (217–219).

The survivor phenotype also demonstrated numerous efflux and transport proteins among the most up-regulated genes **(Figure 4.4D)**. Upregulated efflux genes included inner (WP_016498130 and WP_016499477.1) and outer (WP_016498128.1) membrane components highly homologous to the AcrAD-TolC-type multidrug resistance-nodulation-division (RND) family of efflux pumps and the Mex RND efflux pumps known to facilitate *P. aeruginosa* resistance to aminoglycosides and tetracyclines (233–235). Genes encoding features homologous to multidrug efflux pumps contributing to the virulence of human pathogens were also up-regulated in the survivor phenotype, including a P-type ATPase (WP_016502100) and an additional RND/MmpL (Mycobacterial membrane protein Large) protein (WP_016500594.1) **(Figure 4.4D)**.

Interestingly, among other highly expressed genes by the survivor phenotype was included a formaldehyde dehydrogenase (Fdh) (WP_016497631.1). A recent observation suggests formaldehyde secretion and subsequent higher expression of formaldehyde dehydrogenase to be a predation-resistance trait of *P. aeruginosa* (98). Higher expression of Fdh by the survivor *P. putida* suggests a common strategy to avoid predation might be employed by *Pseudomonas* genus. A variety of membrane-associated proteins were also overexpressed in the survivor phenotype, including an osmotically inducible protein OsmY (WP_0016501632.1), an outer membrane protein A (OmpA) family protein (WP_016501196.1), an FKBP-type peptidyl-prolyl cis-trans isomerase (WP_0165010671), an aquaporin (WP_016498616.1), and a DUF1282 domain-containing hypothetical protein from the Yip1 superfamily (WP_016499858.1) **(Figure 4.4A)**. Afforded these observed differences in gene expression, utilizing classical microbiological assays, we sought to determine if the survivor phenotype demonstrated increased production of the siderophore pyoverdine, increased mucoidy, and antibiotic resistance.

4.3.5. Increased pyoverdine production by survivor phenotype

Significantly upregulated features associated with pyoverdine biosynthesis previously noted from the survivor phenotype in our transcriptomic data suggested that increased pyoverdine production might be an observable survivor trait. Fluorescence of extracellular pyoverdine was quantified from clarified media of parent *P. putida* and the survivor phenotype using methodology established by Imperi *et al* (236,237). Indicative of increased pyoverdine secretion, extracellular fractions from the survivor phenotype exhibited a 3-5 fold increase in fluorescence when compared to extracellular fractions from parent *P. putida* **(Figure 4.5)**. Although the genome of the *P. putida* type strain includes a pyoverdine biosynthetic gene cluster, no structurally elucidated pyoverdines have been characterized from the *P. putida* type strain, and these results merely suggest the presence of fluorescent pyoverdine-like metabolites potentially produced by the strain. Regardless, these results corroborate overexpression of pyoverdine biosynthetic pathway components observed in our transcriptomic analysis and suggest that siderophore pyoverdine production may contribute towards the competition in co-cultured condition.

4.3.6. Increased production of phenazine-1-carboxylic acid by survivor phenotype

Untargeted mass spectrometry was used to identify additional differences in detectable quantities of *P. putida* metabolites, comparing organic phase extracts from parent *P. putida* and the survivor phenotype. Initial principal component analysis (PCA) score plot of resulting data utilizing XCMS (206) demonstrated the survivor phenotype is metabolically distinct from the parent *P. putida* **(Figure 4.6A)**. Additional analysis using Global Natural Product Social Molecular Networking (GNPS) (135) resulted in a library hit for phenazine-1-carboxylic acid

([M+H]$^{+}$=225.066) that was only observed in extracts from the survivor phenotype **(Figure 4.6B)**. Subsequent comparison utilizing XCMS-MRM (206) provided the statistical significance (n=3; p=0.0509) in detected phenazine-1-carboxylic acid (P1CA) between extracts from parent *P. putida* and the survivor phenotype. Interestingly, phenazine production in *P. aeruginosa* contributes to redox maintenance during biofilm formation and promotes efflux-based antibiotic resistance (238–240). Despite no significant change in expression of putative phenazine biosynthesis genes *phzD* (SUD74861.1) and *phzF* (SUD71919.1) from our comparative transcriptomic data (241–244).

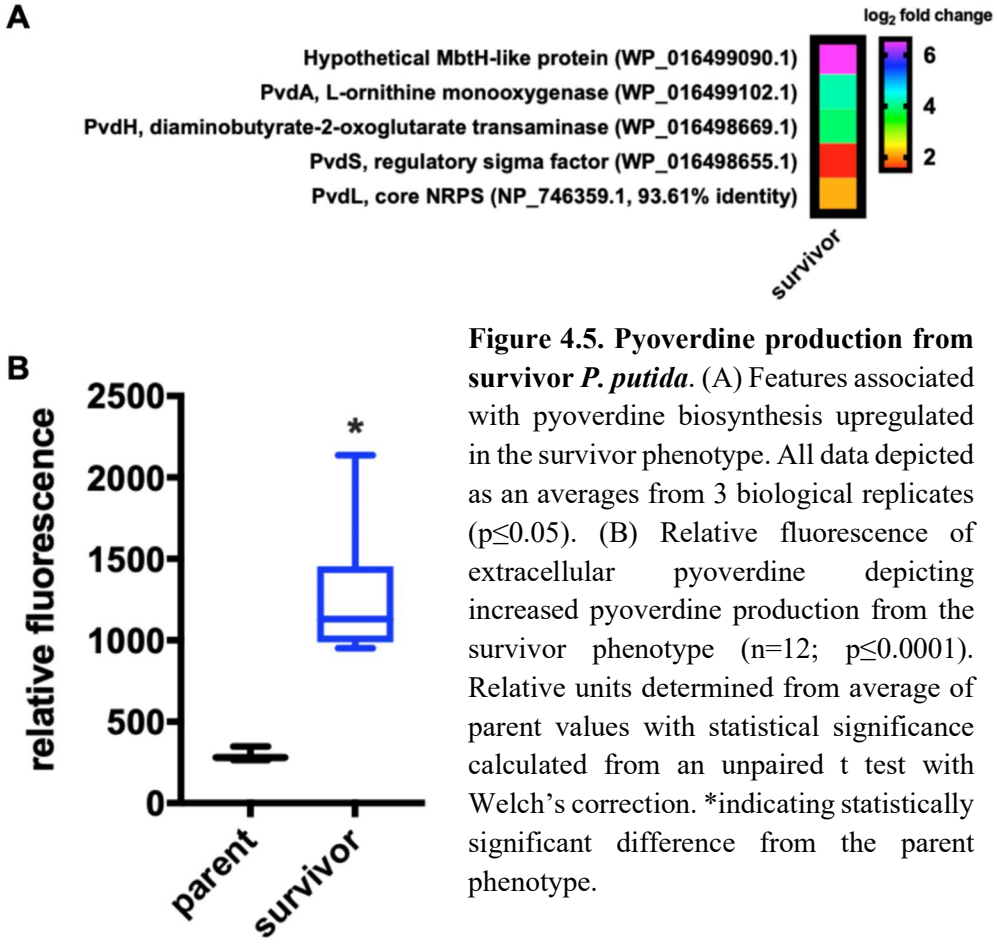

Figure 4.5. Pyoverdine production from survivor *P. putida*. (A) Features associated with pyoverdine biosynthesis upregulated in the survivor phenotype. All data depicted as an averages from 3 biological replicates ($p \leq 0.05$). (B) Relative fluorescence of extracellular pyoverdine depicting increased pyoverdine production from the survivor phenotype (n=12; $p \leq 0.0001$). Relative units determined from average of parent values with statistical significance calculated from an unpaired t test with Welch's correction. *indicating statistically significant difference from the parent phenotype.

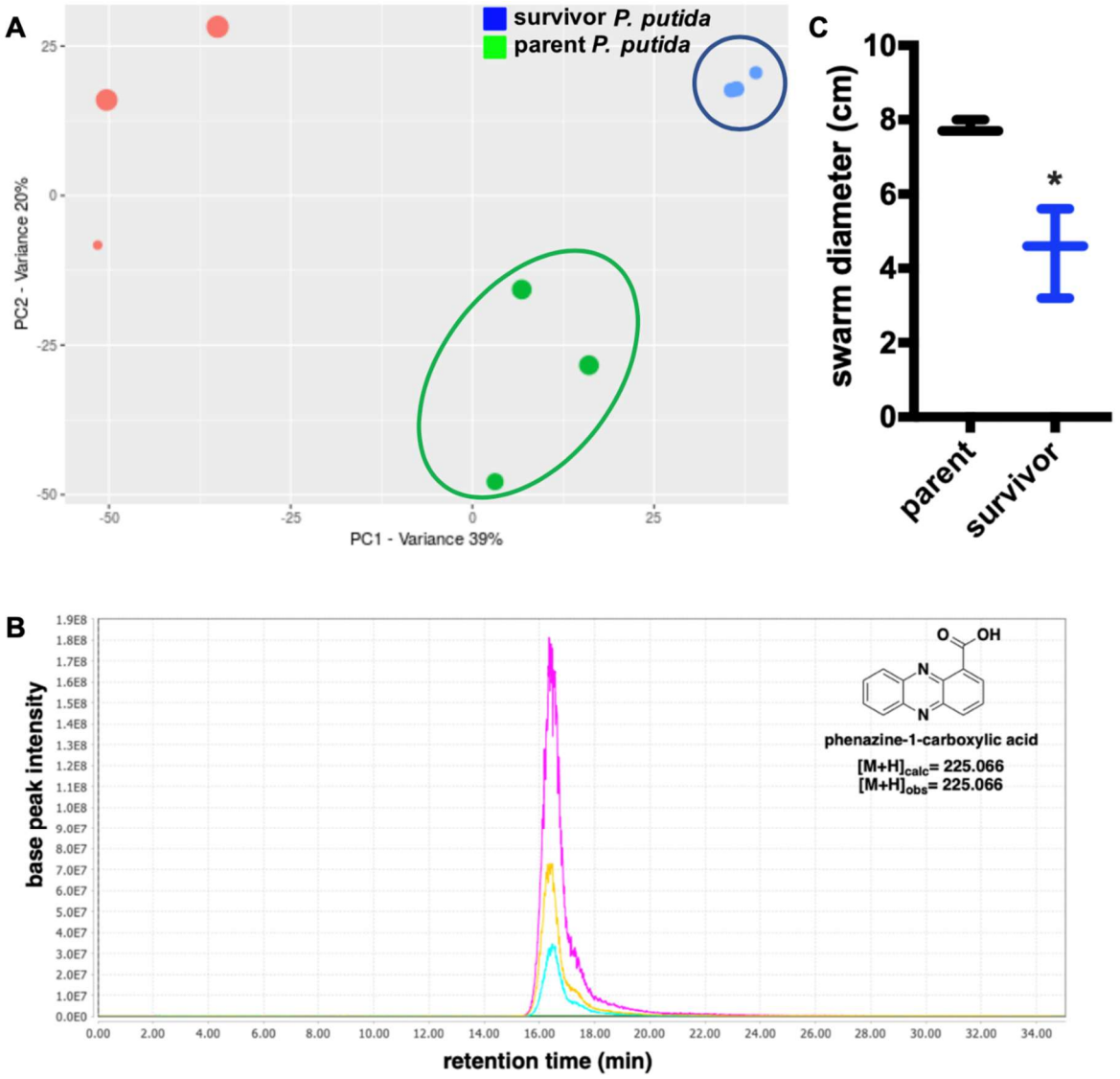

Figure 4.6. Metabolic crude extract analysis of both phenotypes of *P. putida*. (A) Principal component analysis (PCA) score plot of untargeted mass spectrometry data from the crude metabolic extracts from parent *P. putida* (green) and *P. putida* survivor (blue) with extracts from media control in red. Score plot is depicting a differential metabolic profile of two *P. putida* phenotypes. XCMS v3.7.1 was used for constructing PCA score plot. (B) Extracted ion chromatograph (224.9-225.1 m/z) depicting presence of phenazine-1-carboxylic acid in extracts from survivor phenotype replicates (n=3; magenta, yellow, cyan) and absence in extracts from all three parent *P. putida* replicates; n=3; p=0.0509. Chromatograph rendered with MZmine v2.37, and XCMS v3.7.1 was used for statistical analysis. (C) Swarm diameter of *C. ferrugineus* on a lawn of culture supernatant of parent, and survivor *P. putida* phenotypes p=0.0386; statistical significance calculated from an unpaired t test with Welch's correction. *indicating statistically significant difference from the parent phenotype.

We suspect that higher quantities of P1CA detected in extracts from the survivor phenotype may contribute to the increased transcription of efflux pump components **(Figure 4.4D)** observed from the survivor phenotype. However, associations between phenazine production and efflux-mediated resistance have only been reported from *P. aeruginosa*, and any parallels potentially observed in our data require further investigation.

Considering phenazine production has been observed to protect *Pseudomonas aureofaciens* from predatory myxobacteria (92), we sought to investigate the impact of culture supernatant on the swarming of *C. ferrugineus*. After growing parent and survivor phenotypes of *P. putida* to OD_{600} of 1.5, we prepared a uniform lawn on VY/2 agar plate and spotted equal inoculum of *C. ferrugineus* at the center of prepared lawns. Notably, *C. ferrugineus* exhibited significantly smaller swarming diameter on the survivor lawn than the parent phenotype **(Figure 4.6C)**, suggesting that possibly P1CA production contributes to predator avoidance. However, considering we performed a swarming assay on the culture supernatant of *P. putida* phenotypes instead of pure P1CA, the possibility of additional components contributing to lower swarming of *C. ferrugineus* cannot be overlooked. Overall, these results suggest that the survivor phenotype produces significantly greater quantities of phenazine-1-carboxylic acid when compared to parent *P. putida*, and phenazine production contributes to its avoidance of myxobacterial predators.

4.3.7. Increased production of alginate by survivor phenotype

Alginate-based formation of mucoid biofilms has previously been associated with *Pseudomonas* sp. CM10, and *P. aeruginosa* avoidance of the protozoan grazer *Rhynchomonas nasuta* (217,218,245,246). Utilizing an established carbazole assay as well as alginate antibody dot blots (247–249), we sought to determine if the increased transcription of genes known to impact alginate production observed from the survivor phenotype resulted in increased production of alginate when compared to parent *P. putida*. Comparing supernatants from parent *P. putida* with the survivor phenotype, we observed that the survivor phenotype indeed produced more alginate when compared to parent *P. putida* that was not exposed to *C. ferrugineus* **(Figure 4.7)**. This result suggests like other *Pseudomonas* that employ alginate as a protective measure to avoid their eukaryotic predator, *P. putida* utilizes a similar strategy to avoid a prokaryotic predator.

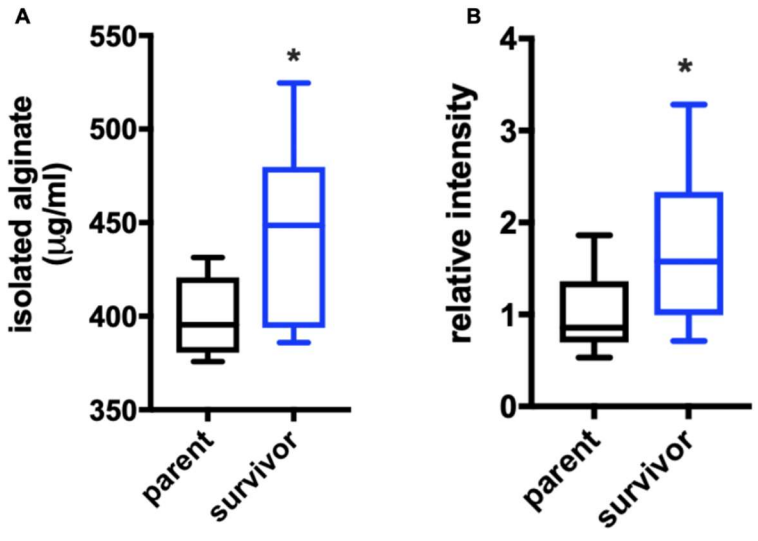

Figure 4.7. *P. putida* survivor phenotype produces higher quantities of alginate. (A) Isolated alginate concentration determined from carbazole assays depicting increased alginate production observed from the survivor phenotype (n=16; p≤0.02). (B) Relative intensities of alginate dot blots confirming alginate production observed from the survivor phenotype (n=10; p=0.039). Relative units determined from average of parent values with statistical significance calculated from an unpaired t test with Welch's correction. *indicating statistically significant difference from the parent phenotype.

4.3.8. Antibiotic resistance of survivor phenotype

We were interested in determining if the survivor phenotype exhibited antibiotic resistance, provided the observation that numerous transport proteins were overexpressed in the survivor phenotype **(Figure 4.4D)**, including RND-type efflux pumps known to contribute to *P. aeruginosa* antibiotic resistance. The survivor phenotype was capable of initially forming colonies on LB agar supplemented with the antibiotics gentamicin (10 µg/ml), kanamycin (50 µg/ml), and tetracycline (10 µg/ml), with no colonies from predation sensitive *P. putida* observed on identical media. Subsequent growth curve assays comparing parent *P. putida* **(Figure 4.8A)** with the survivor phenotype when grown in LB and LB supplemented with antibiotics **(Figure 4.8B)** confirmed that the survivor phenotype was uniquely resistant to gentamicin, kanamycin, and tetracycline. These results combined with the overexpression of efflux-associated proteins observed from the survivor phenotype confirms that *C. ferrugineus* selection provides prey that benefits from antibiotic resistance and suggests efflux-mediated antibiotic resistance to be involved in *P. putida* response to predatory stress.

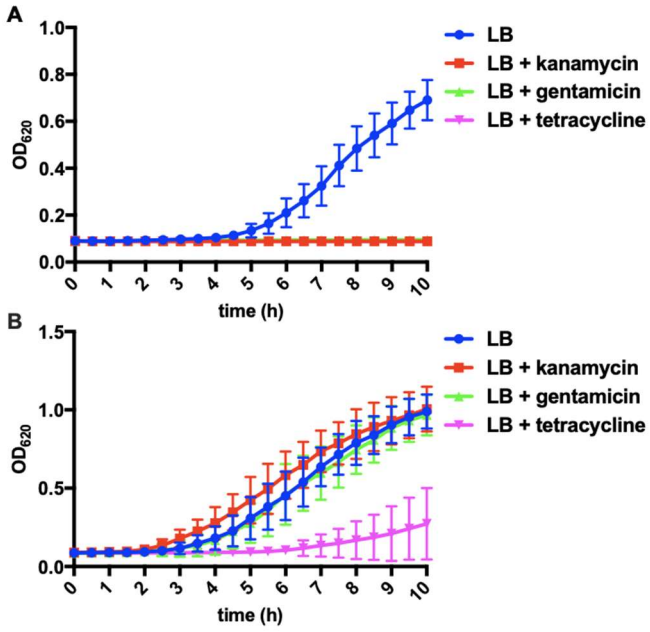

Figure 4.8. *P. putida* survivor phenotype demonstrates resistance to aminoglycosides and tetracycline antibiotics. Growth curves for (A) parent *P. putida* and (B) *P. putida* survivor phenotype depicting antibiotic resistance unique to the survivor phenotype (n=12). LB was supplemented with working concentrations of gentamicin (10 µg/ml), kanamycin (50 µg/ml), and tetracycline (10 µg/ml), where indicated.

4.4. Discussion

Compared to features associated with *P. putida* to avoid protozoan predators (211), the resiliency of *P. putida* during bacterial predator-prey interactions remained underexplored. The predator-prey experiments that utilize *M. xanthus* with various prey such as *B. subtilis* (26,34,105), *E. coli* (53,54), *S. melilotti* (32,35), *P. aeruginosa* (98), and *S. coelicolor* (70) have demonstrated that the predatory stress from myxobacterial predator contributes to the avoidance of predation. In this study, we investigated the predatory interaction of a myxobacterium *C. ferrugineus* with prey *P. putida*. We uncovered a *P. putida* phenotype that *C. ferrugineus* selected in the standard predation assays. Specifically, out of 100 independent predation assays, five times *P. putida* phenotype selection phenomenon occurred. Two times the phenotype was found when we performed assays on nutrient-rich VY/2 media plates and three times on the nutrient-free WAT agar media. All five selected phenotypes avoided subsequent predation by *C. ferrugineus* (data is provided for the three). Selection of the survivor phenotype on nutrient-free as well as nutrient-rich media suggest that instead of nutrient limitation, it's the predatory stress that resulted in the selection of the survivor phenotype. The observed rare occurrence of this phenomenon perhaps could be due to the variability in *C. ferrugineus* phenotype capable to provide an excessive predatory stress.

Utilizing comparative transcriptomics, we found that several features significantly upregulated in *P. putida* survivor phenotype. Comparative transcriptomics provided key features up-regulated in the *P. putida* survivor phenotype that are responsible for iron acquisition. Considering iron as an essential micronutrient for all life forms (220), this metal is a vital component of the competition among several bacterial interactions (71,214,215,226). Up-regulation of the siderophore pyoverdine biosynthetic pathway as well as increased pyoverdine in

extracellular extracts, along with observed upregulation of a TonB-dependent hemin, ferrichrome receptor (WP_016501290.1), and a Ferric iron ABC transporter (WP_016501876.1) (221) from the survivor phenotype suggest a competitive environment for the acquisition of iron. The survivor phenotype not only demonstrated upregulation of siderophore and associated receptor and transporter but also demonstrate other components required for iron acquisition, such as upregulated iron storage Bacterioferritin (WP_143999490.1), and a Bacterioferritin-associated ferredoxin (WP_016488781.1) responsible for the iron release in the cytosol under iron depleted conditions (220). Overall, the survivor phenotype depicts an iron-depleted predator-prey environment that resulted in its selection. Myxobacteria providing iron competing environment to their bacterial prey has been observed previously from *M. xanthus*. Where enhanced production of the primary myxobacterial siderophore myxochelin by *M. xanthus* contributed to an iron-restrictive environment and triggered production of the pigment actinorhodin from *S. coelicolor* (70,71).

Although no significant change in expression of putative phenazine biosynthesis genes *phzD* (SUD74861.1) and *phzF* (SUD71919.1) was found from our comparative transcriptomics data (241–244), the comparative metabolomics demonstrated the survivor phenotype produced phenazine-1-carboxylic acid. Interestingly, no phenazine-1-carboxylic acid was detected in the extracts from the parent *P. putida*. This also emphasizes the inter species competition and predatory stress triggers the production of antibiotics and parallels with the bacillaene production by *B. subtilis* to avoid *M. xanthus* predation (34). While phenazine production has been observed to protect *Pseudomonas aureofaciens* from predatory myxobacteria (92), the production of phenazine and pyoverdine by *P. aeruginosa* also provided it a competitive advantage against *E. coli* (250).

Several features associated with mucoid conversion were also up-regulated in the survivor phenotype, including a 4 genes operon responsible for elevated alginate production in *P. aeruginosa,* and the regulatory transcription factors MucA and MucB were downregulated (227–229,231). We also observed an upregulated OmpA family protein in the survivor phenotype. This OmpA family protein might also correlate with mucoid conversion in the survivor phenotype as *P. aeruginosa* phenotypes that upregulate expression of OmpA also overproduce alginate (251). We confirmed the increased alginate production by the survivor phenotype using established carbazole assays and anti-alginate dot blots. Alginate-based mucoid conversion, microcolonies, and biofilm formation have previously been associated with *Pseudomonas* sp. CM10 and *P. aeruginosa* avoidance of grazing amoeba and could also contribute to the small colony variation observed from our survivor phenotype (218,222,245). Additionally, adaptive mucoid phenotypes have been previously observed in response to myxobacterial predation (54), amoebal grazing (218), macrophages (252), and lytic phages (253). The observed differential attack pattern of *C. ferrugineus* during predator-prey interactions with the survivor phenotype parallel previous observation of mucoid *S. meliloti* phenotypes avoiding *M. xanthus* predation (35). These results provide a clear overlap between features utilized by different *Pseudomonas* species under stress. The findings also afford additional evidence that the coincidental selection of prey virulence factors reported from amoebal predatory stress (209) might also be observed from predator-prey interactions involving myxobacteria.

Comparative transcriptomics also revealed the upregulated key features associated with efflux pumps. Of these, 3 putative RND family transporter components with high homology to the MexAB-OprM and MexCD-OprM efflux systems known to mediate aminoglycosides and tetracyclines antibiotic resistance in *P. aeruginosa* were up-regulated in the survivor phenotype

(234,235). Also of note, the multidrug efflux pump CmeABC serves as a survival mechanism for *Campylobacter jejuni* when engulfed by the predatory amoeba *Acanthamoeba polyphaga* (254). Growth curve analysis determined that the *P. putida* survivor phenotype was indeed resistant to the aminoglycosides kanamycin and gentamicin as well as tetracycline. In contrast, susceptibility to all 3 of these antibiotics was observed from the parent *P. putida*. Although multidrug resistance is associated with *P. aeruginosa* pathogenicity, to the best of our knowledge multidrug resistance has not been observed in a predation survivor bacterium. Both efflux-mediated antibiotic resistance and mucoid conversion have also been attributed to the virulence of clinical isolates of *P. aeruginosa* (230,255–257). Collectively, in this study, we found features associated with the *P. putida* phenotype that overlaps with the features of other Pseudomonads avoiding their eukaryotic predator. Our study emphasizes the predatory stress from the prokaryotic predator as well as the eukaryotic predator selects the same features in different *Pseudomonas* species. It also emphasizes the utility of possibly a similar resistance mechanism utilized by Pseudomonas under the stress situation.

It is worth noticing that predatory stress contributes to the development of phenotypic traits in the prey bacteria overlapping with persistent clinical pathogens (209,213,255). As an example, clinical isolates of persistent *P. aeruginosa* from cystic fibrosis patients exhibit increased mucoidy and small colony variation as well as efflux-mediated antibiotic resistance (256,258,259). Other human pathogens that have demonstrated overlapping factors involved in both virulence and anti-predation strategies include *Legionella pneumophila*, *Escherichia coli*, *Vibrio cholerae*, *Campylobacter jejuni*, *Listeria monocytogenes*, *Mycobacterium leprae*, and *Yersinia enterocolitica* (209,213). Overlapping factors thus far observed to be associated with both virulence and predator avoidance include biofilm formation (212,217,246), quorum signal (260)

and siderophore (261) small molecule biosynthesis, toxin production (262–264), expression of transport proteins such as type III and type VI secretion systems (265,266) and antibiotic resistance-associated efflux pumps (254,267). While the impact of predatory selection on virulence factors have primarily been reported from predator-prey experiments with grazing amoeba, efforts to determine the influence of generalist predators on microbial communities have suggested that bacterial predators also drive adaptation of prey traits that overlap with virulence in bacterial pathogens (54). Recently, Nair *et al.* reported that during predator-prey interactions with *E. coli* prey, the predatory myxobacterium *Myxococcus xanthus* selects for 2 traits associated with virulence, mucoidy and increased expression of the outer membrane protease OmpT (54). Our study adds in these findings and provides the importance of exploring bacterial predator-prey interactions to unravel features overlapping with clinical pathogens.

4.5. Materials and Methods

4.5.1. Bacterial strains and cultivation

The myxobacterium *Cystobacter ferrugineus* strain Cbfe23, DSM 52764, was employed as the predator. Parent *Pseudomonas putida* type strain, ATCC 12633, and the predation selected *P. putida* survivor phenotype resulted were included as prey. *C. ferrugineus* was grown on VY/2 solid (1.4% w/v agar, 0.1% w/v $CaCl_2$ * 2 H_2O, 0.5% w/v Baker's yeast, 500 μM vitamin B12) media for 5-7 days. Luria-Bertani (LB) solid (1.5% agar) and liquid media were utilized for the cultivation of *P. putida*. All bacteria were grown at 30 °C.

4.5.2. Predation assays

Predation experiments were performed on WAT agar (1.5% w/v agar, 0.1% w/v $CaCl_2$, 20 mM HEPES) plates. Prey spot assay was performed as described by Seccareccia et al. (216). Briefly, *P. putida* prey was grown in LB liquid media on a rotary shaker (150 rpm) at 30 °C for 16-18 h. Next, the bacterial cultures were sedimented by centrifugation at 4,000 g for 15 min, and the sedimented cells were washed and resuspended in TM buffer (50 mM Tris HCl, pH 7.8, 10 mM $MgSO_4$) to an OD_{600} of 0.5. Then the agar plates were spotted with 150 µl of the freshly prepared bacterial suspensions, and the spots were dried in a laminar flow hood. Finally, equal size of *C. ferrugineus* was inoculated at the edge of the prey spot. The assay plates were incubated at 30 °C for 14 days or until the full visible swarming of *C. ferrugineus* on the prey spot. The assay was performed with 100 replicates, 60 replicates on WAT agar, and 40 replicates on VY/2 agar plates. Any prey spot with visible biomass of *P. putida* after day 14 was considered as survivor phenotype of *P. putida*, and five observed *P. putida* (three from WAT agar and two from the VY/2 agar plates) were acquired that remained visible after day 14 of the assay. These undigested biomasses of *P. putida* prey were struck on LB agar, and freezer stocks of the colonies appearing from the individual collected phenotype were prepared and stored in -80 °C.

For subsequent predation assays, parent *P. putida* (control) and the survivor phenotypes in triplicate were employed as prey. The direct spot assay was performed as mentioned above on nutrient-free WAT agar and nutrient rich VY/2 agar plates. Statistical significance of recorded time to predation reported was calculated using an unpaired t test with Welch's correction in Prism 7.0d.

4.5.3. CFU assays

The colony forming units (CFU) were calculated as described by DePas *et al.* (246). Briefly, after the full swarming of *C. ferrugineus* over the prey spot, the agar slab under the prey spot was excised and suspended in 2 mL phosphate buffer saline (PBS). Next, a dilution series from this solution was inoculated on the LB plates, and the plates were incubated at 30 °C for 18 hr. Then, CFU/mL was calculated from the viable colonies that appeared on the LB plates. Finally, the CFU/mL of the survivor was compared with CFU/mL of the parent *P. putida,* considered as a control. Statistical significance of all CFU assays was calculated using an unpaired t test with Welch's correction in Prism 7.0d.

4.5.4. RNA sequencing

Triplicate samples of parent *P. putida* (control) and *P. putida* survivor phenotype (obtained from the individual colonies of three independently selected survivor stocks stored in -80 °C) grown in LB at 30 °C for 18 h and pelleted via centrifugation were stored in RNA*later* solution for sequencing. The DNA from *P. putida* type strain cells (200 µL) was extracted using MagAttract HMW DNA Kit (Qiagen). The DNA was eluted in 100 uL AE buffer. The concentration of DNA was evaluated using the Qubit® dsDNA HS Assay Kit (Life Technologies). The library was prepared using Nextera DNA Flex library preparation kit (Illumina) following the manufacturer's user guide. 50 ng DNA was used to prepare the library. The sample underwent the simultaneous fragmentation and addition of adapter sequences. These adapters are utilized during a limited-cycle (6 cycles) PCR in which unique index was added to the sample. Following the library preparation, the final concentration of the library was measured using the Qubit® dsDNA HS Assay Kit (Life Technologies), and the average library size was determined using the Agilent 2100 Bioanalyzer

The library was diluted (to 6.5 pM) and sequenced paired end for 500 cycles using the MiSeq system (Illumina). Total RNA was isolated from triplicate samples of the parent *P. putida* control, the *P. putida* survivor phenotype using the RNeasy PowerSoil Total RNA Kit (Qiagen) following the manufacturer's instructions. 400 µL cell sample was used for extractions. The concentration of total RNA was determined using the Qubit® RNA Assay Kit (Life Technologies). For rRNA depletion, first, 1000 ng of total RNA was used to remove the DNA contamination using Baseline-ZERO™ DNase (Epicentre) following the manufacturer's instructions followed by purification using the RNA Clean & Concentrator-5 columns (Zymo Research). DNA free RNA samples were used for rRNA removal by using RiboMinus™ rRNA Removal Kit (Bacteria; Thermo Fisher Scientific), and final purification was performed using the RNA Clean & Concentrator-5 columns (Zymo Research). rRNA depleted samples were used for library preparation using the KAPA mRNA HyperPrep Kits (Roche) by following the manufacturer's instructions. Following the library preparation, the final concentrations of all libraries were measured using the Qubit® dsDNA HS Assay Kit (Life Technologies), and the average library size was determined using the Agilent 2100 Bioanalyzer (Agilent Technologies). The libraries were then pooled in equimolar ratios of 0.6 nM and sequenced paired end for 300 cycles using the NovaSeq 6000 system (Illumina). Differential expression between the resulting transcriptomes was calculated from pair-wise analysis of trimmed mean of M-values (TMM) normalized read counts (268) including fold change, counts-per-million (CPM), and associated p-values using the R-package, edgeR (269). Differential expression data with p-values ≤ 0.05 were considered statistically significant. Genome and RNA sequencing was conducted by MR DNA (Molecular Research LP). All raw RNAseq data is publicly available at the NCBI Sequence Read Archive (PRJNA577468).

4.5.5. Assessment of extracellular pyoverdine

Extracellular pyoverdine fluorescence was detected from supernatants following methodologies Imperi *et al.* and Barrientos-Moreno *et al.* (236,237). Clarified supernatants from overnight cultivation of 200 µl LB cultures of parent *P. putida* (control) and the survivor phenotype adjusted to an OD_{600} of 0.07 were generated by centrifugation (10,000 rpm, 15m). Fluorescence was recorded at 455 nm upon excitation at 400 nm using a CLARIOstar microplate reader (BMG Labtech Inc., Cary, NC, USA). Sterile LB was used as a negative control to assess background fluorescence. Average relative fluorescence for supernatants from parent *P. putida* (control) and survivor phenotype cultures (n=12) are reported with statistical significance was calculated using an unpaired t test with Welch's correction in Prism 7.0d.

4.5.6. Metabolite extraction and analysis

For metabolomic analysis, the survivor phenotype and parent *P. putida* (control) were cultivated on VY/2 agar plates as described in the predation assay. VY/2 agar plates with TM buffer were used as a negative control. The plates were incubated at 30°C for 14 days. After the incubation period, agar was chopped and extracted with ethyl acetate (EtOAC). The EtOAc extracts were dried in vacuo to produce crude extracts for LC-MS/MS analysis. The crude extracts from each condition were generated in triplicate and analyzed as described in Adaikpoh *et al.* (137). LC-MS/MS generated data was converted to .mzML files using MS-Convert, and the GNPS platform (135) was utilized as a dereplication tool to look for the library hits within publicly available natural products libraries. For the statistical analysis, using XCMSonline (206), multigroup analysis with HPLC orbitrap default settings was employed. MZmine 2.53 was used to generate extracted ion chromatograms (202–204).

4.5.7. Swarming assay with culture supernatant of parent and survivor *P. putida*

P. putida parent and *P. putida* survivor were grown in LB media overnight up to OD_{600} of 1.5. Culture supernatants were acquired after centrifuging the cell cultures at 10,000 rpm for 15 minutes. The supernatants were filtered with a 0.2 µl filter paper. 1 mL of each filtered supernatant was used to make a uniform lawn on a VY/2 agar plate. An equal amount of *C. ferrugineus* was spotted in the middle of the lawn and incubated for 5 days at 30°C. On the fifth day, the diameter of *C. ferrugineus* was measured. Statistical significance was calculated using an unpaired t test with Welch's correction in Prism 7.0d.

4.5.8. Carbazole assays

The alginate was isolated according to Jones *et al*. (270). In brief, both *P. putida* phenotype, the parent and the survivor were grown overnight in 2 ml LB media and adjusted to an OD_{600} of 1.00. Following centrifugation, 1 ml of supernatant was treated with 2% cetyl pyridinium chloride to precipitate the alginate. The precipitated alginate was further collected by centrifugation. It was resuspended in 1 M NaCl and then re-precipitated in cold isopropanol. Precipitated alginate was suspended in 150 µl 0.9% (w/v) saline solution. Following established protocols (247,248), a 50 µL aliquot of the isolated alginate and a dilution series of standard alginic acid (Sigma) were mixed with 200 µL of a solution of 25 mM sodium tetraborate in sulfuric acid and added in a 96-well plate. Next, the plate was heated for 10 min at 100 °C in an oven. After cooling at room temperature for 15 min, 50 µl of a 0.125% carbazole solution in absolute ethanol was added. The plate was re-heated at 100 °C for 10 min in an oven and cooled down at room temperature for 15 min. The plate was read in a CLARIOstar microplate reader at a wavelength of 550 nm. Quantities of alginate per sample (µg/ml) were calculated from the resulting standard curve of purchase alginic acid.

4.5.9. Anti-alginate dot plots

Alginate dot blots were generated using methodology from Lorenz *et al.* with slight modifications (249). Alginate was isolated as previously described, suspended in 150 µl 0.9% (w/v) saline solution, and 2 µl aliquots were pipetted onto a nitrocellulose membrane. After air-drying for 30 min, Tris buffered saline-Tween 20 (TBST) with 5% bovine serum albumin (BSA) was used for membrane blocking for 1 h. Membrane was then washed 3x for 10 min with TBST and subsequently incubated with the alginate antibody (Sigma, monoclonal, anti-mouse) overnight at 4°C. The following day, the membrane was washed 3x for 10 min with TBST, incubated with IRDye 800CW Goat anti-mouse (Sigma) for 30 min, rinsed 2x with TBST, and imaged on a LI-COR Odyssey. Average relative intensities for imaged blots comparing isolated alginate from parent *P. putida* with alginate isolated from the survivor phenotype (n=10) are reported with statistical significance was calculated using an unpaired t test with Welch's correction in Prism 7.0d.

4.5.10. Antibiotic susceptibility assays

The standard growth curve assay was employed to determine the sensitivity of parent *P. putida* (control) and the survivor phenotype towards kanamycin (50 mg/mL), gentamicin (10 mg/mL), and tetracycline (10 mg/mL) antibiotics. The Lauria Bertani (LB) broth without any supplemented antibiotics was used as a control. The test was performed in a 96-well microtiter plate. In a 96-well plate, each well having 200 µL of LB or LB supplemented with an antibiotic was inoculated with a colony of *P. putida.* Next, the absorbance at OD_{620} was recorded using a plate reader every 30 min for 10 hr to examine the growth dynamics of each phenotype. The test was performed in 12 replicates per condition for both phenotypes. Recorded OD_{620} values were plotted using Prism version 7.0d with error bars depicting the standard deviation of replicate data.

4.6. Acknowledgements

I appreciate funding and support from the National Institute of General Medical Sciences of the National Institutes of Health (P20GM130460). I Thank Scot E. Dowd at MR DNA, Molecular Research LP for assistance throughout sequencing services provided, Dr. Sandeep Misra Manager of the Analytical and Biophysical Chemistry Core associated with the Glycoscience Center of Research Excellence (GlyCORE; P20GM130460) for LC-MS/MS analysis, and Prof. Nicole Ashpole for her assistance with anti-alginate dot blot generation and imaging.

Chapter 5

Conclusion and Contribution

5.1. Introduction

Even though myxobacteria consume broadly broad diversity of microbial prey (29,48–51), an individual myxobacterial strain shows variability in its predation rates and unique specificities to several of its prey (29,31). The overlap and distinctions in the predatory capacities among myxobacterial predators not only contribute to the diversity of the soil bacterial communities but also make myxobacteria a spotlight as a therapeutic source against different infectious microbes (7,21,22). In addition to myxobacterial genomic level variabilities of predation capabilities (98), specific features associated with prey organisms also contribute to prey differential susceptibilities to myxobacterial predation (32-35,70,105). Understanding prey specific chemical entities and other features responsible for eliciting predatory responses from myxobacteria and their significance to myxobacterial specialized metabolism would contribute to the understanding of bacterial ecological interactions in the soil as well as to the biologically significant natural products discovery efforts from the myxobacteria. Keeping this in mind, the goal of this study was 1) to compare and contrast the impact of two different classes of prey associated signaling molecules on the responses and metabolism of two myxobacteria, 2) explore features of a prey bacterium that enable it to avoid a myxobacterial predator.

5.2. Results

The comparative analysis of the responses from two myxobacteria, *C. ferrugineus* and *M. xanthus*, when exposed to two distinct structural classes of bacterial prey signals, reveals both myxobacteria demonstrate predatory eavesdropping to these signals. Their responses to acyl-homoserine lactones (AHLs) type signals overlap, and perhaps the L-homoserine lactone structural moiety of AHLs is responsible for triggering this response. In contrast, both employed myxobacteria respond distinctively to the quinolone signal HHQ. Many transcriptional features upregulate in *C. ferrugineus* upon exposure to HHQ, and HHQ profoundly impacts the metabolism of this bacterium. The capability to detoxify HHQ signal to a less toxic PQS-NO is unique to *C. ferrugineus*, and no similar metabolic response is observable from *M. xanthus*. Our findings demonstrate that similar responses to AHLs type signals might contribute to generalist predatory capacities of myxobacteria, and the distinctive responses to HHQ could be a contributor to myxobacterial specificities to their prey.

While investigating the physical predatory interactions between *C. ferrugineus* and *P. putida*, we explored the predatory stress from *C. ferrugineus* results in selecting a *P. putida* phenotype that shows resistance to subsequent *C. ferrugineus* predation. Overproduction of a siderophore pyoverdine, Phenazine-1-Carboxylic acid, alginate, and resistance to aminoglycosides and tetracycline antibiotics are the features unique to this phenotype compared to the parent *P. putida* phenotype. These findings highlight the characteristics that perhaps *Pseudomonas* utilize for their survival and emphasize the contributing role of predatory stress in the phenotypic variability of prey bacteria.

5.3. Contributions

The finding of L-homoserine lactone structural moiety from acyl-homoserine lactone type bacterial prey signaling molecules is sufficient to trigger a general response in myxobacterial predators provides additional evidence to the already observed myxobacterial prey signal eavesdropping phenomenon.

Myxobacterial metabolic responses to the employed prey signal classes corroborate the findings of shared chemical space in the microbial communities, and support signals from the prey trigger specialized metabolites production from the myxobacteria. Our result of *M. xanthus* not responding to HHQ similar to *C. ferrugineus* also emphasizes like differential predatory capacities of individual myxobacterial strains, the responses from different myxobacteria to the prey signals would not be uniform. Therefore, testing individual myxobacterial isolate would be essential to observe the uniqueness of myxobacterial metabolic responses to a prey signal.

Our findings of the distinct traits associated with survivor *P. putida* phenotype selected during *C. ferrugineus* predation and the observed overlap between the adapted traits of the survivor *P. putida* phenotype and traits associated with persistent clinical pathogens suggest the possible features that *Pseudomonads* employ under stress conditions. The results also suggest predatory stress from myxobacteria derives phenotypic diversity of prey bacteria in the microbial communities.

Overall, our study confirms the significant role of chemical components of bacterial prey, including signaling molecules as well as specialized metabolites, in directing their interactions with the predatory myxobacteria.

BIBLIOGRAPHY

1. Garcia R, La Clair J, Müller R. Future Directions of Marine Myxobacterial Natural Product Discovery Inferred from Metagenomics. Mar Drugs. 2018;16(9):303

2. Reichenbach H. The ecology of the myxobacteria. Environ Microbiol. 1999;1(1):15–21.

3. Mohr K. Diversity of Myxobacteria—We Only See the Tip of the Iceberg. Microorganisms. 2018;6(3):84.

4. Reichenbach H, Dworkin M. The myxobacteria. The prokaryotes. 2nd edn. Spriger-Verlag, Berlin, 1992;3418–3487.

5. Wrótniak-Drzewiecka W, Brzezińska AJ, Dahm H, Ingle AP, Rai M. Current trends in myxobacteria research. Ann Microbiol. 2016;66(1):17–33.

6. Berleman JE, Kirby JR. Deciphering the hunting strategy of a bacterial wolfpack. FEMS Microbiol Rev. 2009;33(5):942–57.

7. Herrmann J, Fayad AA, Müller R. Natural products from myxobacteria: novel metabolites and bioactivities. Nat Prod Rep. 2017;34(2):135–60.

8. Kaiser D, Robinson M, Kroos L. Myxobacteria, Polarity, and Multicellular Morphogenesis. Cold Spring Harb Perspect Biol. 2010;2(8):a000380–a000380.

9. Kaiser D, Manoil C, Dworkin M. Myxobacteria: Cell Interactions, Genetics, and Development. Annu Rev Microbiol. 1979;33(1):595–639.

10. Muñoz-Dorado J, Marcos-Torres FJ, García-Bravo E, Moraleda-Muñoz A, Pérez J. Myxobacteria: Moving, Killing, Feeding, and Surviving Together. Front Microbiol. 2016; 7:781.

11. Kaiser D. A Microbial Genetic Journey. Annu Rev Microbiol. 2006 Oct;60(1):1–25.

12. Kaiser D, Crosby C. Cell movement and its coordination in swarms of myxococcus xanthus. Cell Motil. 1983;3(3):227–45.

13. LuNSDORF H, Reichenbach H. Ultrastructural Details of the Apparatus of Gliding Motility of Myxococcus fulvus (Myxobacterales). Microbiology. 1989;135(6):1633–41.

14. Hodgkin J, Kaiser D. Genetics of gliding motility in Myxococcus xanthus (Myxobacterales): Two gene systems control movement. Mol Gen Genet MGG. 1979;171(2):177–91.

15. Li Y, Sun H, Ma X, Lu A, Lux R, Zusman D, et al. Extracellular polysaccharides mediate pilus retraction during social motility of Myxococcus xanthus. Proc Natl Acad Sci. 2003;100(9):5443–8.

16. Mignot T. The elusive engine in Myxococcus xanthus gliding motility. Cell Mol Life Sci. 2007;64(21):2733–45.

17. Mauriello EMF, Mignot T, Yang Z, Zusman DR. Gliding Motility Revisited: How Do the Myxobacteria Move without Flagella? Microbiol Mol Biol Rev. 2010;74(2):229–49.

18. Treuner-Lange A, Bruckskotten M, Rupp O, Goesmann A, Søgaard-Andersen L. Complete Genome Sequence of the Fruiting Myxobacterium Melittangium boletus DSM 14713. Genome Announc. 2017;5(45):e01262-17, e01262-17.

19. Han K, Li Z, Peng R, Zhu L, Zhou T, Wang L, et al. Extraordinary expansion of a Sorangium cellulosum genome from an alkaline milieu. Sci Rep. 2013;3(1):2101.

20. Gregory K, Salvador LA, Akbar S, Adaikpoh BI, Stevens DC. Survey of Biosynthetic Gene Clusters from Sequenced Myxobacteria Reveals Unexplored Biosynthetic Potential. Microorganisms. 2019;7(6):181.

21. Weissman KJ, Müller R. Myxobacterial secondary metabolites: bioactivities and modes-of-action. Nat Prod Rep. 2010;27(9):1276.

22. Reichenbach H. Myxobacteria: a source of new antibiotics. Trends Biotechnol. 1988;6(6):115–21.

23. Oxford AE. Observations Concerning the Growth and Metabolic Activities of Myxococci in a Simple Protein-free Liquid Medium. J Bacteriol. 1947;53(2):129–38.

24. Thiery S, Kaimer C. The Predation Strategy of Myxococcus xanthus. Front Microbiol. 2020;11:2.

25. Schäberle TF, Lohr F, Schmitz A, König GM. Antibiotics from myxobacteria. Nat Prod Rep. 2014;31(7):953.

26. Müller S, Strack SN, Ryan SE, Shawgo M, Walling A, Harris S, et al. Identification of Functions Affecting Predator-Prey Interactions between Myxococcus xanthus and Bacillus subtilis. O'Toole GA, editor. J Bacteriol. 2016;198(24):3335–44.

27. Xiao Y, Wei X, Ebright R, Wall D. Antibiotic Production by Myxobacteria Plays a Role in Predation. J Bacteriol. 2011;193(18):4626–33.

28. Livingstone PG, Morphew RM, Whitworth DE. Genome Sequencing and Pan-Genome Analysis of 23 Corallococcus spp. Strains Reveal Unexpected Diversity, With Particular Plasticity of Predatory Gene Sets. Front Microbiol. 2018;9:3187.

29. Morgan AD, MacLean RC, Hillesland KL, Velicer GJ. Comparative Analysis of Myxococcus Predation on Soil Bacteria. Appl Environ Microbiol. 2010;76(20):6920–7.

30. Livingstone PG, Morphew RM, Whitworth DE. Myxobacteria Are Able to Prey Broadly upon Clinically-Relevant Pathogens, Exhibiting a Prey Range Which Cannot Be Explained by Phylogeny. Front Microbiol. 2017;8:1593.

31. Mendes-Soares H, Velicer GJ. Decomposing Predation: Testing for Parameters that Correlate with Predatory Performance by a Social Bacterium. Microb Ecol. 2013;65(2):415–23.

32. Contreras-Moreno FJ, Muñoz-Dorado J, García-Tomsig NI, Martínez-Navajas G, Pérez J, Moraleda-Muñoz A. Copper and Melanin Play a Role in Myxococcus xanthus Predation on Sinorhizobium meliloti. Front Microbiol. 2020;11:94.

33. DePas WH, Syed AK, Sifuentes M, Lee JS, Warshaw D, Saggar V, et al. Biofilm Formation Protects Escherichia coli against Killing by Caenorhabditis elegans and Myxococcus xanthus. Appl Environ Microbiol. 2014;80(22):7079–87.

34. Müller S, Strack SN, Hoefler BC, Straight PD, Kearns DB, Kirby JR. Bacillaene and Sporulation Protect Bacillus subtilis from Predation by Myxococcus xanthus. Appl Environ Microbiol. 2014;80(18):5603–10.

35. Pérez J, Jiménez-Zurdo JI, Martínez-Abarca F, Millán V, Shimkets LJ, Muñoz-Dorado J. Rhizobial galactoglucan determines the predatory pattern of *M yxococcus xanthus* and protects *S inorhizobium meliloti* from predation: *M. xanthus* predation on *S. meliloti*. Environ Microbiol. 2014;16(7):2341–50.

36. Wang C, Liu X, Zhang P, Wang Y, Li Z, Li X, et al. *Bacillus licheniformis* escapes from *Myxococcus xanthus* predation by deactivating myxovirescin A through enzymatic glucosylation. Environ Microbiol. 2019;21(12):4755–72.

37. Arend KI, Schmidt JJ, Bentler T, Lüchtefeld C, Eggerichs D, Hexamer HM, et al. *Myxococcus xanthus* Predation of Gram-Positive or Gram-Negative Bacteria Is Mediated by Different Bacteriolytic Mechanisms. Appl Environ Microbiol. 2020;87(5):e02382-20.

38. McBride MJ, Zusman DR. Behavioral analysis of single cells of *Myxococcus xanthus* in response to prey cells of *Escherichia coli*. FEMS Microbiol Lett. 1996;137(2–3):227–31.

39. Pan H, He X, Lux R, Luan J, Shi W. Killing of Escherichia coli by Myxococcus xanthus in Aqueous Environments Requires Exopolysaccharide-Dependent Physical Contact. Microb Ecol. 2013;66(3):630–8.

40. Fraleigh, P. C., Burnham, J. C. Myxococcal predation on cyanobacterial populations: nutrient effects. Limnol. Oc. 1988.

41. Kang-Chien L, Casida LE. Survival of myxobacter strain 8 in natural soil in the presence and absence of host cells. Soil Biol Biochem. 1983;15(5):551–5.

42. Rosenberg E, Keller KH, Dworkin M. Cell density-dependent growth of Myxococcus xanthus on casein. J Bacteriol. 1977;129(2):770–7.

43. Pérez J, Moraleda-Muñoz A, Marcos-Torres FJ, Muñoz-Dorado J. Bacterial predation: 75 years and counting!: Bacterial predation. Environ Microbiol. 2016r;18(3):766–79.

44. Shimkets LJ & Kaiser D. Induction of coordinated movement of Myxococcus xanthus cells. J Bacteriol. 1982;152: 451–461.

45. Zhang H, Vaksman Z, Litwin DB, Shi P, Kaplan HB, Igoshin OA. The Mechanistic Basis of Myxococcus xanthus Rippling Behavior and Its Physiological Role during Predation. PLoS Comput Biol. 2012;8(9):e1002715.

46. Berleman JE, Chumley T, Cheung P, Kirby JR. Rippling Is a Predatory Behavior in Myxococcus xanthus. J Bacteriol. 2006;188(16):5888–95.

47. Burnham JC, Collart SA, Highison BW. Entrapment and lysis of the cyanobacterium Phormidium luridum by aqueous colonies of Myxococcus xanthus PCO2. Arch Microbiol. 1981;129(4):285–94.

48. Hillesland KL, Lenski RE, Velicer GJ. Ecological Variables Affecting Predatory Success in Myxococcus xanthus. Microb Ecol. 2007;53(4):571–8.

49. Singh BN. Myxobacteria in Soils and Composts; their Distribution, Number and Lytic Action on Bacteria. J Gen Microbiol. 1947;1(1):1–10.

50. Zhang L, Lueders T. Micropredator niche differentiation between bulk soil and rhizosphere of an agricultural soil depends on bacterial prey. FEMS Microbiol Ecol. 2017.

51. Zhou Y, Zhang X, Yao Q, Zhu H. Both Soil Bacteria and Soil Chemical Property Affected the Micropredator Myxobacterial Community: Evidence from Natural Forest Soil and Greenhouse Rhizosphere Soil. Microorganisms. 2020;8(9):1387.

52. Keane R, Berleman J. The predatory life cycle of Myxococcus xanthus. Microbiology. 2016;162(1):1–11.

53. Livingstone PG, Millard AD, Swain MT, Whitworth DE. Transcriptional changes when Myxococcus xanthus preys on Escherichia coli suggest myxobacterial predators are constitutively toxic but regulate their feeding. Microb Genomics. 2018;4(2).

54. Nair RR, Vasse M, Wielgoss S, Sun L, Yu Y-TN, Velicer GJ. Bacterial predator-prey coevolution accelerates genome evolution and selects on virulence-associated prey defences. Nat Commun. 2019;10(1):4301.

55. Hillesland KL, Velicer GJ, Lenski RE. Experimental evolution of a microbial predator's ability to find prey. Proc R Soc B Biol Sci. 2009;276(1656):459–67.

56. Berleman JE, Kirby JR. Multicellular Development in Myxococcus xanthus Is Stimulated by Predator-Prey Interactions. J Bacteriol. 2007;189(15):5675–82.

57. Charousová I, Medo J, Javoreková S. Isolation, antimicrobial activity of myxobacterial crude extracts and identification of the most potent strains. Arch Biol Sci. 2017;69(3):561–8.

58. Garcia R, Müller R. The Family Nannocystaceae. The Prokaryotes. 2014; 213–29.

59. Wang C, Lv Y, Li A, Yao Q, Feng G, Zhu H. Culture-dependent and -independent methods revealed an abundant myxobacterial community shaped by other bacteria and pH in Dinghushan acidic soils. PLOS ONE. 2020;15(9):e0238769.

60. Zhang F, Braun DR, Rajski SR, DeMaria D, Bugni TS. Enhypyrazinones A and B, Pyrazinone Natural Products from a Marine-Derived Myxobacterium Enhygromyxa sp. Mar Drugs. 2019;17(12):698.

61. Pham VD, Shebelut CW, Diodati ME, Bull CT, Singer M. Mutations affecting predation ability of the soil bacterium Myxococcus xanthus. Microbiology. 2005;151(6):1865–74.

62. Śnieszko SF, McAllister J, Hitchner ER. Further studies on the biology of certain myxobacteria. Bulletin of the Polish Institute of Arts and Sciences in America. 1943; (1):651-664.

63. Mathew S, Dudani A. Lysis of Human Pathogenic Bacteria by Myxobacteria. Nature. 1955 Jan;175(4446):125–125.

64. Livingstone PG, Ingleby O, Girdwood S, Cookson AR, Morphew RM, Whitworth DE. Predatory Organisms with Untapped Biosynthetic Potential: Descriptions of Novel *Corallococcus* Species *C. aberystwythensis* sp. nov., *C. carmarthensis* sp. nov., *C. exercitus* sp. nov., *C. interemptor* sp. nov., *C. llansteffanensis* sp. nov., *C. praedator* sp. nov., *C. sicarius* sp. nov., and *C. terminator* sp. nov. Appl Environ Microbiol. 2019;86(2):e01931-19.

65. Noren, B. Studies on Myxobacteria. Lytic activityon different eubacteria. Sv. Bot. Tidskr., 1955a; 42, 282-294.

66. Barka EA, Vatsa P, Sanchez L, Gaveau-Vaillant N, Jacquard C, Klenk H-P, et al. Taxonomy, Physiology, and Natural Products of Actinobacteria. Microbiol Mol Biol Rev. 2016;80(1):1–43.

67. de Lima Procópio RE, da Silva IR, Martins MK, de Azevedo JL, de Araújo JM. Antibiotics produced by Streptomyces. Braz J Infect Dis. 2012;16(5):466–71.

68. Jacob C, Weissman KJ. Unpackaging the Roles of Streptomyces Natural Products. Cell Chem Biol. 2017;24(10):1194–5.

69. Jakubiec-Krzesniak K, Rajnisz-Mateusiak A, Guspiel A, Ziemska J, Solecka J. Secondary Metabolites of Actinomycetes and their Antibacterial, Antifungal and Antiviral Properties. Pol J Microbiol. 2018;67(3):259–72.

70. Pérez J, Muñoz-Dorado J, Braña AF, Shimkets LJ, Sevillano L, Santamaría RI. Myxococcus xanthus induces actinorhodin overproduction and aerial mycelium formation by Streptomyces coelicolor: Mixed bacterial cultures induce antibiotic production. Microb Biotechnol. 2011;4(2):175–83.

71. Lee N, Kim W, Chung J, Lee Y, Cho S, Jang K-S, et al. Iron competition triggers antibiotic biosynthesis in Streptomyces coelicolor during coculture with Myxococcus xanthus. ISME J. 2020;14(5):1111–24.

72. Casida LE. Bacterial Predators of Micrococcus luteus in Soil †. Appl Environ Microbiol. 1980;39(5):1035–41.

73. Chambers J, Sparks N, Sydney N, Livingstone PG, Cookson AR, Whitworth DE. Comparative Genomics and Pan-Genomics of the Myxococcaceae, including a Description of Five Novel Species: *Myxococcus eversor* sp. nov., *Myxococcus llanfairpwllgwyngyllgogerychwyrndrobwllllantysiliogogogochensis* sp. nov., *Myxococcus vastator* sp. nov., *Pyxidicoccus caerfyrddinensis* sp. nov., and *Pyxidicoccus trucidator* sp. nov. Genome Biol Evol. 2020;12(12):2289–302.

74. Bižić M, Klintzsch T, Ionescu D, Hindiyeh MY, Günthel M, Muro-Pastor AM, et al. Aquatic and terrestrial cyanobacteria produce methane. Sci Adv. 2020;6(3):eaax5343.

75. Echlin P, Morris I. THE RELATIONSHIP BETWEEN BLUE-GREEN ALGAE AND BACTERIA. Biol Rev. 1965;40(2):143–84.

76. Shilo M. Lysis of blue-green algae by myxobacter. J bacteriol. 1970;104(1), 453–461.

77. Daft MJ, Stewart WDP. BACTERIAL PATHOGENS OF FRESHWATER BLUE-GREEN ALGAE. New Phytol. 1971;70(5):819–29.

78. Daft MJ, McCORD SB, Stewart WDP. Ecological studies on algal-lysing bacteria in fresh waters. Freshw Biol. 1975;5(6):577–96.

79. Burnham JC, Collart SA, Daft MJ. Myxococcal predation of the cyanobacterium Phormidium luridum in aqueous environments. Arch Microbiol. 1984;137(3):220–5.

80. Yamamoto Y, Suzuki K. DISTRIBUTION AND ALGAL-LYSING ACTIVITY OF FRUITING MYXOBACTERIA IN LAKE SUWA1. J Phycol. 1990;26(3):457–62.

81. Geitler L. Über Polyangium parasiticum n. sp., eine submerse, parasitische Myxobacteriaceae. Arch Protistenk. 1924;50:67.

82. Abinandan S, Subashchandrabose SR, Venkateswarlu K, Megharaj M. Soil microalgae and cyanobacteria: the biotechnological potential in the maintenance of soil fertility and health. Crit Rev Biotechnol. 2019;39(8):981–98.

83. Rego A, Raio F, Martins TP, Ribeiro H, Sousa AGG, Séneca J, et al. Actinobacteria and Cyanobacteria Diversity in Terrestrial Antarctic Microenvironments Evaluated by Culture-Dependent and Independent Methods. Front Microbiol. 2019;10:1018.

84. Havens KE. Cyanobacteria blooms: effects on aquatic ecosystems. Cyanobacterial Harmful Algal Blooms: State of the Science and Research Needs. Springer New York; 2008;619:733–47.

85. Schäberle TF, Goralski E, Neu E, Erol Ö, Hölzl G, Dörmann P, et al. Marine Myxobacteria as a Source of Antibiotics—Comparison of Physiology, Polyketide-Type Genes and Antibiotic Production of Three New Isolates of Enhygromyxa salina. Mar Drugs. 2010;8(9):2466–79.

86. Wu B, Hardy MK, Howe HB. Antimicrobial activity of a myxobacterium against bluegreen algae. Bacteriol Proc. 1968;48.

87. Kim, Sung-Taek, Yun, Sung-Chul. Selection of KYC 3270, a Cellulolytic Myxobacteria of Sorangium cellulosum, against Several Phytopathogens and a Potential Biocontrol Agent against Gray Mold in Stored Fruit. Plant Pathol J. 2011;27(3):257–65.

88. Yun, Sung-Chul. Selection and a 3-Year Field Trial of Sorangium cellulosum KYC 3262 Against Anthracnose in Hot Pepper. Plant Pathol J. 2014;30(3):279–87.

89. Hocking D, Cook FD. Myxobacteria exert partial control of damping-off and root disease in container-grown tree seedlings. Can J Microbiol. 1972;18(10):1557–60.

90. Homma Y. Perforation and Lysis of Hyphae of *Rhizoctonia solani* and Conidia of *Cochliobolus miyabeanus* by Soil Myxobacteria. Phytopathology. 1984;74(10):1234.

91. Snieszko SF, McAllister J, Hitchner ER. On the biology of certain myxobacteria. J. Bact. 1941;41:26-27.

92. Bull CT, Shetty KG, Subbarao KV. Interactions Between Myxobacteria, Plant Pathogenic Fungi, and Biocontrol Agents. Plant Dis. 2002;86(8):889–96.

93. Dahm H, Brzezińska J, Wrótniak-Drzewiecka W, Golińska P, Różycki H, Rai M. Myxobacteria as a potential biocontrol agent effective against pathogenic fungi of economically important forest trees. Dendrobiology. 2015;74:13–24.

94. Meliah S, Kusumawati DI, Ilyas M. Preliminary study of myxobacteria as biocontrol agents for panama disease pathogen, tropical race 4 *Fusarium odoratissimum*. IOP Conf Ser Earth Environ Sci. 2020;457:012060.

95. Li Z, Ye X, Chen P, Ji K, Zhou J, Wang F, et al. Antifungal potential of Corallococcus sp. strain EGB against plant pathogenic fungi. Biol Control. 2017;110:10–7.

96. Ye X, Li Z, Luo X, Wang W, Li Y, Li R, et al. A predatory myxobacterium controls cucumber Fusarium wilt by regulating the soil microbial community. Microbiome. 2020;8(1):49.

97. Li Z, Ye X, Liu M, Xia C, Zhang L, Luo X, et al. A novel outer membrane β-1,6-glucanase is deployed in the predation of fungi by myxobacteria. ISME J. 2019;13(9):2223–35.

98. Sutton D, Livingstone PG, Furness E, Swain MT, Whitworth DE. Genome-Wide Identification of Myxobacterial Predation Genes and Demonstration of Formaldehyde Secretion as a Potentially Predation-Resistant Trait of Pseudomonas aeruginosa. Front Microbiol. 2019;10:2650.

99. Wang D, Fu J, Zhou R, Li Z, Xie Y, Liu X, et al. Formation of sclerotia in *Sclerotinia ginseng* and composition of the sclerotial exudate. PeerJ. 2018;6:e6009.

100. Rieusset L, Rey M, Muller D, Vacheron J, Gerin F, Dubost A, et al. Secondary metabolites from plant-associated *Pseudomonas* are overproduced in biofilm. Microb Biotechnol. 2020;13(5):1562–80.

101. Butcher RA, Schroeder FC, Fischbach MA, Straight PD, Kolter R, Walsh CT, et al. The identification of bacillaene, the product of the PksX megacomplex in Bacillus subtilis. Proc Natl Acad Sci. 2007;104(5):1506–9.

102. Jousset A, Rochat L, Péchy-Tarr M, Keel C, Scheu S, Bonkowski M. Predators promote defence of rhizosphere bacterial populations by selective feeding on non-toxic cheaters. ISME J. 2009;3(6):666–74.

103. Olsén A, Jonsson A, Normark S. Fibronectin binding mediated by a novel class of surface organelles on Escherichia coli. Nature. 1989;338(6217):652–5.

104. Jones KM. Increased Production of the Exopolysaccharide Succinoglycan Enhances Sinorhizobium meliloti 1021 Symbiosis with the Host Plant Medicago truncatula. J Bacteriol. 2012;194(16):4322–31.

105. Müller S, Strack SN, Ryan SE, Kearns DB, Kirby JR. Predation by Myxococcus xanthus Induces Bacillus subtilis To Form Spore-Filled Megastructures. Appl Environ Microbiol. 2015;81(1):203–10.

106. Ellis BM, Fischer CN, Martin LB, Bachmann BO, McLean JA. Spatiochemically Profiling Microbial Interactions with Membrane Scaffolded Desorption Electrospray Ionization-Ion

Mobility-Imaging Mass Spectrometry and Unsupervised Segmentation. Anal Chem. 2019;91(21):13703–11.

107. Trowitzsch W, Wray V, Gerth K, Höfle G. Structure of myxovirescin A, a new macrocylic antibiotic from gliding bacteria. J Chem Soc Chem Commun. 1982;(23):1340–2.

108. Pinoy M.E. Sur la nécessité d'une association bactérienne pour la développement d'une Myxobactérie, Chondromyces crocatus. C. R. Acad. Sci. Paris. 1913; 157:77-78.

109. Petters S, Söllinger A, Bengtsson MM, Urich T. The soil microbial food web revisited with metatranscriptomics - predatory *Myxobacteria* as keystone taxon? Microbiology. 2018.

110. Petters S, Groß V, Söllinger A, Pichler M, Reinhard A, Bengtsson MM, et al. The soil microbial food web revisited: Predatory myxobacteria as keystone taxa? ISME J. 2021.

111. Honghui Zhu., Influence of different prey strains on isolation myxobacteria in saline-alkaline soils of Xinjiang, Weishe. 2013.

112. Schäberle TF, Lohr F, Schmitz A, König GM. Antibiotics from myxobacteria. Nat Prod Rep. 2014;31(7):953.

113. Baumann S, Herrmann J, Raju R, Steinmetz H, Mohr KI, Hüttel S, et al. Cystobactamids: Myxobacterial Topoisomerase Inhibitors Exhibiting Potent Antibacterial Activity. Angew Chem Int Ed. 2014;53(52):14605–9.

114. Cortina NS, Revermann O, Krug D, Müller R. Identification and Characterization of the Althiomycin Biosynthetic Gene Cluster in Myxococcus xanthus DK897. ChemBioChem. 2011;12(9):1411–6.

115. Keller L, Plaza A, Dubiella C, Groll M, Kaiser M, Müller R. Macyranones: Structure, Biosynthesis, and Binding Mode of an Unprecedented Epoxyketone that Targets the 20S Proteasome. J Am Chem Soc. 2015;137(25):8121–30.

116. Nadmid S, Plaza A, Garcia R, Müller R. Cystochromones, Unusual Chromone-Containing Polyketides from the Myxobacterium *Cystobacter* sp. MCy9104. J Nat Prod. 2015;78(8):2023–8.

117. Fleischmann R, Adams M, White O, Clayton R, Kirkness E, Kerlavage A, et al. Whole-genome random sequencing and assembly of Haemophilus influenzae Rd. Science. 1995;269(5223):496–512.

118. Wenzel SC, Müller R. The impact of genomics on the exploitation of the myxobacterial secondary metabolome. Nat Prod Rep. 2009;26(11):1385.

119. Feng Z, Qi J, Tsuge T, Oba Y, Kobayashi T, Suzuki Y, et al. Construction of a Bacterial Artificial Chromosome Library for a Myxobacterium of the Genus *Cystobacter* and Characterization of an Antibiotic Biosynthetic Gene Cluster. Biosci Biotechnol Biochem. 2005;69(7):1372–80.

120. Amiri Moghaddam J, Crüsemann M, Alanjary M, Harms H, Dávila-Céspedes A, Blom J, et al. Analysis of the Genome and Metabolome of Marine Myxobacteria Reveals High Potential for Biosynthesis of Novel Specialized Metabolites. Sci Rep. 2018;8(1):16600.

121. Chai Y, Shan S, Weissman KJ, Hu S, Zhang Y, Müller R. Heterologous Expression and Genetic Engineering of the Tubulysin Biosynthetic Gene Cluster Using Red/ET Recombineering and Inactivation Mutagenesis. Chem Biol. 2012;19(3):361–71.

122. Chai Y, Pistorius D, Ullrich A, Weissman KJ, Kazmaier U, Müller R. Discovery of 23 Natural Tubulysins from Angiococcus disciformis An d48 and Cystobacter SBCb004. Chem Biol. 2010;17(3):296–309.

123. Rabe P, Citron CA, Dickschat JS. Volatile Terpenes from Actinomycetes: A Biosynthetic Study Correlating Chemical Analyses to Genome Data. ChemBioChem. 2013;14(17):2345–54.

124. Fields FR, Lee SW, McConnell MJ. Using bacterial genomes and essential genes for the development of new antibiotics. Biochem Pharmacol. 2017;134:74–86.

125. Skinnider MA, Johnston CW, Gunabalasingam M, Merwin NJ, Kieliszek AM, MacLellan RJ, et al. Comprehensive prediction of secondary metabolite structure and biological activity from microbial genome sequences. Nat Commun. 2020;11(1):6058.

126. Shapland EB, Holmes V, Reeves CD, Sorokin E, Durot M, Platt D, et al. Low-Cost, High-Throughput Sequencing of DNA Assemblies Using a Highly Multiplexed Nextera Process. ACS Synth Biol. 2015;4(7):860–6.

127. Chavali AK, Rhee SY. Bioinformatics tools for the identification of gene clusters that biosynthesize specialized metabolites. Brief Bioinform. 2018;19(5):1022–34.

128. Weber T, Blin K, Duddela S, Krug D, Kim HU, Bruccoleri R, et al. antiSMASH 3.0—a comprehensive resource for the genome mining of biosynthetic gene clusters. Nucleic Acids Res. 2015;43(W1):W237–43.

129. Blin K, Shaw S, Steinke K, Villebro R, Ziemert N, Lee SY, et al. antiSMASH 5.0: updates to the secondary metabolite genome mining pipeline. Nucleic Acids Res. 2019;47(W1):W81–7.

130. Blin K, Kim HU, Medema MH, Weber T. Recent development of antiSMASH and other computational approaches to mine secondary metabolite biosynthetic gene clusters. Brief Bioinform. 2019;20(4):1103–13.

131. van der Lee TAJ, Medema MH. Computational strategies for genome-based natural product discovery and engineering in fungi. Fungal Genet Biol. 2016;89:29–36.

132. Wishart DS. Computational Approaches to Metabolomics. In: Matthiesen R, editor. Bioinformatics Methods in Clinical Research. Totowa, NJ: Humana Press; Methods in Molecular Biology. 2010;593:283–313.

133. Machushynets NV, Wu C, Elsayed SS, Hankemeier T, van Wezel GP. Discovery of novel glycerolated quinazolinones from Streptomyces sp. MBT27. J Ind Microbiol Biotechnol. 2019;46(3–4):483–92.

134. van der Hooft JJJ, Wandy J, Barrett MP, Burgess KEV, Rogers S. Topic modeling for untargeted substructure exploration in metabolomics. Proc Natl Acad Sci. 2016;113(48):13738–43.

135. Wang M, Carver JJ, Phelan VV, Sanchez LM, Garg N, Peng Y, et al. Sharing and community curation of mass spectrometry data with Global Natural Products Social Molecular Networking. Nat Biotechnol. 2016;34(8):828–37.

136. Mohimani H, Gurevich A, Shlemov A, Mikheenko A, Korobeynikov A, Cao L, et al. Dereplication of microbial metabolites through database search of mass spectra. Nat Commun. 2018;9(1):4035.

137. Adaikpoh BI, Akbar S, Albataineh H, Misra SK, Sharp JS, Stevens DC. Myxobacterial Response to Methyljasmonate Exposure Indicates Contribution to Plant Recruitment of Micropredators. Front Microbiol. 2020;11:34.

138. Raju R, Mohr KI, Bernecker S, Herrmann J, Müller R. Cystodienoic acid: a new diterpene isolated from the myxobacterium Cystobacter sp. J Antibiot (Tokyo). 2015;68(7):473–5.

139. Akbar S, Dowd SE, Stevens DC. Draft Genome Sequence of Cystobacter ferrugineus Strain Cbfe23. Genome Announc. 2017;5(6):e01601-16, e01601-16.

140. Li Y, Weissman KJ, Müller R. Myxochelin Biosynthesis: Direct Evidence for Two- and Four-Electron Reduction of a Carrier Protein-Bound Thioester. J Am Chem Soc. 2008;130(24):7554–5.

141. Sasse F, Sieinmetz H, Heil J, Höfle G, Reichenbach H. Tubulysins, New Cytostatic Peptides from Myxobacteria Acting on Microtubuli. Production, Isolation, Physico-chemical and Biological Properties. J Antibiot (Tokyo). 2000;53(9):879–85.

142. Steinmetz H, Glaser N, Herdtweck E, Sasse F, Reichenbach H, Höfle G. Isolation, Crystal and Solution Structure Determination, and Biosynthesis of Tubulysins—Powerful Inhibitors of Tubulin Polymerization from Myxobacteria. Angew Chem Int Ed. 2004;43(37):4888–92.

143. Lang E, Schumann P, Tindall BJ, Mohr KI, Spröer C. Reclassification of Angiococcus disciformis, Cystobacter minus and Cystobacter violaceus as Archangium disciforme comb. nov., Archangium minus comb. nov. and Archangium violaceum comb. nov., unification of the families Archangiaceae and Cystobacteraceae, and emended descriptions of the families Myxococcaceae and Archangiaceae. Int J Syst Evol Microbiol. 2015;65(Pt_11):4032–42.

144. Overbeek R, Olson R, Pusch GD, Olsen GJ, Davis JJ, Disz T, et al. The SEED and the Rapid Annotation of microbial genomes using Subsystems Technology (RAST). Nucleic Acids Res. 2014;42(D1):D206–14.

145. Angiuoli SV, Gussman A, Klimke W, Cochrane G, Field D, Garrity GM, et al. Toward an Online Repository of Standard Operating Procedures (SOPs) for (Meta)genomic Annotation. OMICS J Integr Biol. 2008;12(2):137–41.

146. Landwehr W, Wolf C, Wink J. Actinobacteria and Myxobacteria—Two of the Most Important Bacterial Resources for Novel Antibiotics. How to Overcome the Antibiotic Crisis. Cham: Springer International Publishing; 2016;398:273–302.

147. Korp J, Vela Gurovic MS, Nett M. Antibiotics from predatory bacteria. Beilstein J Org Chem. 2016;12:594–607.

148. Miller MB, Bassler BL. Quorum Sensing in Bacteria. Annu Rev Microbiol. 2001;55(1):165–99.

149. Federle MJ, Bassler BL. Interspecies communication in bacteria. J Clin Invest. 2003;112(9):1291–9.

150. Shiner EK, Rumbaugh KP, Williams SC. Interkingdom signaling: Deciphering the language of acyl homoserine lactones. FEMS Microbiol Rev. 2005;29(5):935–47.

151. Huang Y, Ki J, Case R, Qian P. Diversity and acyl-homoserine lactone production among subtidal biofilm-forming bacteria. Aquat Microb Ecol. 2008;52:185–93.

152. Acharya D, Miller I, Cui Y, Braun DR, Berres ME, Styles MJ, et al. Omics Technologies to Understand Activation of a Biosynthetic Gene Cluster in *Micromonospora* sp. WMMB235: Deciphering Keyicin Biosynthesis. ACS Chem Biol. 2019;14(6):1260–70.

153. Rateb ME, Hallyburton I, Houssen WE, Bull AT, Goodfellow M, Santhanam R, et al. Induction of diverse secondary metabolites in Aspergillus fumigatus by microbial co-culture. RSC Adv. 2013;3(34):14444.

154. Seyedsayamdost MR, Chandler JR, Blodgett JAV, Lima PS, Duerkop BA, Oinuma K-I, et al. Quorum-Sensing-Regulated Bactobolin Production by *Burkholderia thailandensis* E264. Org Lett. 2010;12(4):716–9.

155. Reen FJ, Mooij MJ, Holcombe LJ, McSweeney CM, McGlacken GP, Morrissey JP, et al. The Pseudomonas quinolone signal (PQS), and its precursor HHQ, modulate interspecies and interkingdom behaviour: Quinolone signal molecules modulate interkingdom behaviour. FEMS Microbiol Ecol. 2011;77(2):413–28.

156. Heeb S, Fletcher MP, Chhabra SR, Diggle SP, Williams P, Cámara M. Quinolones: from antibiotics to autoinducers. FEMS Microbiol Rev. 2011;35(2):247–74.

157. Wratten SJ, Wolfe MS, Andersen RJ, Faulkner DJ. Antibiotic Metabolites from a Marine Pseudomonad. Antimicrob Agents Chemother. 1977;11(3):411–4.

158. Diggle SP, Matthijs S, Wright VJ, Fletcher MP, Chhabra SR, Lamont IL, et al. The Pseudomonas aeruginosa 4-Quinolone Signal Molecules HHQ and PQS Play

Multifunctional Roles in Quorum Sensing and Iron Entrapment. Chem Biol. 2007;14(1):87–96.

159. Dubern J-F, Diggle SP. Quorum sensing by 2-alkyl-4-quinolones in Pseudomonas aeruginosa and other bacterial species. Mol Biosyst. 2008;4(9):882.

160. Vial L, Lépine F, Milot S, Groleau M-C, Dekimpe V, Woods DE, et al. Burkholderia pseudomallei, B. thailandensis, and B. ambifaria Produce 4-Hydroxy-2-Alkylquinoline Analogues with a Methyl Group at the 3 Position That Is Required for Quorum-Sensing Regulation. J Bacteriol. 2008;190(15):5339–52.

161. Diggle SP, Lumjiaktase P, Dipilato F, Winzer K, Kunakorn M, Barrett DA, et al. Functional Genetic Analysis Reveals a 2-Alkyl-4-Quinolone Signaling System in the Human Pathogen Burkholderia pseudomallei and Related Bacteria. Chem Biol. 2006;13(7):701–10.

162. Thierbach S, Birmes FS, Letzel MC, Hennecke U, Fetzner S. Chemical Modification and Detoxification of the *Pseudomonas aeruginosa* Toxin 2-Heptyl-4-hydroxyquinoline *N* -Oxide by Environmental and Pathogenic Bacteria. ACS Chem Biol. 2017;12(9):2305–12.

163. Müller C, Birmes FS, Niewerth H, Fetzner S. Conversion of the Pseudomonas aeruginosa Quinolone Signal and Related Alkylhydroxyquinolines by Rhodococcus sp. Strain BG43. Appl Environ Microbiol. 2014;80(23):7266–74.

164. Lloyd DG, Whitworth DE. The Myxobacterium Myxococcus xanthus Can Sense and Respond to the Quorum Signals Secreted by Potential Prey Organisms. Front Microbiol. 2017;8.

165. Albataineh H, Duke M, Misra SK, Sharp JS, Stevens DC. Identification of a solo acylhomoserine lactone synthase from the myxobacterium Archangium gephyra. Sci Rep. 2021;11(1):3018.

166. Whitworth DE, Zwarycz A. A Genomic Survey of Signalling in the Myxococcaceae. Microorganisms. 2020;8(11):1739.

167. Velicer GJ, Kroos L, Lenski RE. Loss of social behaviors by Myxococcus xanthus during evolution in an unstructured habitat. Proc Natl Acad Sci. 1998;95(21):12376–80.

168. Kraemer SA, Toups MA, Velicer GJ. Natural variation in developmental life-history traits of the bacterium Myxococcus xanthus: Natural variation in Myxococcus developmental phenotypes. FEMS Microbiol Ecol. 2010.

169. Kaiser D. Social gliding is correlated with the presence of pili in Myxococcus xanthus. Proc Natl Acad Sci. 1979;76(11):5952–6.

170. Yu Y-TN, Cooper E, Velicer GJ. A conserved stem of the Myxococcus xanthus sRNA Pxr controls sRNA accumulation and multicellular development. Sci Rep. 2017;7(1):15411.

171. Cossey SM, Yu Y-TN, Cossu L, Velicer GJ. Kin discrimination and outer membrane exchange in Myxococcus xanthus: Experimental analysis of a natural population. Lai E-M, editor. PLOS ONE. 2019;14(11):e0224817.

172. Chen I-CK, Velicer GJ, Yu Y-TN. Divergence of functional effects among bacterial sRNA paralogs. BMC Evol Biol. 2017;17(1):199.

173. Yu Y-TN, Kleiner M, Velicer GJ. Spontaneous Reversions of an Evolutionary Trait Loss Reveal Regulators of a Small RNA That Controls Multicellular Development in Myxobacteria. J Bacteriol. 2016;198(23):3142–51.

174. Nair RR, Fiegna F, Velicer GJ. Indirect evolution of social fitness inequalities and facultative social exploitation. Proc R Soc B Biol Sci. 2018;285(1875):20180054.

175. Krug D, Zurek G, Revermann O, Vos M, Velicer GJ, Müller R. Discovering the Hidden Secondary Metabolome of Myxococcus xanthus: a Study of Intraspecific Diversity. Appl Environ Microbiol. 2008;74(10):3058–68.

176. Xiao G, Déziel E, He J, Lépine F, Lesic B, Castonguay M-H, et al. MvfR, a key Pseudomonas aeruginosa pathogenicity LTTR-class regulatory protein, has dual ligands. Mol Microbiol. 2006;62(6):1689–99.

177. Cao H, Krishnan G, Goumnerov B, Tsongalis J, Tompkins R, Rahme LG. A quorum sensing-associated virulence gene of Pseudomonas aeruginosa encodes a LysR-like transcription regulator with a unique self-regulatory mechanism. Proc Natl Acad Sci. 2001;98(25):14613–8.

178. Ueki T, Inouye S. Identification of an activator protein required for the induction of fruA, a gene essential for fruiting body development in Myxococcus xanthus. Proc Natl Acad Sci. 2003;100(15):8782–7.

179. Ogawa M, Fujitani S, Mao X, Inouye S, Komano T. FruA, a putative transcription factor essential for the development of *Myxococcus xanthus*. Mol Microbiol. 1996;22(4):757–67.

180. Hoang Y, Kroos L. Ultrasensitive Response of Developing *Myxococcus xanthus* to the Addition of Nutrient Medium Correlates with the Level of MrpC. J Bacteriol. 2018;200(22):e00456-18.

181. Robinson M, Son B, Kroos D, Kroos L. Transcription factor MrpC binds to promoter regions of hundreds of developmentally-regulated genes in Myxococcus xanthus. BMC Genomics. 2014;15(1):1123.

182. McLaughlin PT, Bhardwaj V, Feeley BE, Higgs PI. MrpC, a CRP/Fnr homolog, functions as a negative autoregulator during the *Myxococcus xanthus* multicellular developmental program: Negative autoregulation by MrpC. Mol Microbiol. 2018;109(2):245–61.

183. Gallagher LA, McKnight SL, Kuznetsova MS, Pesci EC, Manoil C. Functions Required for Extracellular Quinolone Signaling by Pseudomonas aeruginosa. J Bacteriol. 2002;184(23):6472–80.

184. Deziel E, Lepine F, Milot S, He J, Mindrinos MN, Tompkins RG, et al. Analysis of Pseudomonas aeruginosa 4-hydroxy-2-alkylquinolines (HAQs) reveals a role for 4-hydroxy-2-heptylquinoline in cell-to-cell communication. Proc Natl Acad Sci. 2004;101(5):1339–44.

185. Schertzer JW, Brown SA, Whiteley M. Oxygen levels rapidly modulate Pseudomonas aeruginosa social behaviours via substrate limitation of PqsH: O2 controls P. aeruginosa quorum sensing via PqsH. Mol Microbiol. 2010;77(6):1527–38.

186. Medema MH, Kottmann R, Yilmaz P, Cummings M, Biggins JB, Blin K, et al. Minimum Information about a Biosynthetic Gene cluster. Nat Chem Biol. 2015;11(9):625–31.

187. Walsh CT, Fischbach MA. Natural Products Version 2.0: Connecting Genes to Molecules. J Am Chem Soc. 2010;132(8):2469–93.

188. Skinnider MA, Merwin NJ, Johnston CW, Magarvey NA. PRISM 3: expanded prediction of natural product chemical structures from microbial genomes. Nucleic Acids Res. 2017;45(W1):W49–54.

189. Berleman JE, Allen S, Danielewicz MA, Remis JP, Gorur A, Cunha J, et al. The lethal cargo of Myxococcus xanthus outer membrane vesicles. Front Microbiol. 2014;5.

190. Evans AGL, Davey HM, Cookson A, Currinn H, Cooke-Fox G, Stanczyk PJ, et al. Predatory activity of Myxococcus xanthus outer-membrane vesicles and properties of their hydrolase cargo. Microbiology. 2012;158(11):2742–52.

191. Goh E-B, Yim G, Tsui W, McClure J, Surette MG, Davies J. Transcriptional modulation of bacterial gene expression by subinhibitory concentrations of antibiotics. Proc Natl Acad Sci. 2002;99(26):17025–30.

192. Seyedsayamdost MR. High-throughput platform for the discovery of elicitors of silent bacterial gene clusters. Proc Natl Acad Sci. 2014;111(20):7266–71.

193. Onaka H, Tabata H, Igarashi Y, Sato Y, Furumai T. Goadsporin, a Chemical Substance which Promotes Secondary Metabolism and Morphogenesis in Streptomycetes. I. Purification and Characterization. J Antibiot (Tokyo). 2001;54(12):1036–44.

194. Pimentel-Elardo SM, Sørensen D, Ho L, Ziko M, Bueler SA, Lu S, et al. Activity-Independent Discovery of Secondary Metabolites Using Chemical Elicitation and Cheminformatic Inference. ACS Chem Biol. 2015;10(11):2616–23.

195. Okada BK, Wu Y, Mao D, Bushin LB, Seyedsayamdost MR. Mapping the Trimethoprim-Induced Secondary Metabolome of *Burkholderia thailandensis*. ACS Chem Biol. 2016;11(8):2124–30.

196. Moon K, Xu F, Seyedsayamdost MR. Cebulantin, a Cryptic Lanthipeptide Antibiotic Uncovered Using Bioactivity-Coupled HiTES. Angew Chem Int Ed. 2019;58(18):5973–7.

197. Xu F, Nazari B, Moon K, Bushin LB, Seyedsayamdost MR. Discovery of a Cryptic Antifungal Compound from *Streptomyces albus* J1074 Using High-Throughput Elicitor Screens. J Am Chem Soc. 2017;139(27):9203–12.

198. Bredenbruch F, Nimtz M, Wray V, Morr M, Müller R, Häussler S. Biosynthetic Pathway of Pseudomonas aeruginosa 4-Hydroxy-2-Alkylquinolines. J Bacteriol. 2005;187(11):3630–5.

199. Toyofuku M, Nakajima-Kambe T, Uchiyama H, Nomura N. The Effect of a Cell-to-Cell Communication Molecule, Pseudomonas Quinolone Signal (PQS), Produced by P. aeruginosa on Other Bacterial Species. Microbes Environ. 2010;25(1):1–7.

200. Machan ZA, Taylor GW, Pitt TL, Cole PJ, Wilson R. 2-Heptyl-4-hydroxyquinoline *N* -oxide, an antistaphylococcal agent produced by *Pseudomonas aeruginosa*. J Antimicrob Chemother. 1992;30(5):615–23.

201. Michael Love SA. DESeq2. Bioconductor; 2017. Available from: https://bioconductor.org/packages/DESeq2

202. Katajamaa M, Miettinen J, Oresic M. MZmine: toolbox for processing and visualization of mass spectrometry based molecular profile data. Bioinformatics. 2006;22(5):634–6.

203. Olivon F, Grelier G, Roussi F, Litaudon M, Touboul D. MZmine 2 Data-Preprocessing To Enhance Molecular Networking Reliability. Anal Chem. 2017;89(15):7836–40.

204. Pluskal T, Castillo S, Villar-Briones A, Orešič M. MZmine 2: Modular framework for processing, visualizing, and analyzing mass spectrometry-based molecular profile data. BMC Bioinformatics. 2010;11(1):395.

205. Smith CA, Want EJ, O'Maille G, Abagyan R, Siuzdak G. XCMS: Processing Mass Spectrometry Data for Metabolite Profiling Using Nonlinear Peak Alignment, Matching, and Identification. Anal Chem. 2006;78(3):779–87.

206. Domingo-Almenara X, Montenegro-Burke JR, Ivanisevic J, Thomas A, Sidibé J, Teav T, et al. XCMS-MRM and METLIN-MRM: a cloud library and public resource for targeted analysis of small molecules. Nat Methods. 2018;15(9):681–4.

207. Albataineh H, Stevens D. Marine Myxobacteria: A Few Good Halophiles. Mar Drugs. 2018;16(6):209.

208. Findlay BL. The Chemical Ecology of Predatory Soil Bacteria. ACS Chem Biol. 2016;11(6):1502–10.

209. Erken M, Lutz C, McDougald D. The Rise of Pathogens: Predation as a Factor Driving the Evolution of Human Pathogens in the Environment. Microb Ecol. 2013;65(4):860–8.

210. Justice SS, Hunstad DA, Cegelski L, Hultgren SJ. Morphological plasticity as a bacterial survival strategy. Nat Rev Microbiol. 2008;6(2):162–8.

211. Seiler C, van Velzen E, Neu TR, Gaedke U, Berendonk TU, Weitere M. Grazing resistance of bacterial biofilms: a matter of predators' feeding trait. FEMS Microbiol Ecol. 2017;93(9).

212. Weitere M, Bergfeld T, Rice SA, Matz C, Kjelleberg S. Grazing resistance of Pseudomonas aeruginosa biofilms depends on type of protective mechanism, developmental stage and protozoan feeding mode. Environ Microbiol. 2005;7(10):1593–601.

213. Sun S, Noorian P, McDougald D. Dual Role of Mechanisms Involved in Resistance to Predation by Protozoa and Virulence to Humans. Front Microbiol. 2018;9:1017.

214. Traxler MF, Seyedsayamdost MR, Clardy J, Kolter R. Interspecies modulation of bacterial development through iron competition and siderophore piracy: Xenosiderophores alter development in actinomycetes. Mol Microbiol. 2012;86(3):628–44.

215. Harrison F, Paul J, Massey RC, Buckling A. Interspecific competition and siderophore-mediated cooperation in Pseudomonas aeruginosa. ISME J. 2008;2(1):49–55.

216. Seccareccia I, Kost C, Nett M. Quantitative Analysis of Lysobacter Predation. Schottel JL, editor. Appl Environ Microbiol. 2015;81(20):7098–105.

217. Matz C, Bergfeld T, Rice SA, Kjelleberg S. Microcolonies, quorum sensing and cytotoxicity determine the survival of Pseudomonas aeruginosa biofilms exposed to protozoan grazing. Environ Microbiol. 2004;6(3):218–26.

218. Matz C, Deines P, JÃ¼rgens K. Phenotypic variation in Pseudomonas sp. CM10 determines microcolony formation and survival under protozoan grazing. FEMS Microbiol Ecol. 2002;39(1):57–65.

219. Queck S-Y, Weitere M, Moreno AM, Rice SA, Kjelleberg S. The role of quorum sensing mediated developmental traits in the resistance of Serratia marcescens biofilms against protozoan grazing. Environ Microbiol. 2006;8(6):1017–25.

220. Andrews SC, Robinson AK, Rodríguez-Quiñones F. Bacterial iron homeostasis. FEMS Microbiol Rev. 2003;27(2–3):215–37.

221. Wandersman C, Delepelaire P. Bacterial Iron Sources: From Siderophores to Hemophores. Annu Rev Microbiol. 2004;58(1):611–47.

222. Drake EJ, Cao J, Qu J, Shah MB, Straubinger RM, Gulick AM. The 1.8 Å Crystal Structure of PA2412, an MbtH-like Protein from the Pyoverdine Cluster of Pseudomonas aeruginosa. J Biol Chem. 2007;282(28):20425–34.

223. Felnagle EA, Barkei JJ, Park H, Podevels AM, McMahon MD, Drott DW, et al. MbtH-Like Proteins as Integral Components of Bacterial Nonribosomal Peptide Synthetases. Biochemistry. 2010;49(41):8815–7.

224. Parker DL, Lee S-W, Geszvain K, Davis RE, Gruffaz C, Meyer J-M, et al. Pyoverdine synthesis by the Mn(II)-oxidizing bacterium Pseudomonas putida GB-1. Front Microbiol. 2014;5.

225. Ringel MT, Brüser T. The biosynthesis of pyoverdines. Microb Cell. 2018;5(10):424–37.

226. Weaver VB, Kolter R. Burkholderia spp. Alter Pseudomonas aeruginosa Physiology through Iron Sequestration. J Bacteriol. 2004;186(8):2376–84.

227. Hassett DJ, Howell ML, Ochsner UA, Vasil ML, Johnson Z, Dean GE. An operon containing fumC and sodA encoding fumarase C and manganese superoxide dismutase is controlled by the ferric uptake regulator in Pseudomonas aeruginosa: fur mutants produce elevated alginate levels. J Bacteriol. 1997;179(5):1452–9.

228. Hassett DJ, Howell ML, Sokol PA, Vasil ML, Dean GE. Fumarase C activity is elevated in response to iron deprivation and in mucoid, alginate-producing Pseudomonas aeruginosa: cloning and characterization of fumC and purification of native fumC. J Bacteriol. 1997;179(5):1442–51.

229. Damron FH, Goldberg JB. Proteolytic regulation of alginate overproduction in Pseudomonas aeruginosa: Proteolytic regulation of alginate. Mol Microbiol. 2012;84(4):595–607.

230. Deretic V, Martin DW, Schurr MJ, Mudd MH, Hibler NS, Curcic R, et al. Conversion to Mucoidy in Pseudomonas aeruginosa. Nat Biotechnol. 1993;11(10):1133–6.

231. Li S, Lou X, Xu Y, Teng X, Liu R, Zhang Q, et al. Structural basis for the recognition of MucA by MucB and AlgU in *Pseudomonas aeruginosa*. FEBS J. 2019;286(24):4982–94.

232. Martin DW, Schurr MJ, Mudd MH, Deretic V. Differentiation of Pseudomonas aeruginosa into the alginate-producing form: inactivation of mucB causes conversion to mucoidy. Mol Microbiol. 1993;9(3):497–506.

233. Garneau-Tsodikova S, Labby KJ. Mechanisms of resistance to aminoglycoside antibiotics: overview and perspectives. MedChemComm. 2016;7(1):11–27.

234. Li X-Z, Plésiat P, Nikaido H. The Challenge of Efflux-Mediated Antibiotic Resistance in Gram-Negative Bacteria. Clin Microbiol Rev. 2015;28(2):337–418.

235. Aeschlimann JR. The Role of Multidrug Efflux Pumps in the Antibiotic Resistance of *Pseudomonas aeruginosa* and Other Gram-Negative Bacteria. Pharmacotherapy. 2003;23(7):916–24.

236. Barrientos-Moreno L, Molina-Henares MA, Pastor-García M, Ramos-González MI, Espinosa-Urgel M. Arginine Biosynthesis Modulates Pyoverdine Production and Release in *Pseudomonas putida* as Part of the Mechanism of Adaptation to Oxidative Stress. J Bacteriol. 2019;201(22):e00454-19.

237. Imperi F, Tiburzi F, Visca P. Molecular basis of pyoverdine siderophore recycling in Pseudomonas aeruginosa. Proc Natl Acad Sci. 2009;106(48):20440–5.

238. Dietrich LEP, Price-Whelan A, Petersen A, Whiteley M, Newman DK. The phenazine pyocyanin is a terminal signalling factor in the quorum sensing network of Pseudomonas aeruginosa. Mol Microbiol. 2006;61(5):1308–21.

239. Sakhtah H, Koyama L, Zhang Y, Morales DK, Fields BL, Price-Whelan A, et al. The *Pseudomonas aeruginosa* efflux pump MexGHI-OpmD transports a natural phenazine that controls gene expression and biofilm development. Proc Natl Acad Sci. 2016;113(25):E3538–47.

240. Schiessl KT, Hu F, Jo J, Nazia SZ, Wang B, Price-Whelan A, et al. Phenazine production promotes antibiotic tolerance and metabolic heterogeneity in Pseudomonas aeruginosa biofilms. Nat Commun. 2019;10(1):762.

241. Blankenfeldt W, Parsons JF. The structural biology of phenazine biosynthesis. Curr Opin Struct Biol. 2014;29:26–33.

242. Blankenfeldt W, Kuzin AP, Skarina T, Korniyenko Y, Tong L, Bayer P, et al. Structure and function of the phenazine biosynthetic protein PhzF from Pseudomonas fluorescens. Proc Natl Acad Sci. 2004;101(47):16431–6.

243. Mavrodi DV, Peever TL, Mavrodi OV, Parejko JA, Raaijmakers JM, Lemanceau P, et al. Diversity and Evolution of the Phenazine Biosynthesis Pathway. Appl Environ Microbiol. 2010;76(3):866–79.

244. Parsons JF, Song F, Parsons L, Calabrese K, Eisenstein E, Ladner JE. Structure and Function of the Phenazine Biosynthesis Protein PhzF from *Pseudomonas fluorescens* 2-79 ‡. Biochemistry. 2004;43(39):12427–35.

245. Matz C, Kjelleberg S. Off the hook – how bacteria survive protozoan grazing. Trends Microbiol. 2005;13(7):302–7.

246. Matz C, McDougald D, Moreno AM, Yung PY, Yildiz FH, Kjelleberg S. Biofilm formation and phenotypic variation enhance predation-driven persistence of Vibrio cholerae. Proc Natl Acad Sci. 2005;102(46):16819–24.

247. Al Ahmar R, Kirby BD, Yu HD. Culture of Small Colony Variant of Pseudomonas aeruginosa and Quantitation of its Alginate. J Vis Exp. 2020;(156):60466.

248. Knutson CA, Jeanes A. A new modification of the carbazole analysis: Application to heteropolysaccharides. Anal Biochem. 1968;24(3):470–81.

249. Lorenz C, Dougherty TJ, Lory S. Transcriptional responses of *Pseudomonas aeruginosa* to inhibition of lipoprotein transport by a small molecule inhibitor. J Bacteriol. 2020;JB.00452-20, jb;JB.00452-20v1.

250. Khare A, Tavazoie S. Multifactorial Competition and Resistance in a Two-Species Bacterial System. Zhang J, editor. PLOS Genet. 2015;11(12):e1005715.

251. Yang F, Gu J, Zou J, Lei L, Jing H, Zhang J, et al. PA0833 Is an OmpA C-Like Protein That Confers Protection Against Pseudomonas aeruginosa Infection. Front Microbiol. 2018;9:1062.

252. Miskinyte M, Sousa A, Ramiro RS, de Sousa JAM, Kotlinowski J, Caramalho I, et al. The Genetic Basis of Escherichia coli Pathoadaptation to Macrophages. Monack DM, editor. PLoS Pathog. 2013;9(12):e1003802.

253. Scanlan PD, Buckling A. Co-evolution with lytic phage selects for the mucoid phenotype of Pseudomonas fluorescens SBW25. ISME J. 2012;6(6):1148–58.

254. Vieira A, Ramesh A, Seddon AM, Karlyshev AV. CmeABC Multidrug Efflux Pump Contributes to Antibiotic Resistance and Promotes Campylobacter jejuni Survival and Multiplication in Acanthamoeba polyphaga. McBain AJ, editor. Appl Environ Microbiol. 2017;83(22):e01600-17.

255. Leong W, Lutz C, Williams J, Poh YH, Yee BYK, Chua C, et al. *Pseudomonas aeruginosa* isolates co-incubated with *Acanthamoeba castellanii* exhibit phenotypes similar to chronic cystic fibrosis isolates. Microbiology; 2020.

256. Winstanley C, O'Brien S, Brockhurst MA. Pseudomonas aeruginosa Evolutionary Adaptation and Diversification in Cystic Fibrosis Chronic Lung Infections. Trends Microbiol. 2016;24(5):327–37.

257. Mulcahy LR, Burns JL, Lory S, Lewis K. Emergence of Pseudomonas aeruginosa Strains Producing High Levels of Persister Cells in Patients with Cystic Fibrosis. J Bacteriol. 2010;192(23):6191–9.

258. Malone J. Role of small colony variants in persistence of Pseudomonas aeruginosa infections in cystic fibrosis lungs. Infect Drug Resist. 2015;237.

259. Maunders E, Welch M. Matrix exopolysaccharides; the sticky side of biofilm formation. FEMS Microbiol Lett. 2017;364(13).

260. Sun S, Kjelleberg S, McDougald D. Relative Contributions of Vibrio Polysaccharide and Quorum Sensing to the Resistance of Vibrio cholerae to Predation by Heterotrophic Protists. PLoS ONE. 2013;8(2):e56338.

261. Butt AT, Thomas MS. Iron Acquisition Mechanisms and Their Role in the Virulence of Burkholderia Species. Front Cell Infect Microbiol. 2017;7:460.

262. Chekabab SM, Daigle F, Charette SJ, Dozois CM, Harel J. Shiga toxins decrease enterohaemorrhagic *Escherichia coli* survival within *Acanthamoeba castellanii*. FEMS Microbiol Lett. 2013;344(1):86–93.

263. Lainhart W, Stolfa G, Koudelka GB. Shiga Toxin as a Bacterial Defense against a Eukaryotic Predator, Tetrahymena thermophila. J Bacteriol. 2009;191(16):5116–22.

264. Meltz Steinberg K, Levin BR. Grazing protozoa and the evolution of the *Escherichia coli* O157:H7 Shiga toxin-encoding prophage. Proc R Soc B Biol Sci. 2007;274(1621):1921–9.

265. Matz C, Moreno AM, Alhede M, Manefield M, Hauser AR, Givskov M, et al. Pseudomonas aeruginosa uses type III secretion system to kill biofilm-associated amoebae. ISME J. 2008;2(8):843–52.

266. Riquelme S, Varas M, Valenzuela C, Velozo P, Chahin N, Aguilera P, et al. Relevant Genes Linked to Virulence Are Required for Salmonella Typhimurium to Survive Intracellularly in the Social Amoeba Dictyostelium discoideum. Front Microbiol. 2016.

267. Pombinho R, Camejo A, Vieira A, Reis O, Carvalho F, Almeida MT, et al. Listeria monocytogenes CadC Regulates Cadmium Efflux and Fine-tunes Lipoprotein Localization to Escape the Host Immune Response and Promote Infection. J Infect Dis. 2017;215(9):1468–79.

268. Dillies M-A, Rau A, Aubert J, Hennequet-Antier C, Jeanmougin M, Servant N, et al. A comprehensive evaluation of normalization methods for Illumina high-throughput RNA sequencing data analysis. Brief Bioinform. 2013;14(6):671–83.

269. Robinson MD, McCarthy DJ, Smyth GK. edgeR: a Bioconductor package for differential expression analysis of digital gene expression data. Bioinformatics. 2010;26(1):139–40.

270. Jones CJ, Ryder CR, Mann EE, Wozniak DJ. AmrZ Modulates Pseudomonas aeruginosa Biofilm Architecture by Directly Repressing Transcription of the psl Operon. J Bacteriol. 2013;195(8):1637–44.

APPENDIX

Table X. Abbreviations of microorganisms

A. globiformis	*Agrobacter globiformis*
B. licheniformis	*Bacillus licheniformis*
B. subtilis	*Bacillus subtilis*
C. nebraskensis	*Clavibacter nebraskensis*
C. exiguus	*Corallococcus exiguus*
C. destructans	*Cylindrocarpon destructans*
C. ferrugineus	*Cystobacter ferrugineus*
E. coli	*Escherichia coli*
F. oxysporum	*Fusarium oxysporum*
K. pneumoniae	*Klebsiella pneumoniae*
M. flavescens	*Myxococcus flavescens*
M. fulvus	*Myxococcus fulvus*
M. macrosporus	*Myxococcus macrosporus*
M. stipitatus	*Myxococcus stipitatus*
M. virescens	*Myxococcus virescens*
M. xanthus	*Myxococcus xanthus*
N. muscorum	*Nostoc muscorum*
P. luridum	*Phormidium luridum*
P. aeruginosa	*Pseudomonas aeruginosa*
P. aureofaciens	*Pseudomonas aureofaciens*
P. fluorescens	*Pseudomonas fluorescens*
P. putida	*Pseudomonas putida*
P. syringae	*Pseudomonas syringae*
P. mirabilis	*Proteus mirabilis*
R. solani	*Rhizoctonia solani*
R. vitis	*Rhizobium vitis*

S. cerevisiae	*Saccharomyces cerevisiae*
S. typhosa	*Salmonella typhosa*
S. minor	*Sclerotinia minor*
S. meliloti	*Sinorhizobium meliloti*
S. aureus	*Staphylococcus aureus*
S. saprophyticus	*Staphylococcus saprophyticus*
S. coelicolor	*Streptomyces coelicolor*
V. dahlia	*Verticillium dahlia*

Table 3.1: Impact of prey signaling molecules on myxobacterial genes included in biosynthetic gene clusters

exposure experiment	antiSMASH annotation	accession	cluster ID	cluster type	antiSMASH category	log_2fold change
M. xanthus	hypothetical protein	WP_011551417.1	1.2	betalactone/NRPS	other gene	-3.79
C6-AHL	hypothetical protein	WP_011552481.1	1.5	Tfu-related	other gene	-3.19
	TetR/AcrR family transcriptional regulator	WP_011552861.1	1.6	NRPS-PKS	regulatory gene	2.38
	AAA family ATPase	WP_011554508.1	1.18	NRPS-PKS	other gene	-3.12
	hypothetical protein/YcaO-like protein	WP_011554909.1	1.20	thiopeptide/bacteriocin	core biosynthetic gene	-2.39
	beta-ketoacyl synthase	WP_011556328.1	1.22	ladderane/lanthipeptide	additional biosynthetic gene	-4.64
	beta-ketoacyl-[acyl-carrier-protein] synthase family protein	WP_011556332.1	1.22	ladderane/lanthipeptide	additional biosynthetic gene	-4.81
C. ferrugineus	alpha/beta fold hydrolase	WP_084735772.1	1.2	NRPS	additional biosynthetic gene	-6.59
C6-AHL	alpha/beta hydrolase fold domain-containing protein	WP_071896420.1	1.3	T3PKS	additional biosynthetic gene	-6.87
	D-alanine--D-alanine ligase	WP_071896998.1	1.3	T3PKS	other gene	-3.94
	UDP-glucose	WP_071896852.1	1.5	terpene	additional biosynthetic gene	-3.05
	fatty acid desaturase	WP_071897173.1	2.3	NRPS	other gene	-3.92
	DUF938 domain-containing protein	WP_071897649.1	2.4	terpene	other gene	-6.92
	phage holin family protein	WP_071897879.1	2.5	terpene	other gene	7.63
	hypothetical protein	WP_071897877.1	2.5	terpene	other gene	-6.72
	iron-containing redox enzyme family protein	WP_071898518.1	3.2	NRPS	other gene	6.71
	hypothetical protein	WP_071900459.1	5.1	NRPS	other gene	-8.45
	hypothetical protein	WP_071900730.1	6.2	T1PKS	other gene	-7.15
	hypothetical protein	WP_071902147.1	9.2	lanthipeptide	other gene	**-2.89**
	YdeI/OmpD-associated family protein	WP_071902672.1	11.1	terpene	other gene	-4.02
	MBL fold metallo-hydrolase	WP_071902711.1	11.2	NRPS-PKS	other gene	-5.22
	hypothetical protein	WP_071902727.1	11.2	NRPS-PKS	other gene	**8.75**
	peptidoglycan DD-metalloendopeptidase family protein	WP_071902970.1	12.1	thiopeptide	other gene	**7.23**
	hypothetical protein	WP_071903089.1	12.2	terpene	other gene	1.96
	aldehyde dehydrogenase family protein	WP_071903959.1	16.2	NRPS	additional biosynthetic gene	2.18
	alcohol dehydrogenase AdhP	WP_071903960.1	16.2	NRPS	additional biosynthetic gene	2.40
	hypothetical protein	WP_071904220.1	17.1	bacteriocin	other gene	6.37
M. xanthus						
HHQ	DUF4215 domain-containing protein	WP_011554915.1	1.20	thiopeptide/bacteriocin	other gene	-4.41
C. ferrugineus	MarR family transcriptional regulator	WP_071896979.1	1.2	NRPS	regulatory gene	5.83
HHQ	response regulator	WP_071896419.1	1.3	T3PKS	regulatory gene	4.96
	hypothetical protein	WP_071896846.1	1.5	terpene	other gene	-7.39
	chemotaxis protein CheW	WP_071897126.1	2.2	T3PKS	other gene	6.13
	response regulator	WP_071897195.1	2.3	NRPS	other gene	6.13
	hypothetical protein	WP_071897642.1	2.4	terpene	other gene	4.74
	suppressor of fused domain protein	WP_071898529.1	3.2	NRPS	other gene	4.21
	hypothetical protein	WP_071898691.1	3.3	terpene	other gene	-4.31
	MvdC family ATP-grasp ribosomal peptidematurase	WP_071901228.1	7.2	lanthipeptide/microviridin	additional biosynthetic gene	5.38
	TerC family protein	WP_071901260.1	7.3	NRPS	other gene	4.55
	dienelactone hydrolase family protein	WP_084736693.1	8.1	terpene	other gene	-5.84
	aquaporin	WP_071902141.1	9.2	lanthipeptide	other gene	5.16
	hypothetical protein	WP_071902715.1	11.2	NRPS-PKS	other gene	-5.25
	acyl-CoA thioesterase	WP_071903088.1	12.2	terpene	other gene	6.05
	HAMP domain-containing histidine kinase	WP_071903679.1	15.1	LAP	regulatory gene	5.43
	MFS transporter	WP_071904585.1	19.1	T1PKS	transport-related gene	5.04

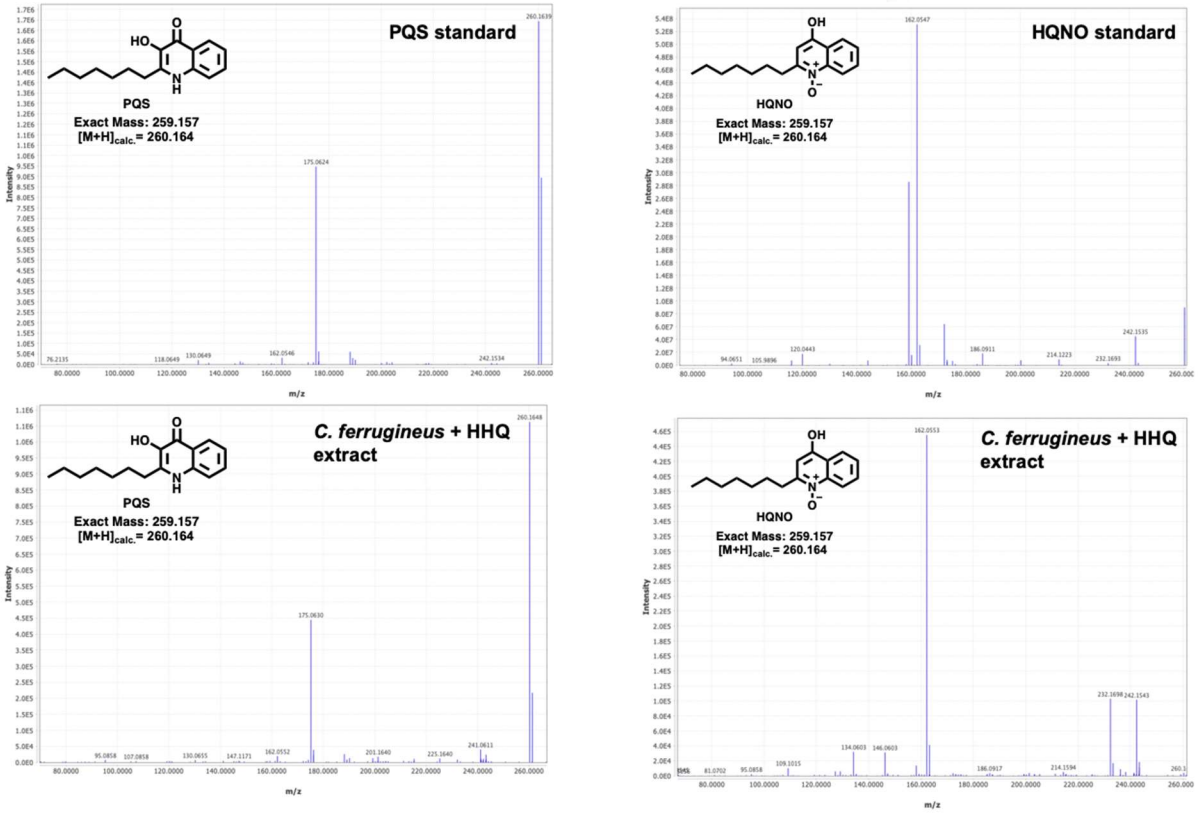

Figure 3.12. Comparison of MS/MS spectra of HHQ oxidized products from *C. ferrugineus* extract with the commercial standards.

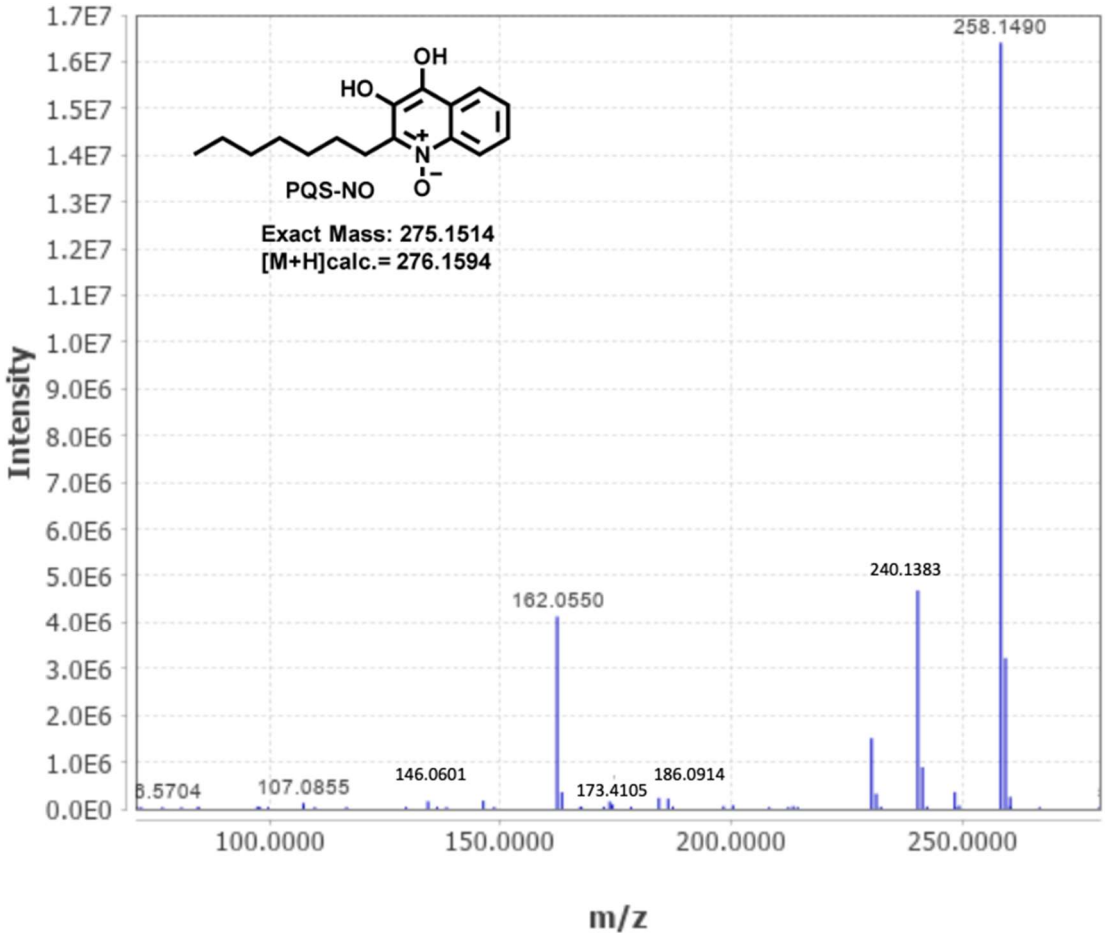

Figure 3.13. MS/MS spectra of PQS-NO from HHQ exposed *C. ferrugineus* extract.

VITA

Shukria Akbar was born in Abu Dhabi, United Arab Emirates, and was brought up in Lahore, Pakistan. She graduated from the School of Pharmacy, University of the Punjab, Pakistan, in 2014 with a professional degree of Doctor of Pharmacy. She then worked as a hospital pharmacist in Surgimed Hospital, Pakistan, before starting her Ph.D. As a graduate student, Shukria joined Professor Cole Stevens research group in the Department of BioMolecular Sciences, School of Pharmacy at the University of Mississippi in 2016. She is currently a Ph.D. candidate in the Pharmaceutical Sciences and conducting her graduate research on investigating the interactions of predatory myxobacteria with their prey and prey signaling molecules.